PB-227 023

NITRIC OXICE MEASUREMENTS IN A SIMULATED SPARK IGNITION ENGINE

James L. Hodges, et al

Stevens Institute of Technology
Hoboken, New Jersey

31 January 1971

DISTRIBUTED BY:

NTIS
National Technical Information Service
U. S. DEPARTMENT OF COMMERCE
5285 Port Royal Road, Springfield Va. 22151

Mechanical Engineering
Report ME-RT-70008

PB 227 023

"NITRIC OXIDE MEASUREMENTS IN A SIMULATED SPARK IGNITION ENGINE"

by

James L. Hodges
Lubomyr Kurylko
Robert F. McAlevy III

January 31, 1971

This is an interim progress report on research funded by a grant No. AP00847-01A1 from the Environmental Protection Agency, Air Pollution Control Office.

submitted by

Robert F. McAlevy III

Robert F. McAlevy III
Principal Investigator

Mechanical Engineering Department
Stevens Institute of Technology
Hoboken, New Jersey 07030

Reproduced by
NATIONAL TECHNICAL
INFORMATION SERVICE
U S Department of Commerce
Springfield VA 22151

The major portion of this report has been submitted by James L. Hodges to Stevens Institute of Technology in partial fulfillment of the requirements for the degree of Doctor of Philosophy in Mechanical Engineering.

ABSTRACT

Nitrogen oxides emitted from spark ignition engines play a significant role in the production of photochemical smog.

Nitric oxide concentration in automotive engine exhaust corresponds closely to chemical equilibrium concentrations at combustion temperatures, indicating that nitric oxide concentration "freezes" during, or immediately after, the completion of combustion.

In order to determine the means by which nitric oxide is produced in engines, a device which simulates pertinent thermochemical engine processes was designed, tested and used to acquire relevant data.

A nitric oxide product gas monitoring apparatus was developed which related absorption of ultraviolet radiation at the $(0,0)\gamma$ band of nitric oxide to the NO concentration in the combustion product gas a few seconds after combustion was complete. It was determined that the rate of expansion of the product gas immediately after attainment of peak pressure does not have a substantial effect on measured product gas concentration of NO.

A time-resolved nitric oxide monitoring technique, intended to monitor NO concentration during, and subsequent to the completion of combustion was also devised. Limited qualitative data were acquired.

TABLE OF CONTENTS

Page

Title Page

Abstract ii

Table of Contents iii

List of Figures iv

I. Background 1

A. Photochemistry of Smog Formation 1

B. Previous Work 2

C. Nitric Oxide Emission Control Devices 10

II. Introduction 13

III. Experimental Spark Ignition Engine Analog Device 16

A. Design Criteria 16

B. Description and Operation of Analog Apparatus 17

C. Performance of the S.I. Engine Analog Device 24

D. Evaluation of the S.I. Engine Analog Device 32

IV. Nitric Oxide Ultraviolet Absorption Monitoring Technique 34

A. General 34

B. The Electronic Energy States of the Nitric Oxide Molecule 34

C. Selection of An Absorption Band 37

1. Signal Level 37

2. Window and Lens Materials 38

3. Ultraviolet Radiation Sources 39

4. Ultraviolet Radiation Detectors 40

5. Interfering Species 40

6. Discussion 43

D. The $(0,0)\gamma$ Band of Nitric Oxide 43

1. General 43

2. The Integrated Absorption Coefficient of the $(0,0)\gamma$ Band 45

page

3. The Spectral Absorption Coefficient of the (0,0)γ Band 49
4. Depopulation of the Ground Electronic State of the NO Molecule 51

E. Experimental Procedure 54
1. General 55
2. Calibration 55
3. NO Concentration Measurements 58
4. Discussion 65

V. Time Resolved Nitric Oxide Concentration Measurements 73
A. General 73
B. Experimental Considerations 73
1. The Schumann-Runge Bands and Continuum of O_2 73
2. Population Distribution of the NO γ Bands with Temperature 76
3. Vibrational Relaxation of Nitric Oxide 76
4. Change in Band Shape with Temperature 80
C. Description of Apparatus 80
1. General 80
2. Spectrometer Entrance Slit Width 82
3. Spectroscopic Film 83
4. Flash Tube 84
D. Experimental Results 84
E. Discussion 85

VI. Future Work 88
A. Steady State Apparatus 88
B. Time-Resolved Apparatus 88
C. Theoretical Model 89

VII. Significant Results of This Investigation 90

APPENDICES

A. Methods of Monitoring Nitric Oxide in Automobile Exhaust 92
B. Spark Ignition Analog Device Engineering Drawings 96
C. Poppet Valve-Cam Assembly Design 101

page

D. Spectroscopic Apparatus Description, Testing and Alignment 112

E. Theoretical Equilibrium Nitric Oxide Concentration 119

Bibliography 135

LIST OF FIGURES

Figure	Title	Page
1.	Automotive Engine Analog Device	18
2.	Analog Device Electrical Schematic	20
3.	Theoretical Dependence of Expansion Rate on Motor Speed	22
4.	S.I. Analog Device Plumbing Schematic	25
5.	Peak S.I. Engine Pressure As a Function of Engine Speed	26
6.	Peak S.I. Engine Expansion Rate As A Function of Engine Speed	27
7.	Comparison of Pressure Traces Obtained With S.I. Engine and The Analog Device	29
8.	Typical Analog Device Pressure Histories	31
9.	Energy Level Diagram of The NO Molecule	35
10.	Theoretical Nitric Oxide Half-Life As A Function of Product Gas Pressure	42
11.	Steady State Ultraviolet Nitric Oxide Concentration Monitoring Apparatus	46
12.	Dependence of The Integral of The Log of The Reciprocal Fractional Transmission ($(0,0)\gamma$ Band) On Nitric Oxide Optical Density	48
13.	Comparison of Theoretical and Measured Peak Spectral Absorbance of The $(0,0)\gamma$ Band of Nitric Oxide	50
14.	Log of The Peak Measured Spectral Transmittance of The $(0,0)\gamma$ Band As A Function of The Nitric Oxide Partial Pressure	52
15.	Reference Gas Absorption Scans of The $(0,0)\gamma$ Band of Nitric Oxide	56
16.	Calibration Curves For The Nitric Oxide Ultraviolet Monitoring Technique	57

Figure	Title	Page
17.	Dependence of Product Gas Nitric Oxide Concentration on Equivalence Ratio: 25psia Initial Pressure	59
18.	Dependence of Product Gas Nitric Oxide Concentration On Equivalence Ratio: 50psia Initial Pressure	60
19.	Dependence of Product Gas Nitric Oxide Concentration On Equivalence Ratio: 75psia Initial Pressure	61
20.	Dependence of Product Gas Nitric Oxide Concentration On Equivalence Ratio: 100psia Initial Pressure	62
21.	Dependence of Product Gas Nitric Oxide Concentration On Equivalence Ratio: 125psia	63
22.	Dependence of Product Gas Nitric Oxide Concentration On Initial Pressure	64
23.	Comparison of Theoretical and Measured Peak Combustion Pressure	70
24.	Theoretical Schumann-Runge Absorption At Elevated Temperatures	75
25.	Effect of Resolution On Product Gas Absorption With Time	77
26.	Theoretical Population Distribution of Vibrational Quantum States of NO As A Function of Temperature	78
27.	Transient Ultraviolet Nitric Oxide Concentration Monitoring Apparatus	81
28.	Time-Resolved Nitric Oxide Absorption Spectrum	86
29.	Combustion Chamber Body	97
30.	Combustion Chamber Cover-Top	98
31.	Combustion Chamber Cover-Bottom	99
32.	Valve Housing Assembly	100

Figure	Title	Page
33.	Poppet Valve Dimensions	105
34.	Cam Profile Generation	108
35.	Photomultiplier Circuit Diagram	114
36.	2537 Å Hg Line As A Function of Spectrometer Entrance And Exit Slit Width	118
37.	Theoretical Flame Temperature And Peak Equilibrium Nitric Oxide Concentration Computer Program Flow Chart	124

I. BACKGROUND

A. Photochemistry of Smog Formation.

The automotive spark ignition engine is responsible for about 40 percent of the man-made nitrogen oxides (NO_x) found in the atmosphere (1). These nitrogen oxides consist principally of nitric oxide (NO) and nitrogen dioxide (NO_2). Very little nitrogen dioxide is found in engine exhaust, but the nitric oxide which is present is rapidly converted to NO_2 once emitted into the atmosphere (2). The toxicity of nitrogen dioxide, at concentrations typical of the urban environment, is not well established although there is some indication that, at present levels, nitrogen dioxide is deleterious to health (1, 3, 4). At high concentrations the toxicity of nitrogen dioxide is reasonably well defined for short term exposure (5).

The toxicogenic nature of nitric oxide is unambiguous; there is firm evidence that the nitric oxide emitted from spark ignition engines is an intimate participant in those atmospheric reactions whose primary product is photochemical smog (2, 6, 7). Nitric oxide acts as a catalyst in these reactions, which involve unburned hydrocarbons, nitric oxide, nitrogen dioxide, molecular and atomic oxygen, ozone and ultraviolet light. Details of this complex series of reactions are not yet understood. However, a suggested mechanism involves absorption of radiation by the ONOO intermediate (7);

$$NO + O_2 \rightarrow ONOO \qquad (1)$$

$$ONOO + NO \rightarrow 2NO_2 \qquad (2)$$

$$ONOO + h\nu \rightarrow ONOO^* \qquad (3)$$

$$ONOO^* \rightarrow NO_2 + O \qquad (4)$$

$$NO_2 + h\nu \rightarrow NO + O \qquad (5)$$

$$O + O_2 \rightarrow O_3 \qquad (6)$$

The ozone produced will react with and deteriorate both rubber and plant life and will also attack unburned hydrocarbons, which are constituents of automotive exhaust, to form organic nitrates, acids, etc. (8). It is this conglomerate of organic compounds which is commonly referred to as photochemical smog.

B. Previous Work

In order to provide a rational basis for the design of equipment to inhibit the formation of nitric oxide, or to reduce the concentration of nitric oxide already formed in spark ignition engines, it was necessary to determine how nitric oxide emission levels respond to changes in pertinent engine parameters.

Most early studies invariably involved an analysis of the steady state exhaust gas concentration of nitric oxide as a function of such engine operating parameters as air-fuel ratio, spark advance, compression ratio, rpm, etc. Emission levels have been found most sensitive to changes in air-fuel ratio and spark advance. In a gross sense, one can say that anything which tends to increase peak cycle temperature or oxygen atom concentration will also increase nitric oxide emission. That is, measured exhaust gas concentration of nitric oxide corresponds more closely to equilibrium concentrations at peak cycle temperature than exhaust gas temperature, indicating that the processes which lead to excessive NO emission are not equilibrium processes; nitric oxide concentration "freezes", either during combustion or the early part of the expansion stroke.

The presence of nitric oxide in automotive exhaust gas was recognized as early as 1937, long before atmospheric air pollution became a problem (9).

One of the earliest, and most comprehensive studies dealing specifically with nitric oxide emission from spark ignition engines was performed by Wimmer and McReynolds (10). They monitored the concentration of nitric oxide in an experimental engine using a modified version of the Saltzman Method (a compilation of common NO exhaust gas monitoring techniques is presented in Appendix A). A degree of time resolution was obtained by withdrawing samples of the combustion product gas through a quick-opening sampling valve, designed to open briefly during some stage of the power stroke. However, all data reported were obtained at 160° after top dead center, well after important processes had in all cases ceased.

It was determined on the basis of free energy change and evaluation of equilibrium and rate constants that nitric oxide is the only nitrogen oxide present in the exhaust gas in significant quantity. Later measurements have substantiated this deduction (11).

An equilibrium computer program was developed by them to predict concentrations of NO, N_2, O_2, H_2, H_2O, CO_2, CO, H, O, OH and N at peak temperature. Predicted theoretical values for NO concentration were then compared with measured NO concentration in the exhaust gas. It was found that for rich mixtures the exhaust gas concentration of nitric oxide agreed closely with peak temperature equilibrium values, implying that nitric oxide decomposition does not occur during expansion. However, over-advancing the spark resulted in measured values considerably below those at peak temperature equilibrium. Measured NO concentration for fuel lean mixtures were also significantly lower than peak temperature values.

An attempt was made to correlate measured NO concentration with that predicted on the basis of available kinetic data. At low temperatures the literature suggested that a simple bimolecular mechanism prevailed (12);

$$2NO \rightarrow O_2 + N \qquad (7)$$

and at higher temperatures the Zeldovich mechanism predominated (13);

$$NO + O \rightarrow O_2 + N \qquad (8)$$

$$NO + N \rightarrow N_2 + O \qquad (9)$$

During combustion it was assumed that reaction rates were sufficient to maintain equilibrium nitric oxide concentrations. During product gas expansion only decomposition reactions were considered.

For rich mixtures, since little oxygen is present, it was argued that equation (7) is applicable. Bimolecular decomposition was thought, however, far too slow to permit any NO decomposition during expansion, a result not in consonance with experimental results for advanced spark timing. It was concluded that bimolecular decomposition does not adequately describe the means by which nitric oxide decomposes in spark ignition engines. For lean mixtures the bimolecular reaction was neglected and the Zeldovich mechanism (reactions (8) and (9)) was considered. It was found that theoretical results predicted a degree of decomposition in excess of that observed.

Interpretation of results was speculative; anomolies were tentatively attributed to a possible departure from equilibrium oxygen atom concentration, etc.

More recent work has indicated that the formation and decomposition of nitric oxide do not proceed directly. That is, the Zeldovich mechanism, or a slight modification thereof, is the predominant mechanism of nitric oxide formation and decomposition at conditions typical of operating spark ignition engines.

The first attempt to monitor nitric oxide concentration in.situ. in an actual engine during the power stroke was performed by Newhall (14). Absolute infrared emission at the 5.3μ fundamental band of nitric oxide (corresponding to a transition between the ground and first excited vibrational state) was related directly to nitric oxide concentration during combustion and expansion of the product gas.

Calibration of monitoring apparatus is difficult when making absolute emission measurements. This is particularly true when observation windows, mounted in the engine block, are susceptible to to progressive contamination. In Newhall's work the partial pressure of carbon dioxide was sufficiently high to permit the assumption that radiation emitted at the nearby 4.26μ band of CO_2 closely approximated that of a black body. Calculated product gas temperatures were used to relate infrared emission at this band to instrument response.

In order to relate gas emission at 5.3μ to nitric oxide concentration allowance must be made for the existence of potential interfering species. The 5.3μ NO band is flanked by two strong bands; CO_2 at 4.26μ and H_2O at 6.27μ (15). An attempt was made by Newhall to correct for interference by CO_2, but no allowance was made for possible interference by H_2O. Results of an analysis of the performance of NDIR instruments, which relate exhaust gas concentration of nitric oxide to absorbance of I.R. radiation at the 5.3μ band, indicate substantial interference by H_2O, CO_2 and CO (16).

Newhall's experimental results indicated that freezing always occured early in the expansion stroke. Measured nitric oxide concentration was consistently higher than equilibrium concentration based on the thermodynamic state of the gas at peak cycle temperature.

This was attributed to local gas temperatures substantially in excess of the bulk, or average, product gas temperature.

A comprehensive theoretical kinetic analysis of nitric oxide decomposition during expansion was developed. The initial state of expansion was considered to be that point at which product gas temperature was a maximum. Initially, (that is, immediately after the completion of combustion) all species were assumed in equilibrium.

Results obtained by assuming that the predominant kinetic mechanism was the direct decomposition of NO were compared with variations of the Zeldovich mechanism. The direct decomposition scheme was eventually discarded in favor of the Zeldovich mechanism. All atoms were assumed in equilibrium with their respective molecules. Predicted trends were in good agreement with published data.

An analytical model describing the formation of nitric oxide in high pressure flames was developed by Eyzat and Guibet (17). The basis for this development was the simple bimolecular reaction,

$$2NO \rightarrow O_2 + N_2 \qquad (10)$$

There is now general agreement, however, that neither the formation nor decomposition of nitric oxide proceed directly.

Lavoie, Heywood and Keck have also developed a theoretical model of nitric oxide formation and decomposition in spark ignition engines (18). This treatment considered, for the first time, the temperature gradients which will occur in the combustion chamber of spark ignition engines as a consequence of the compression, during combustion, of the gas ahead of and behind the flame. In an attempt to bracket the true physical process, nitric oxide concentration histories based upon an unmixed model (where local cooling rates assumed no mixing or heat transfer occured between neighboring gas elements) were compared with concentration histories based upon a completely mixed model (no temperature gradients exist within the combustion chamber). The unmixed model described the physical situation more closely than did the fully mixed model. Kinetic rate equations were based on a modified version of the Zeldovich mechanism. Atomic oxygen was assumed in equilibrium with its molecule and atomic nitrogen was assumed in the steady state. It was found that, in engines, nitric oxide kinetics are rate limited during combustion as well as expansion and in some cases freezing of nitric oxide can actually occur during combustion.

Time resolved in. situ. temperature and nitric oxide concentration measurements were also obtained, using a CFR spark ignition research engine (19). The continuous emission of visible light resulting from two photochemical recombination reactions was related to both temperature and NO concentration. The two reactions are;

$$CO + O \rightarrow CO_2 + h\nu \qquad (11)$$

$$NO + O \rightarrow NO_2 + h\nu \qquad (12)$$

Measurement of the intensity of emission at two convenient wavelengths and determination of total pressure allowed calculation of, in the first case, the temperature (assuming the C-O-H system in equilibrium) and in the second, using the calculated temperature, the nitric oxide concentration (there is some evidence that carbon monoxide freezes during the latter stages of expansion, an event which would introduce a systematic error in temperatures measured at the end of expansion (20)). A second method of monitoring temperature was developed, in which emission by the OH radical was related to the transient gas temperature. The measured temperatures had the same functional behavior, although the measured temperature using the OH technique was always the higher of the two. This was attributed to failure of the model used to represent the OH emission band.

Their spectroscopic apparatus was calibrated using a dummy window mount and tungsten strip lamp. Experimental procedure was verified by monitoring several wave lengths in each of the continua (measured NO concentration should be independent of monitored wave length) and by adding known quantities of nitric oxide to the incoming charge. Observation windows were mounted throughout the combustion chamber so that NO concentration could be determined as a function of both space and time. Experimental results compared favorably with theory. Nitric oxide concentration in the early burned gas was higher than NO concentration in the late burned gas, although measured concentration in the early burned gas was lower and in the late burned gas higher than was predicted on the basis of the kinetic model. Addition of nitric oxide to the incoming charge resulted in measured concentrations, during the power stroke, considerably higher than was detected with no NO added. This observation is in apparent contradiction with an aspect of the work of Newhall (14), who reported no discernible difference between measured NO concentration after combustion with and without NO added to the incoming charge. The reason for this discrepancy is not known.

LaVoie, *et. al.* also reported difficulty obtaining reproducible engine pressure traces; data reduction was performed only on those cycles with peak pressure within 10 p.s.i. of a given pressure.

C. Nitric Oxide Emission Control Devices

The desirability of reducing nitric oxide emission from spark ignition engines is apparent. There are presently, however, no commercially feasible means of accomplishing this aim. Numerous systems are under study.

The exhaust gas recycle method reduces peak combustion temperatures by diluting the incoming charge with between 10 and 20 percent of the exhaust gas (21, 22). This method does result in a reduction in exhaust gas concentration of nitric oxide, however, fuel economy, power and that subjective quality termed the "drivability" of the automobile are reputed to suffer. Water injected in the incoming charge also reduces NO concentration by suppressing peak cycle temperature, but an impractical amount of water would have to be added in order to obtain a significant reduction in NO concentration (23).

Although there are numerous means available of tuning an engine to reduce nitric oxide emission levels, a consequence of these techniques is often a considerable increase in the emission of unburned hydrocarbons and carbon monixide (21, 22). For example, enriching the fuel-air mixture and retarding the spark will result in a substantial reduction in exhaust gas concentration of nitric oxide. However, unburned hydrocarbon emission will increase significantly with rich mixtures and carbon monoxide concentration levels are known to increase rapidly with spark retardation. Similarly, the exhaust manifold reactor, designed to reduce hydrocarbon emission levels by injecting air into the exhaust manifold (which is maintained at higher than normal temperatures) can, under certain conditions, increase nitric oxide emission levels (24).

Catalytic devices, some based on the heterogeneous reduction of carbon monoxide by nitric oxide, are under study (25, 26). There is good evidence that catalytic reactors are susceptible to progressive contamination by the tetraethyl lead common to most automotive gasoline (27). As a consequence, a practical catalytic device has not yet been developed.

In spite of the current paucity of practical means of reducing nitric oxide emission levels, projected California standards intended to lower atmospheric concentration of nitric oxide have incorporated maximum allowable nitric oxide emission levels from spark ignition engines. By 1971 maximum tolerable nitric oxide emission will be

4.0 grams per mile, by 1972, 3.0 grams per mile and by 1974, 1.3 grams per mile. The 1974 level corresponds, for an average car, to about 340 parts per million (ppm) nitric oxide (22).

II. INTRODUCTION

Although high temperature nitric oxide kinetics have been studied extensively in furnace and shock tube experiments, and the substantial qualitative validity of the Zeldovich chain mechanism as applied to spark ignition engines has been established (12, 13), the details of nitric oxide formation and decomposition in engines are still, to a degree, unclear. Shock tube and furnace experiments provide a desirable environment for research in that the state and species distribution of the reacting gas are well defined with time. This is not the case with a spark ignition engine. Strong temperature and concentration gradients within the combustion chamber, existence of possible hyper-equilibrium states in flames and interference by competing reactions all tend to proscribe direct application of results of shock tube experiments to combustion processes in spark ignition engines. Nitric oxide kinetics have also been studied in stationary flames (28), thereby overcoming, as regards application to spark ignition engines, some of the disadvantages of the shock tube experiments. The problems of state definition and determination of the change of thermodynamic state with both space and time remain, however. In a situation in which departure from chemical equilibrium is virtually certain, accurate determination of the rate at which the thermodynamic state of the gas changes with time is equally as important as the acquisition of precise kinetic data.

There have been relatively few attempts to obtain *in. situ.* time resolved nitric oxide concentration measurements directly, using spark ignition engines. This is substantially attributable to formidable experimental problems. Both LaVoie, et. al. (18) and Newhall (14) have used spectroscopic monitoring techniques, methods in which, typically, acquisition of a signal is considerably less difficult than the unambiguous relation of that signal to some physical quantity, such as NO concentration. Nevertheless, time resolved spectroscopic monitoring techniques are probably the most practical means of acquiring the necessary data (rapid-opening valves have been used, however, to withdraw samples of the reacting gas during the power stroke (29), and results compare reasonably with those of LaVoie, et. al. (18)).

The spark ignition engine itself causes additional experimental problems; cycle-to-cycle variations in peak cylinder pressure (up to 15 percent standard deviation (30)) can introduce an unacceptable degree of data scatter for NO concentration measurements. Transient studies referred to previously (18, 31) have reported problems of excessive cyclic variations in peak pressure which necessitated selective sampling of matching pressure traces.

In spark ignition engines many second order effects, such as spark advance, piston motion during combustion and fall in volumetric efficiency with rpm necessarily complicate interpretation of experimental results. For example, although spark advance has a strong influence on exhaust gas nitric oxide concentration, it does so indirectly; advancing the spark will result in an increase in peak cycle temperature, with a consequent increase in peak equilibrium nitric oxide concentration (22, 32). Since spark advance is usually increased with increasing rpm, the competing decrease in volumetric efficiency with rpm can render assignment of cause-effect relationships difficult.

Additionally, in engines the possible range of such variables as peak compression pressure, rate of expansion and fuel-air ratio is relatively low. For these reasons it was decided to develop a "model" of the combustion-expansion process in an engine in which the essential features of those processes considered relevant to the formation and decomposition of nitric oxide in spark ignition engines were preserved and effects and parameters not directly related to pertinent thermochemical processes were eliminated. An experimental analog device was constructed based on this model.

The subject program also included development of a nitric oxide concentration monitoring technique, based on absorption of ultraviolet light by the (0,0)γ band of nitric oxide. The technique was used to follow nitric oxide concentration a few seconds after combustion. Limited _in._ _situ._ time resolved data have also been acquired.

III. EXPERIMENTAL SPARK IGNITION ENGINE ANALOG DEVICE

A. Design Criteria

In order to develop criteria for the design of a S.I. engine analog device it was necessary to determine the disadvantages peculiar to the spark ignition engine, as regards application to NO concentration measurements.

There is good evidence that the extent of cyclic dispersion of peak pressure and rate of pressure increase in spark ignition engines is a strong function of the motion of the fuel-air charge in the vicinity of the spark plug during the early stages of ignition (30, 33, 34). Quantitative relationships between rate of pressure increase and mixture motion have not yet been determined, but it has been postulated that mixture motion tends to disturb the flame front shape, either locally (through turbulence), or on a larger scale (mixture swirl) and influence indirectly the combustion rate and rate of pressure increase.

Pressure traces obtained by igniting quiescent fuel-air mixtures should be considerably more reproducible than would be the case if the charge were moving. The first of the design criteria, then, stipulates that motion of the charge should be negligibly small in the analog device prior to ignition. Such a system would be considerably more susceptible to detonation, since flame velocity will be reduced as a consequence of gas quiescence. The tendency of the "end gas" to detonate can be reduced, however, by reducing flame path length; for example, by using multiple spark plugs.

There is also evidence that, particularly for lean mixtures, inhomogeneous distribution of fuel and air can effect reproducibility of pressure traces (30). A means must therefore be made available of insuring proper and uniform distribution of fuel within the combustion chamber prior to ignition.

An actual engine is constrained to deliver at least enough useful work to overcome frictional losses. This constraint need not be applied, however, to the design of an analog device.

Independent, experimental parameters should bear more directly on the physical and chemical processes leading to excessive nitric oxide emission from engines than the traditional engine operating parameters (compression ratio, spark advance, etc.).

Finally, the design of the mechanical analog should provide a more convenient means of monitoring pertinent thermochemical processes than does the S.I. engine.

B. Description and Operation of Analog Apparatus

The spark ignition engine analog device consists essentially of a cylindrical, constant volume combustion chamber measuring 3.25 inches in diameter and 1.50 inches high, approximately the general shape and dimension of the combustion chamber in an actual engine (figure 1).

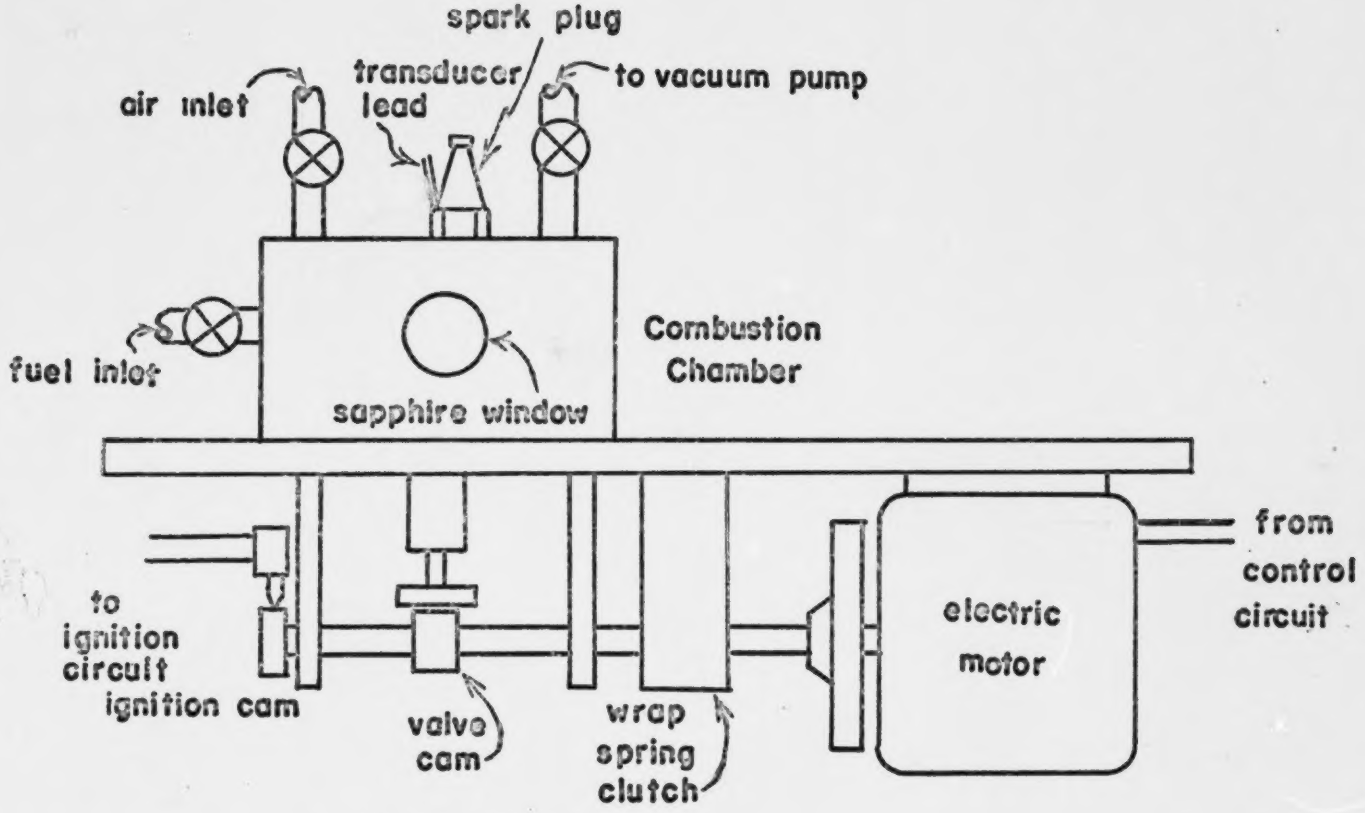
spark plug
air inlet
transducer lead
to vacuum pump
fuel inlet
Combustion Chamber
sapphire window
from control circuit
to ignition circuit
ignition cam
valve cam
wrap spring clutch
electric motor

AUTOMOTIVE ENGINE ANALOG DEVICE

FIGURE 1

A single spark plug was mounted in one end of the combustion chamber, along the axis of symmetry, with a cam-driven poppet valve in the other, also mounted along the axis of symmetry. Drawings and dimensions of the apparatus are presented in Appendix B.

To initiate a test cycle a microsyringe (Hamilton Co., model 725) was used to inject, through a teflon capped ball valve, doubly distilled iso-octane fuel into the evacuated combustion chamber. As a consequence of the low total pressure the fuel vaporized immediately upon injection. The chamber, maintained at a constant, predetermined temperature by a temperature controller (Thermoelectric Co., model 400) was then pressurized with dry air (a schematic of the electrical system of the apparatus is presented in figure 2). A short time interval was provided to allow for complete mixing of fuel and air.

Immediately after ignition combustion proceeded as in an engine, although at a slower rate. After the completion of combustion (determined as that point in time at which combustion chamber pressure was a maximum), the poppet valve opened, allowing some of the product gas to leave the chamber and thereby producing a programmed reduction in combustion chamber pressure with time.

If a control volume is constructed about a portion of the product gas which, at a given time, is inside the chamber, it can be argued that the work done by that gas and its change in state with time will be identical with that of a corresponding volume element in an actual

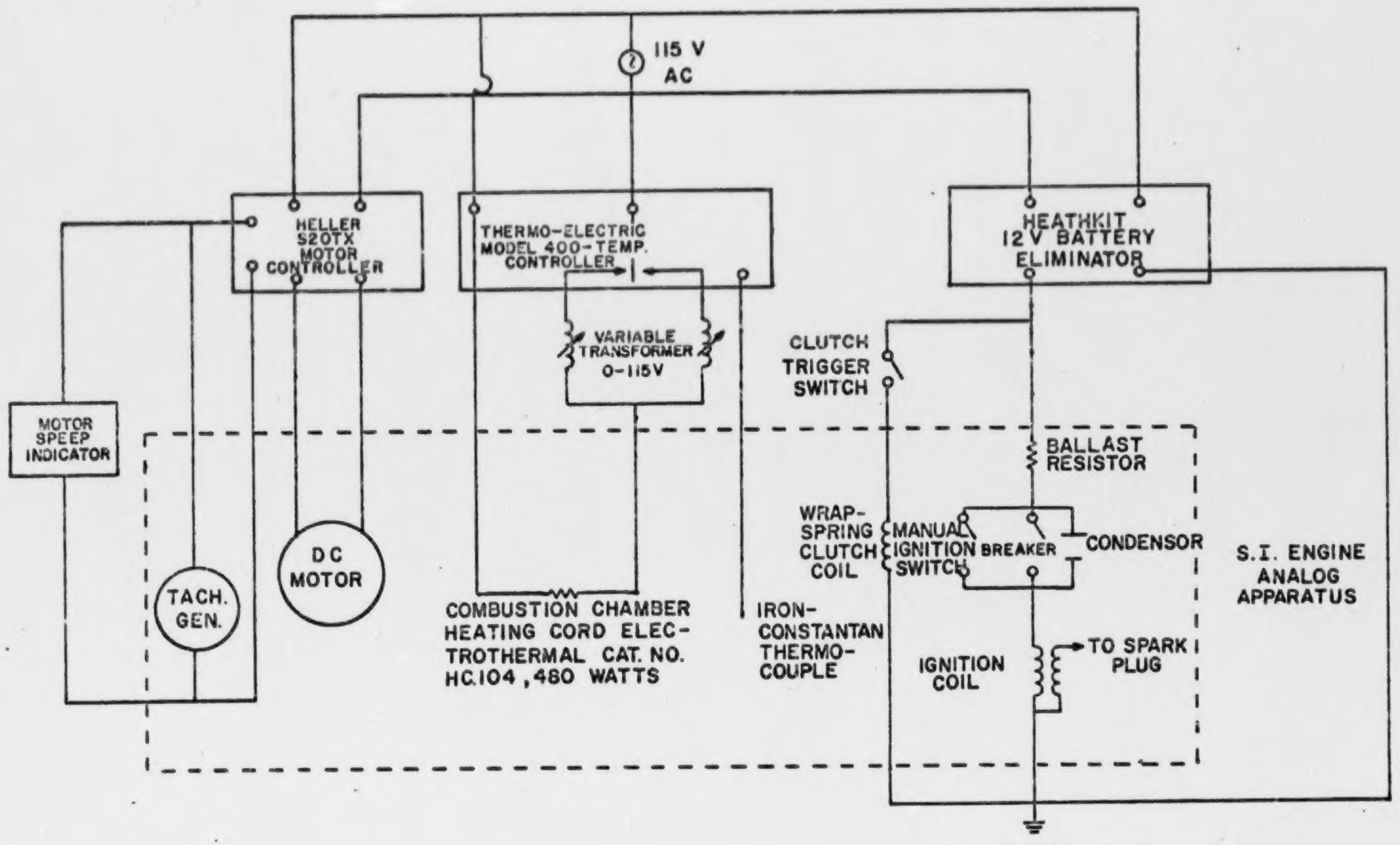
115 V
AC
HELLER
S20TX
MOTOR
CONTROLLER
THERMO-ELECTRIC
MODEL 400-TEMP.
CONTROLLER
HEATHKIT
12 V BATTERY
ELIMINATOR
VARIABLE
TRANSFORMER
0-115V
CLUTCH
TRIGGER
SWITCH
MOTOR
SPEEP
INDICATOR
BALLAST
RESISTOR
WRAP-
SPRING
CLUTCH
COIL
MANUAL
IGNITION
SWITCH
BREAKER
CONDENSOR
S.I. ENGINE
ANALOG
APPARATUS
DC
MOTOR
TACH.
GEN.
COMBUSTION CHAMBER
HEATING CORD ELEC-
TROTHERMAL CAT. NO.
HC.104 ,480 WATTS
IRON-
CONSTANTAN
THERMO-
COUPLE
IGNITION
COIL
TO SPARK
PLUG

ANALOG DEVICE ELECTRICAL SCHEMATIC

FIGURE 2

engine. The only distinction is that in an engine the product gas does work on a moving piston whereas in the analog device the gas within the chamber does work to expel part of the gas mixture.

The poppet valve cam profile necessary to provide the requisite valve area-time relationship (and consequently rate of pressure decrease) was determined by coupling equations for choked flow and isentropic expansion with the perfect gas law. Details of the cam design are provided in Appendix C.

The time interval between ignition and poppet valve opening (poppet valve time delay) was controlled by mounting the poppet valve cam and a conventional ignition breaker point cam assembly on a common shaft which was connected, through a solenoid operated wrap-spring clutch (Precision Specialties, Inc., model SA-500-A), to a continuously operating, speed regulated DC motor (Heller, model S20 TX). As the clutch solenoid engaged the cam shaft rotated for precisely one revolution. Following this the clutch automatically disengaged. Valve time delay was therefore a function of both motor speed and the relative angular position of the two cams. The ignition breaker point assembly could be rotated about the ignition cam providing, in effect, a means of adjusting the relative angular position of the two cams (and thereby the valve time delay). An analysis of poppet valve performance, based on equations developed in Appendix C, indicated that rate of pressure decrease in the chamber was not a strong function of motor rpm (see figure 3). This conclusion was

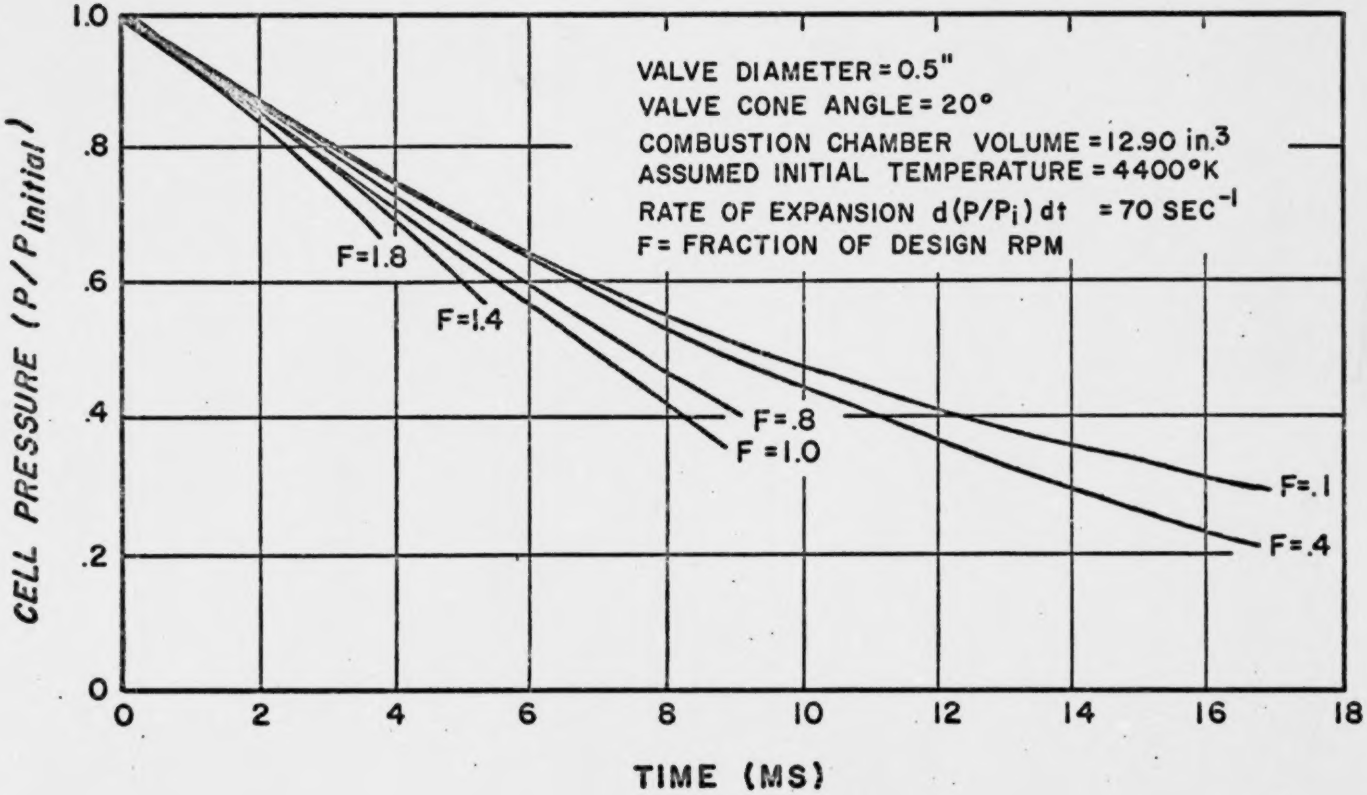

THEORETICAL DEPENDENCE OF EXPANSION RATE ON MOTOR SPEED

FIGURE 3

substantiated experimentally. In practice, since poppet valve time delay varied directly with motor speed, both motor rpm and relative cam position were used to provide the requisite poppet valve time delay.

The process of adjusting time delay generally proceeded as follows: first, for a given operating condition a constant volume combustion pressure trace was obtained in order to determine the time required to complete combustion (maximize chamber pressure). Then the chamber was pressurized with dry air and the clutch engaged. Relative cam position and motor rpm were adjusted so that valve opening, as determined by observing on the oscilloscope pressure trace that point at which cell pressure dropped abruptly, coincided with peak constant volume combustion pressure.

Chamber pressure was monitored using a Kistler model 601A pressure transducer mounted in a modified Champion D-16 spark plug. The output from a Kistler model 504 pressure transducer charge amplifier was displayed on a Tektronix model 564 storage oscilloscope with type 3A3 dual trace differential amplifier and type 2B64 time base plug-in units.

In practice it was difficult to prevent leakage of the fuel-air mixture across the poppet valve seat during the time interval provided for mixing of fuel and air (just prior to ignition). It was found that a good seal could be maintained by lapping the poppet valve into the valve seat. However, after a few firings the seal was lost, due either to erosion of the valve seat or the deposition of solid matter on the valve or valve seat by the high temperature product gas. The effect of this leakage was an arbitrary and random variation in initial cell pressure prior to ignition and a consequent reduction in the reproducibility of pressure traces during combustion. The problem was solved by raising exhaust manifold pressure to coincide with combustion chamber pressure prior to ignition. The combustion chamber discharge rate during expansion was not affected by changes in back pressure as long as exit flow was choked at the poppet valve. Under operating conditions flow remained choked during the first half of the expansion, after which, it is believed, important chemical processes had ceased. A schematic of the analog device is presented in figure 4.

C. Performance of the S.I. Engine Analog Device

In order to obtain representative values for pertinent operating parameters, to provide a basis for the design of the analog device, a variable compression ratio CFR spark ignition research engine was instrumented for the acquisition of pressure histories during the power stroke. Typical examples of maximum combustion pressure, maximum motored chamber pressure, and the normalized rate of expansion were obtained for different engine speeds and compression ratios. The results are presented in figures 5 and 6. Optimum spark advance was used in all cases. No means were available for accurately

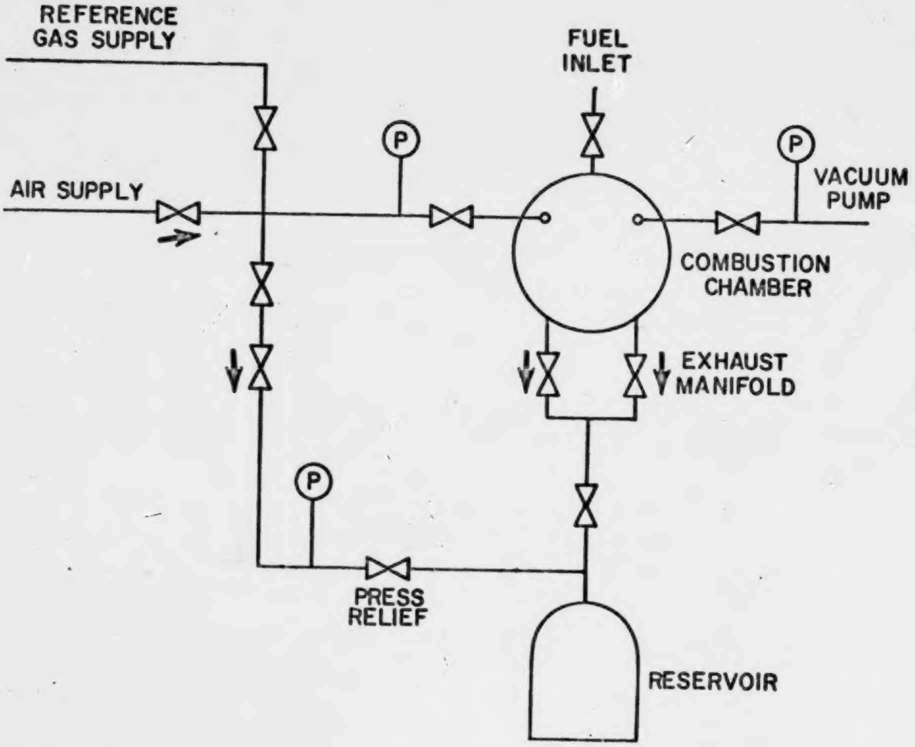
REFERENCE GAS SUPPLY
FUEL INLET
P
P
VACUUM PUMP
AIR SUPPLY
COMBUSTION CHAMBER
EXHAUST MANIFOLD
P
PRESS RELIEF
RESERVOIR

S.I. ENGINE ANALOG DEVICE PLUMBING SCHEMATIC

FIGURE 4

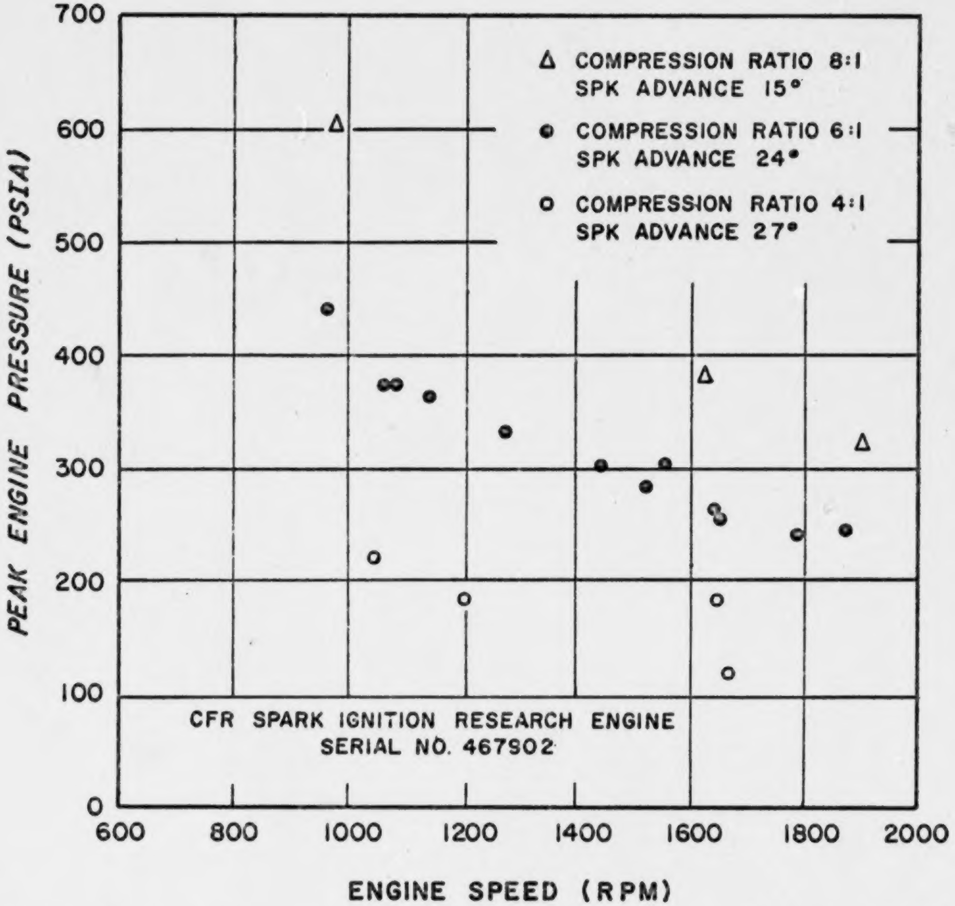

PEAK S.I. ENGINE PRESSURE AS A FUNCTION OF ENGINE SPEED

FIGURE 5

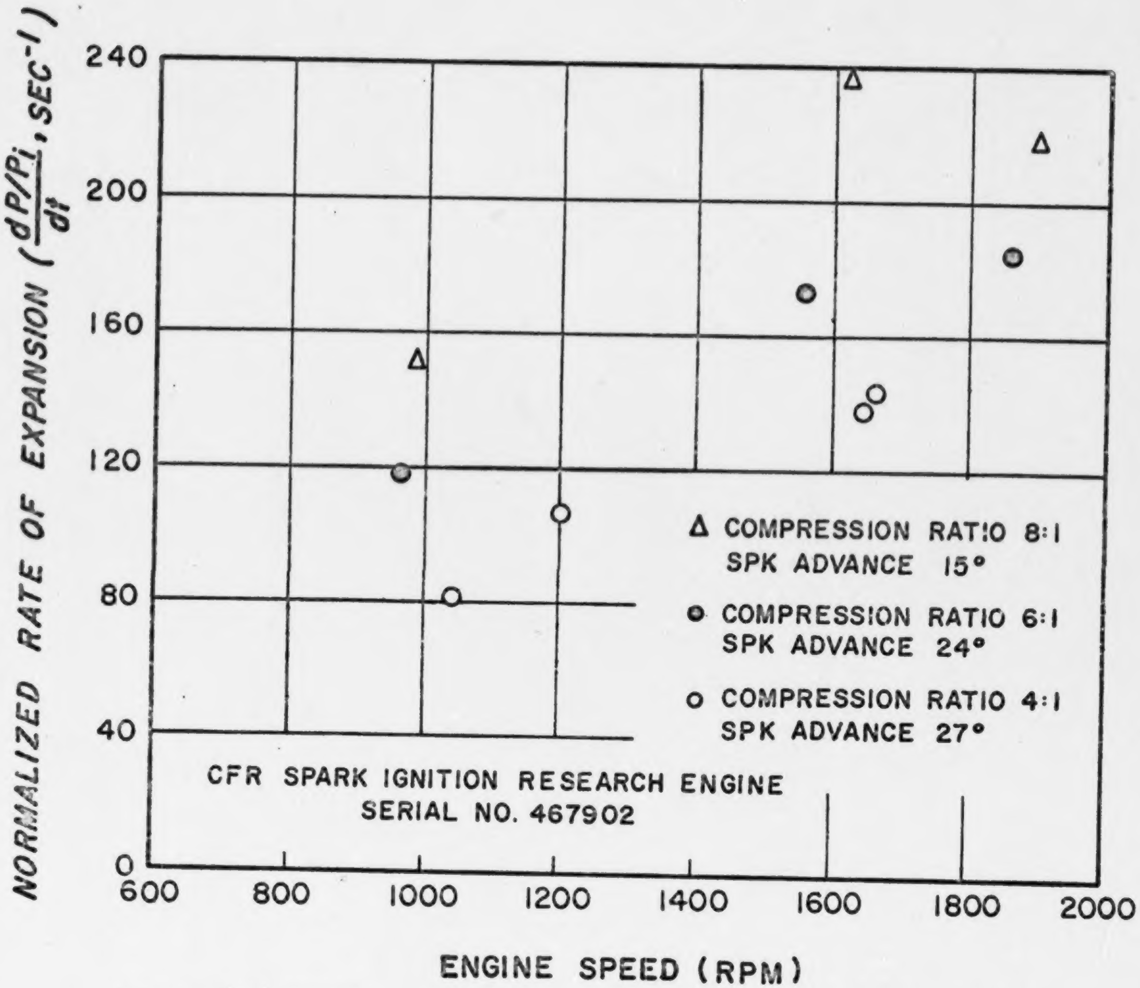

PEAK S.I. ENGINE EXPANSION RATE AS A FUNCTION OF ENGINE SPEED

FIGURE 6

monitoring fuel-air ratio, but slightly rich mixtures were always used, as evidenced by the maximization of peak chamber pressure with changes in fuel-air ratio. Normalized rate of expansion ranged from about 80 to 240 $\sec^{-1}$. Peak combustion pressures ranged from 115 to 600 psia, and maximum motored pressure ranged from 65 to 190 psia.

Analog device pressure traces were obtained with and without expansion of the product gas after combustion at inital pressures between 25 and 125 psia and initial temperatures ranging from 250 to 450°F. Equivalence ratio, ϕ, (ratio of fuel actually added to stoichiemetric fuel required) ranged from 0.8 to 1.2. No detonation was observed in any of the runs.

Oscillographs are presented in figure 7 which compare the superposition of two pressure traces obtained with the analog device (by burning at constant volume and by expanding the gas at a programmed rate after peak pressure), with two successive pressure traces obtained using a CFR research engine. Pressure traces obtained with the analog device are typically much more reproducible than those obtained with an engine. The lower rate of pressure rise in the analog reflects the lower combustion rates and flame speeds resulting from a lack of gas turbulence, as well as a longer flame path length, as compared to an actual engine.

Rate of expansion is also somewhat lower than would be expected in an engine. Maximum rate of expansion is limited by the mechanical

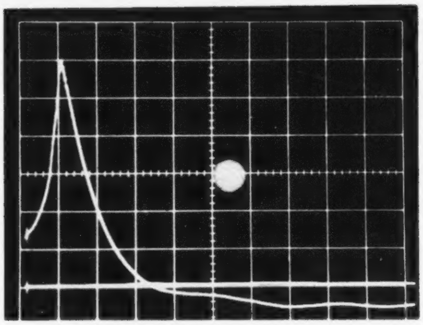

8:1 COMPRESSION RATIO
980 RPM
100 psi/div
5 ms/div

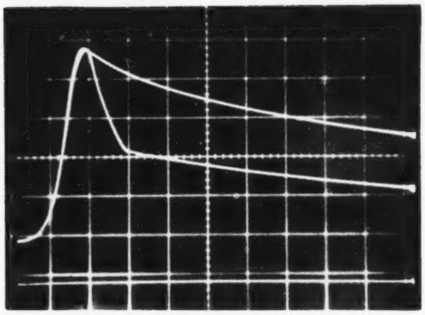

INITIAL TEMPERATURE: 350°F
INITIAL PRESSURE: 125 psia
EQUIVALENCE RATIO: 1.1

100 psi/div
20 ms/div

Note: Analog device pressure traces represent superposition of constant volume and expansion runs

COMPARISON OF PRESSURE TRACES OBTAINED
WITH S.I. ENGINE AND THE ANALOG DEVICE

FIGURE 7

design of the apparatus; the practical limit is imposed by the inability of the flat-face cam follower to follow the abrupt changes in cam profile required to achieve higher expansion rates. Maximum rate of expansion could be increased by using another type of cam-follower assembly, and by installing a larger camshaft clutch. It will be shown, however, that this is not necessary since the slight difference in the rates of expansion characteristic of S.I. engines and the analog device (typically a factor of four) does not have a significant influence on those processes which lead to "freezing" of nitric oxide in the product gas during, or after, combustion.

The abrupt change in slope of the analog device pressure trace which can be observed during expansion is attributable to poppet valve closure.

Figure 8 presents a series of typical pressure traces obtained with the analog device. Superposition of constant volume and expansion runs provides an estimate of the degree of reproducibility of which the apparatus is capable. Reproducibility is generally excellent for rich, stoichiometric and moderately lean mixtures. For extremely lean mixtures however, as the limits of ignition are approached, a random variation in the rate of pressure rise and peak measured pressure can be observed. Interpretation of this effect is speculative; it is possible that errors in metering of fuel are responsible, however microsyringes of different capacities were used in these experiments. A small syringe, operating near maximum

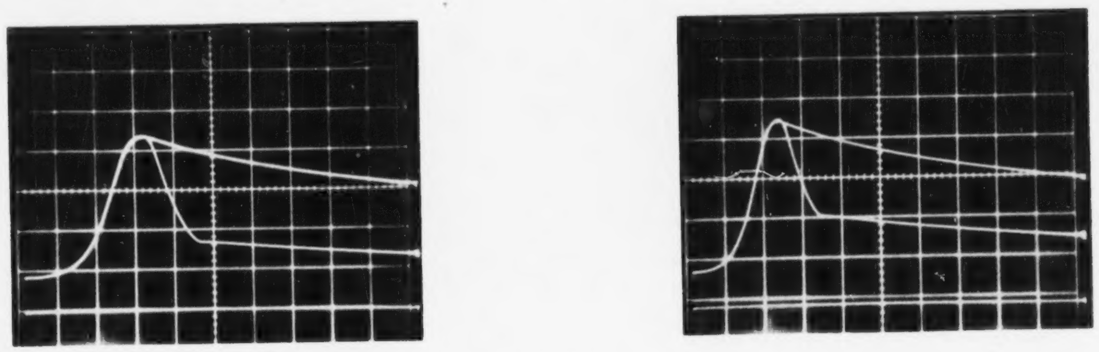

EQUIVALENCE RATIO: 0.88

20 ms/div
100 psi/div

EQUIVALENCE RATIO: 0.98

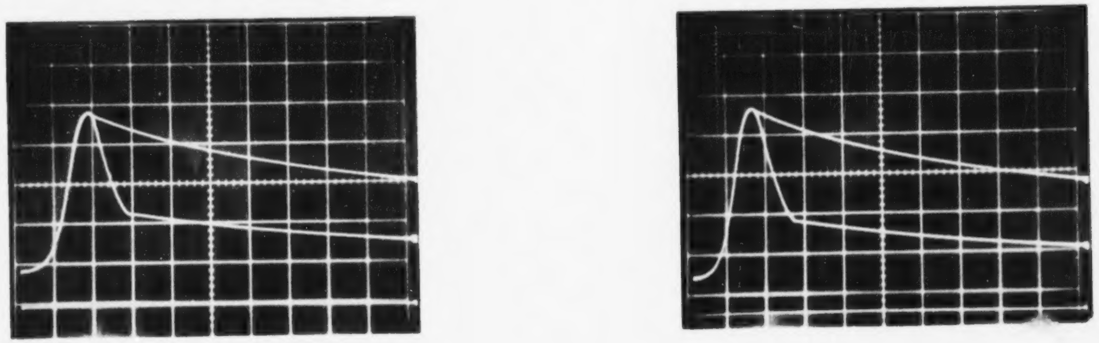

EQUIVALENCE RATIO: 1.08

INITIAL TEMPERATURE: 350^{o}F
INITIAL PRESSURE: 100 psia

EQUIVALENCE RATIO: 1.18

Note: Pressure traces represent superposition of constant volume and expansion runs

TYPICAL ANALOG DEVICE PRESSURE HISTORIES

FIGURE 8

capacity, should be more capable of precise metering of fuel than a larger syringe operating near minimum capacity. When possible two syringes of different sizes were used in successive identical runs with no discernible difference in results. There is evidence that inhomogeneity of the fuel-air mixture can, with lean mixtures, result in cyclic variation in rate of pressure rise and peak pressure (30).

D. Evaluation of the S.I. Engine Analog Device

As far as can be determined from combustion gas pressure traces, it appears that the S.I. engine analog device is a reasonable alternative, for research purposes, to the spark ignition engine. However, the utility of the device can best be established by determining how well it meets the initial design criteria.

Reproducibility of peak combustion pressure and rate of pressure rise was always far in excess of that possible with an engine. Cyclic variations were discernible only for very lean mixtures, near the limits of ignition. The first two design criteria (gas quiescence and fuel-air homogeneity) were stipulated with the intent of reducing cyclic pressure variations. Although it is impossible to determine the degree of gas quiescence or inhomogeneity, the reproducibility of pressure traces is readily determined, hence the analog device satisfies at least the intent of the first two design criteria.

The third criterion, that the range of operation of the device need not be impaired by the necessity of performing useful work, was easily met. Rates of expansion ranged from zero to something less than that possible with an engine.

The fourth criterion was also easily satisfied. Experimental operating parameters such as initial temperature, initial pressure, equivalence ratio and rate of expansion bear more directly on important chemical processes than do corresponding operating parameters in engines (spark advance, compression ratio, rpm, etc.).

There was a possibility that the pressure waves generated as a consequence of the abrupt opening of the poppet valve after combustion could interfere with and alter the chemical processes leading to nitric oxide formation. A brief review of the literature of pressure transients in closed vessels consequent to the rapid expansion of the contained gases did not provide data at conditions typical of the analog device (usually initial pressures were much lower, and rates of expansion much higher). Extrapolation of data which were available indicated that the effect of pressure discontinuities in the analog device should be negligibly small (35).

Analysis of analog device combustion pressure traces revealed no evidence of wave action within the combustion chamber. The time response of the pressure transducer assembly was sufficient to record such transients.

IV. NITRIC OXIDE ULTRAVIOLET ABSORPTION MONITORING TECHNIQUE

A. General

A nitric oxide exhaust gas concentration monitoring technique was developed in which the spectral absorbance of the combustion product gas at a particular wavelength was related, a few seconds after the completion of combustion, directly to the concentration of nitric oxide within the gas.

B. The Electronic Energy States of the Nitric Oxide Molecule.

The nitric oxide molecule is a diatomic, polar molecule which possesses emission and absorption bands in both the infrared and ultraviolet regions of the electromagnetic spectrum (36, 37, 38). The numerous electronic energy states of the molecule have been studied extensively (9, 36, 37). The ground electronic state is a $X^2\Pi$ and the first excited an $A^2\Sigma^+$ state. The γ band system of the molecule corresponds to a transition between these two states. Bands resulting from transitions between the ground and the next excited state ($B^2\Pi$) are called β bands, transitions from ground to the third excited state ($C^2\Sigma^+$) characterize the δ band system, and the ϵ band system represents transitions between ground and the $D^2\Sigma^+$ state. An energy level diagram for the ground and some pertinent excited electronic states is presented in figure 9. Applicable potential curves appear in reference 36.

The bands in a particular band system which appear in either

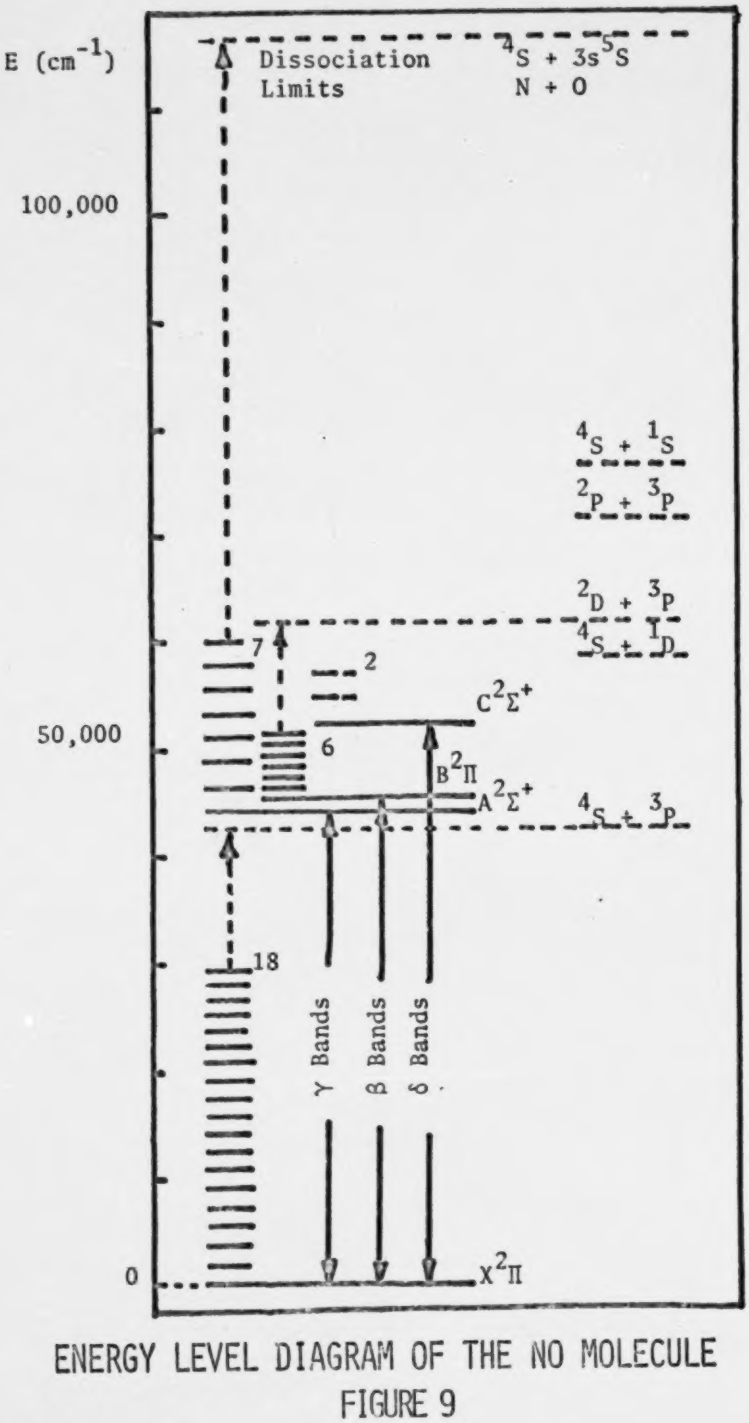
E (cm^{-1})
100,000
50,000
0
Dissociation Limits
$^4S + 3s\,^5S$
N + O
$^4S + {}^1S$
$^2P + {}^3P$
$^2D + {}^3P$
$^4S + {}^1D$
$^4S + {}^3P$
7
2
6
18
$C^2\Sigma^+$
$B^2\Pi$
$A^2\Sigma^+$
$X^2\Pi$
γ Bands
β Bands
δ Bands

ENERGY LEVEL DIAGRAM OF THE NO MOLECULE
FIGURE 9

emission or absorption depend upon the relative population distribution of the vibrational states in the ground electronic state (a function of the thermodynamic temperature, provided the system is in thermodynamic equilibrium). At low temperatures virtually all nitric oxide molecules are in both electronic and vibrational ground states, therefore any electronic energy transitions at low temperature will have to originate from the ground vibrational of the ground electronic state (thereby precluding observable emission) (39, 40). In absorption then, at low temperatures (0,0), (1,0), (2,0), etc. bands can be observed in most systems (corresponding to transitions between $v'' = 0$ of the $X^2\Pi$ ground state, and $v' = 0,1,2,\ldots$ of the respective excited electronic state). Since transitions from the ground electronic and vibrational states to higher electronic and vibrational states involve progressively higher changes in energy, these series will always proceed toward shorter wave lengths. Thus the (0,0) bands of the γ and δ systems appear at about 2265 and 1910 Å, respectively (36). Within a band system transitions from the ground state to higher vibrational levels of excited electronic states also involve progressively higher changes in energy level. Transitions from excited vibrational states of the ground electronic state involve smaller energy changes however, and so these progressions extend towards the red. For example, in the γ system the (0,1), (0,2) and (0,3) bands appear at high temperature at 2370.2, 2478.7 and 2595.7 Å, respectively (36). At low temperatures only the (0,0) band can be observed.

Above 1900 Å, at room temperature, all bands are discrete and identifiable. Below 1900 Å there is considerable overlap, rendering classification difficult. There is also some evidence of predissociation (41). Below 1500 Å absorption continua have been observed.

The choice of a particular band within this series of systems depends upon the adequacy of the signal (absorbance), the presence of potential interfering species, and the characteristics of available light sources, detectors and window materials at the prescribed wavelength.

C. Selection of an Absorption Band.

1. Signal Level.

It was desirable to select a band which would provide, under conditions typical of this experimental work, an absorbance (defined as one minus the ratio of intensity of monochromatic radiation before and after absorption, $1-{}^{I\nu}/I\nu_o$) which ranged between .2 and .8. In order to obtain an approximation of the required absorption coefficient, a simple Beer-Lambert relation was assumed (37).

$$\alpha_\nu = 1-{}^{I\nu}/I\nu_o = 1-e^{-k_\nu \ell'}$$

Where α_ν is the spectral absorbance of the gas

k_ν is the spectral absorption coefficient

ℓ' is the optical path length corrected to STP

Then, keeping the optical density constant,

$$P_{NOSTP}\,\ell' = P_{NO}\,\ell$$

$$P_{NO} = P\,X_{NO}/RT$$

$$\ell' = (P/P_{STP})\,(T_{STP}/T)\,X_{NO}\ell$$

Where P_{NO} is the partial density of nitric oxide

P is the total gas pressure

ℓ is the actual optical path length

X_{NO} is the nitric oxide concentration

T is the gas temperature

Typically, $P = 100$psia

$X_{NO} = 3500$ PPM

$T = 810^{o}R$

and $\ell = 3.25$ inches

If these values are substituted in equations (5)

Then, for $\alpha_{\nu} = .2$, $k_{\nu} = 1.77\ cm^{-1}$

for $\alpha_{\nu} = .8$, $k_{\nu} = 12.8\ cm^{-1}$

The selected band therefore, should have an absorption coefficient of the order of 10 cm^{-1}. At low temperatures the (0,0), (1,0), (2,0), (3,0) and (4,0) bands of the γ system, as well as the (0,0) band of the δ system all fall within this range (40).

2. Windows and Lens Materials.

Considering the nature of the environment to which the combustion chamber windows will be exposed, physical properties of the window material are equally as important as optical properties.

Many ultraviolet transmitting materials are available (42, 43). For example, the lithium, magnesium, calcium and sodium flourides will transmit U.V. radiation to 1200-1300 Å. However, the physical properties of all these materials is quite poor. Lithium and sodium flouride are extremely hygroscopic, an undesirable feature considering the quantity of water vapor present in the combustion product gas, and are susceptible to scratching. Calcium flouride is known to soften, and reacts with atmospheric moisture above 600°C. Magnesium flouride also undergoes a thermal reaction with water above 500°C, and is sensitive to thermal shock. In fact there are only two materials available with excellent physical properties; Sapphire ($A\ell_2O_3$) and U.V. grade quartz (SiO_2). Neither material is soluble in water, both are extremely hard and are essentially chemically inert over a wide temperature range. Optical properties are adequate; the useful U.V. transmission of U.V. grade sapphire extends to 1450 Å, that of quartz to 1850 Å. Linde synthetic U.V. grade sapphire was chosen as a window material. Stress calculations are presented in Appendix D.

3. Ultraviolet Radiation Sources.

A continuous source of U.V. radiation was required in order that change in signal strength with wavelength due to absorption by nitric oxide could be easily distinguished from background emission.

The simplest and the most convenient source of continuous radiation in the U.V. is the high pressure electric arc lamp (44).

Emission is approximately thermal, corresponding to color temperatures between 3500 and 8000°K. If an arc is discharged through a gas such as xenon at high pressure, overlap of broadened emission lines results, in the U.V., in approximately continuous emission. Color temperatures attained are considerably higher than is possible with the carbon arc (about 6600°K compared to 3840°K) and consequently gas radiance is higher by a factor of about 23 in the near ultraviolet. Useful emission ranges from the near infrared through the visible to beyond 1900 Å. The lamp output is stable within 1 percent over a period of several hours even though operated in still air (no forced cooling is required). A high pressure xenon lamp was therefore chosen as a source of ultraviolet radiation for this work.

4. Ultraviolet Radiation Detectors.

The photomultiplier is the only detector useful in the ultraviolet region of the spectrum. An EMI Electronics, Ltd. model 6256B photomultiplier was used, with an S-13 response which extends, through the use of fused silica windows, to about 1650Å.

5. Interfering Species.

In order that product gas absorbance at a particular wavelength be unambiguously related to the nitric oxide concentration of that gas, it is necessary that nitric oxide be the only constituent of the exhaust gas which absorbs at the given wavelength. Absorption spectra of the paraffins, and CO, CO_2, H_2O, H_2, N_2, NO, NO_2 and O_2 molecules were inspected to determine sources of interference at low temperatures (39, 45). The Schumann-Runge bands of oxygen absorb radiation up to 1800Å (39), however the only molecule inspected which will absorb radiation appreciably in the region between 1900-2500 Å at low temperatures is nitrogen dioxide. Little NO_2 is formed during and immediately after combustion (10, 11). However, if the product gas is allowed to stand at elevated pressures and temperatures the NO present will, under certain conditions, be converted to NO_2 (at 350°F, the equilibrium constant for the reaction $2NO + O_2 \rightarrow 2NO_2$ is about 5.3 x 10^5 atm^{-1} (7)). Since interference by this specie can be appreciable, an estimate of the time available for measurement (before substantial NO_2 formation) after combustion was needed. Considering the reaction,

$$2NO + O_2 \rightarrow 2NO_2 \qquad (1)$$

Using a rate constant $k = 3350\ M^{-2}\ sec^{-1}$ obtained from reference (7),

$$-\frac{dNO}{dt} = 2k\ (NO)^2(O_2) \qquad (2)$$

For lean mixtures the O_2 product gas concentration was approximately constant, and the nitric oxide half life can be given by

$$\tau_{1/2} = \left[2k\ (O_2)(NO_i)\right]^{-1} \qquad (3)$$

$$\text{or } \tau_{1/2} = \left[2k\ X_{O_2}\ X_{NO_i}\right]^{-1} \left(\frac{RT}{P}\right)^2 \quad (4)$$

assuming $T = 350°F$ ($450°K$) and X_{NO_i} = 4000 ppm, the nitric oxide half life ($\tau_{1/2}$) was calculated as a function of the pressure and initial oxygen concentration. Results are presented in figure 10. Data were reasonably consistent with these predictions. The formation of

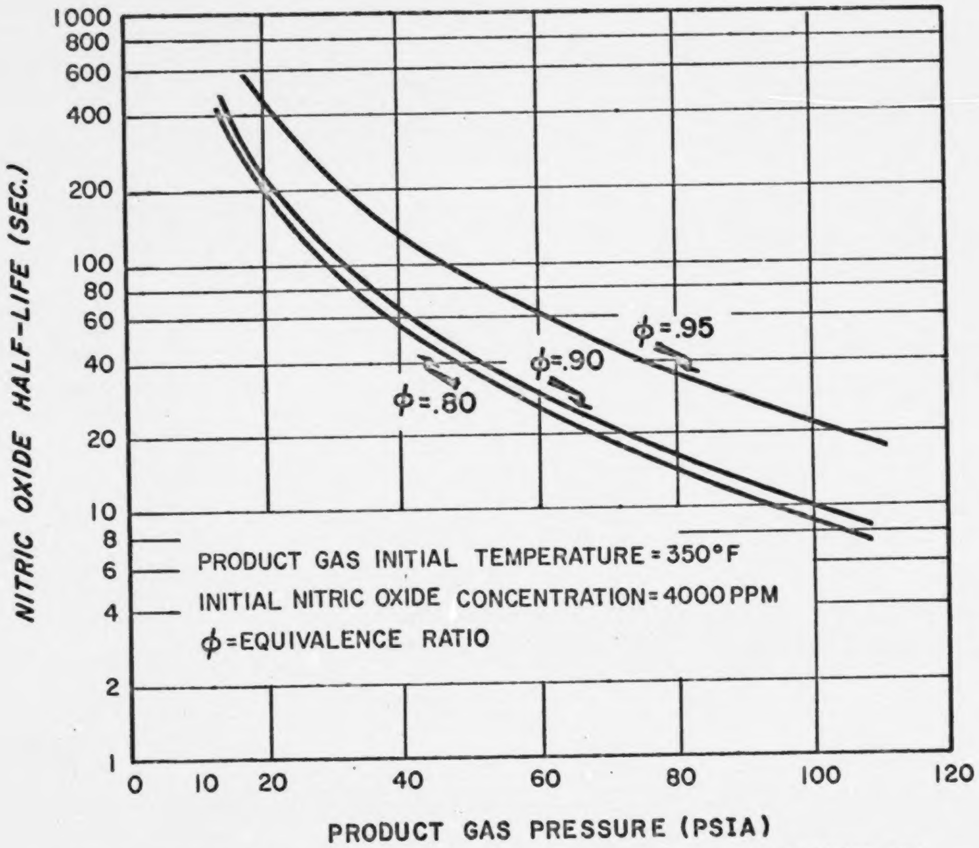

THEORETICAL NITRIC OXIDE HALF-LIFE AS A FUNCTION OF PRODUCT GAS PRESSURE

FIGURE 10

nitrogen dioxide with time was followed after combustion by monitoring product gas spectral absorbance. The product gas acquired the distinct brown color characteristic of nitrogen dioxide concurrently with the increase in spectral absorbance with time.

The principle impediment to the acquisition of product gas nitric oxide concentration at higher pressures was the rapid conversion of NO to NO_2.

6. Discussion

On the basis of the previous considerations it was possible to decide which of the useful absorption bands of nitric oxide (the (0,0), (1,0), (2,0), (3,0), and (4,0) bands of the γ system and the (0,0) band of the δ system) would be most suited to the subject program. Lamp emission, window transmittance and photomultiplier response all fall off with decreasing wavelength. The average spectral absorption coefficient of NO_2 is relatively constant throughout the region between 1900 and 2300 Å (absorbance is not continuous, however, there are strong overlapping bands (39)). For these reasons it was decided to relate spectral absorbance at the nitric oxide band of longest observable wavelength, the (0,0) γ band, to nitric oxide product gas concentration.

D. The (0,0)γ Band of Nitric Oxide.

1. General

The width of any particular band within a system (which is characterized by a given electronic and vibrational transition) depends upon the rotational transitions that occur simultaneously with changes in electronic and vibrational energy levels (37). This rotational fine structure can usually not be seen with moderate resolution monochromators (of the order of 1Å resolution).

The shape of the $(0,0)\gamma$ band (and any other band involving a transition to, or from the ground electronic state) is also influenced by the spin-splitting of the $X^2\Pi$ ground state into $X^2\Pi_{1/2}$ and $X^2\Pi_{3/2}$ states. That is, the two heads of the band correspond to degenerate states distinguished only by the relative orientation of the spin angular momentum (46).

The spectral absorbance at each of the band heads can be related to product gas NO concentration. However, when measurements are limited by the resolution for the monitoring apparatus, as would be the case when an instrument of a few angstroms resolution is used to monitor absorbance of a band which is comprised of many discrete rotational lines, the measured spectral absorption coefficient will not coincide with the actual spectral absorption coefficient (which is an extremely strong function of wavelength), but will represent an average of the actual absorption coefficient over the interval of instrument resolution. As a consequence it may exhibit a fictitious pressure dependence. To determine the influence of instrumental error it was necessary to compare measurements made using the experimental apparatus with published data.

2. The Integrated Absorption Coefficient of the (0,0)γ Band.

One way in which it is possible to determine whether experimental absorption measurements are valid, providing the gas is not optically thick, is to calculate the integrated or absolute absorptivity of the band (37).

The spectral absorbance of the (0,0)γ band was measured as a function of wavelength and the total pressure of a reference gas (which contained 4040 parts per million (PPM) nitric oxide, balance N_2, as determined by the manufacturer's mass spectometric analysis). A schematic of the monitoring apparatus is presented in figure 11. A description of the equipment used, as well as calibration, testing and alignment procedures can be found in Appendix D.

In order to calculate the integrated, or absolute absorbance of the band, the measured band profiles were approximated by triangles, transmittances $(I_{\nu}/I_{\nu o})$ were calculated on the basis of these profiles and the inverse transmittance was plotted as a function of wave number on a semi-log graph. These curves were integrated with a planimeter and the integral of the log of the reciprocal transmittance was plotted as a function of gas optical thickness (the product of absorbing path length and partial pressure of the absorbing gas). The result should have been, if valid absorption measurements were made, a straight line, indicating the equivalency of the measured and actual

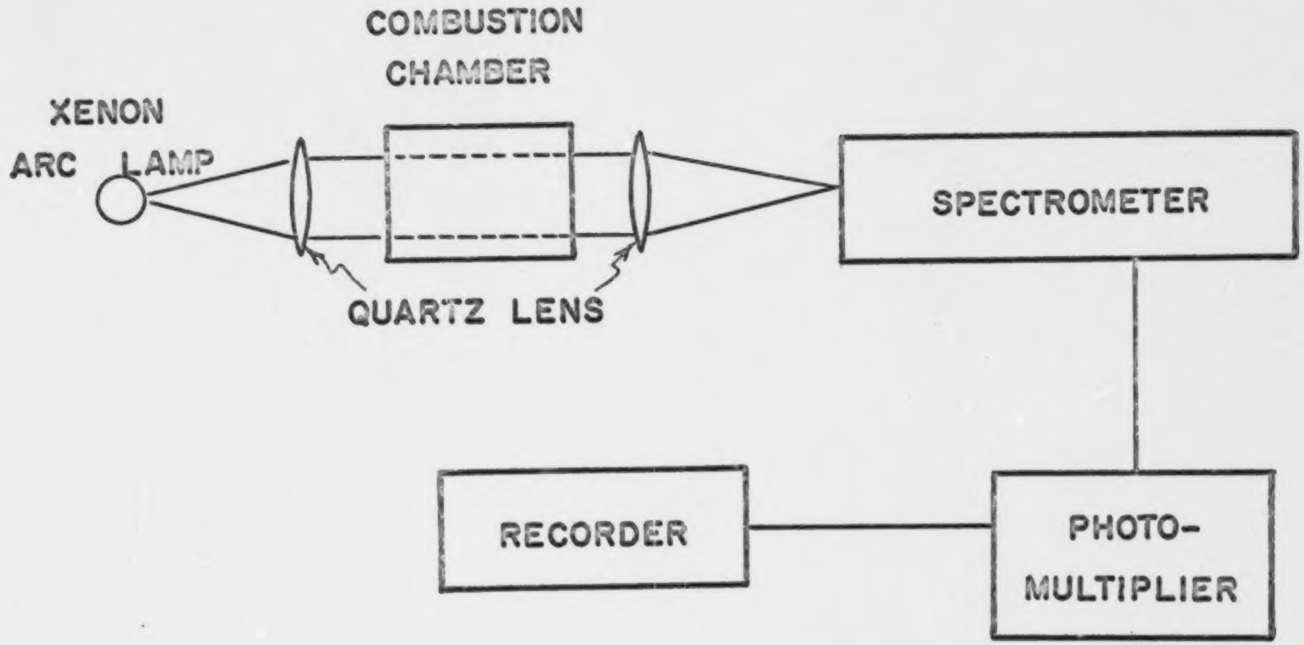
COMBUSTION CHAMBER
XENON ARC LAMP
QUARTZ LENS
SPECTROMETER
RECORDER
PHOTO-MULTIPLIER

STEADY STATE ULTRAVIOLET NITRIC OXIDE
CONCENTRATION MONITORING APPARATUS
FIGURE 11

spectral absorption coefficients (37). The slope of this line is proportional to the f-number, or oscillator strength of the molecule and is invariant with changes in pressure, temperature and concentration. Although values calculated in this work exhibited some curvature the degree of correlation was reasonable, considering the technique used to reduce the data (certainly not a valid procedure if precise spectral data are required), and the resolving power of the monochromator (about 1.6 Å) (see figure 12).

It was concluded that at conditions typical of operating spark ignition engines, gas pressure is sufficiently high to ensure that the rotational lines of the band will overlap (37). This means that the actual spectral absorbance will be a relatively weak function of wavelength, and be closely approximated by absorbance measured with an instrument of a few angstroms resolution.

It should be noted that Penner attempted to broaden the $(0,0)\gamma$ band by adding helium to the test gas, keeping the partial density of nitric oxide constant. No change in the integrated absorption coefficient of the band was detected. In the present work nitrogen was added to the reference gas, with the partial density of nitric oxide maintained constant, and no change in integrated intensity, band shape or peak spectral absorbance was observed. At pressures and temperatures characteristic of this experiment then, the peak spectral absorbance of the $(0,0)\gamma$ NO band is a function only of the partial density of nitric oxide.

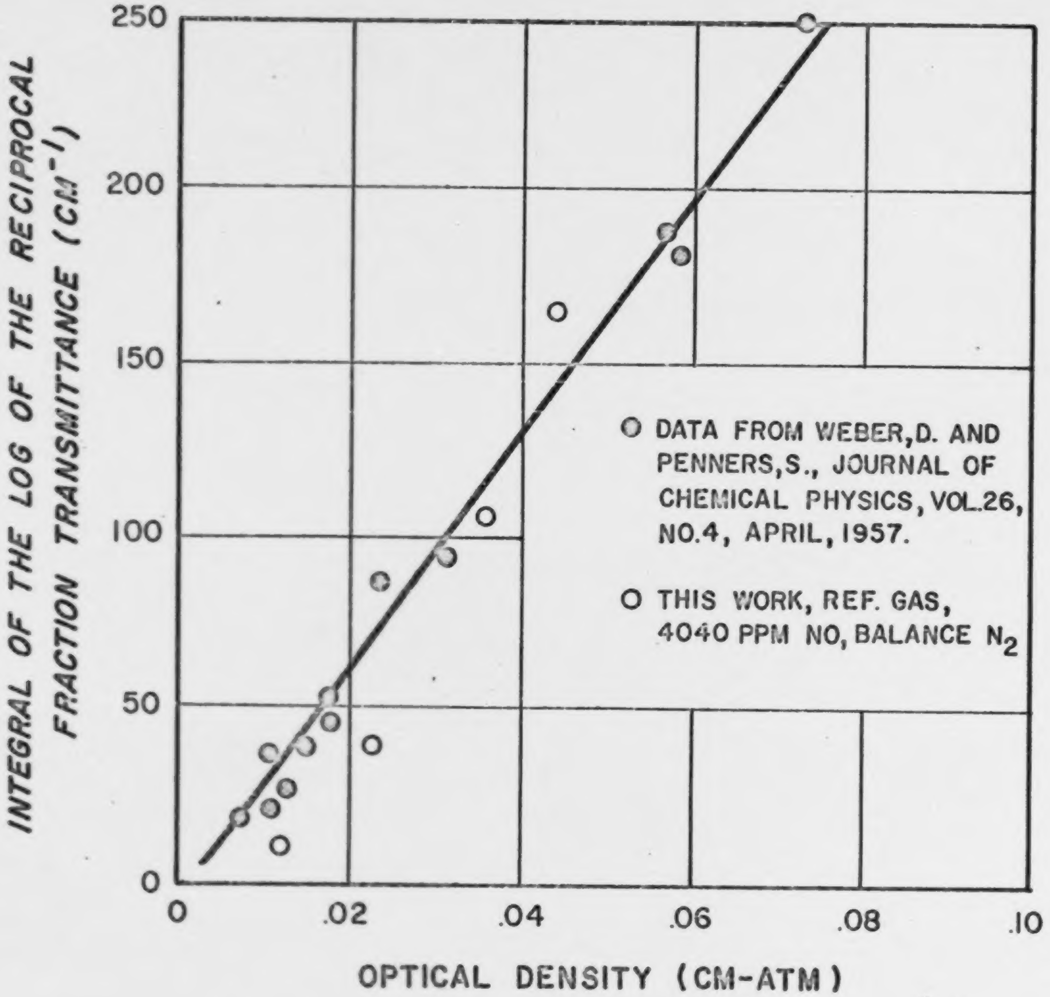

DEPENDENCE OF THE INTEGRAL OF THE LOG OF THE RECIPROCAL FRACTIONAL TRANSMISSION ((0,0) γ BAND) ON NITRIC OXIDE OPTICAL DENSITY

FIGURE 12

3. The Spectral Absorption Coefficient of the (0,0)γ Band.

Figure 13 compares the measured peak spectral absorbance of the reference gas (at the 2262.5Å band head) with theoretical curves which assume a Beer-Lambert relation between absorbance, the absorption coefficient (which is constant) and the equivalent optical path length. Measured and theoretical absorbances are expressed as a function of the partial pressure of nitric oxide; the combustion chamber temperature was maintained constant, at 810°R. The theoretical curve which seems to best fit the data corresponds to a spectral absorption coefficient of about 30 cm^{-1}. Correlation is good at moderately high pressures. However, at lower pressures the measured peak absorbance is considerably less than would be expected on the basis of the Beer-Lambert law. This is almost certainly due to instrumental error since the measured absorbance curve, if extrapolated to zero absorbance, does not intersect the absicca at the origin. At these low pressures the absorption band width is of the order of the instrumental resolution (see Appendix D). Under these conditions a measured peak absorbance would be expected which was lower than actual peak absorbance.

The assumption that the product ($k_\nu \ell'$) is a linear function of the partial density of NO may be, in the present case, an oversimplification. The physical model on which it is based assumes that the process of absorption of radiation by one molecule is unaffected by the presence of other molecules (47). It is not valid when pressure broadening by inert species influences absorption band shape, or when

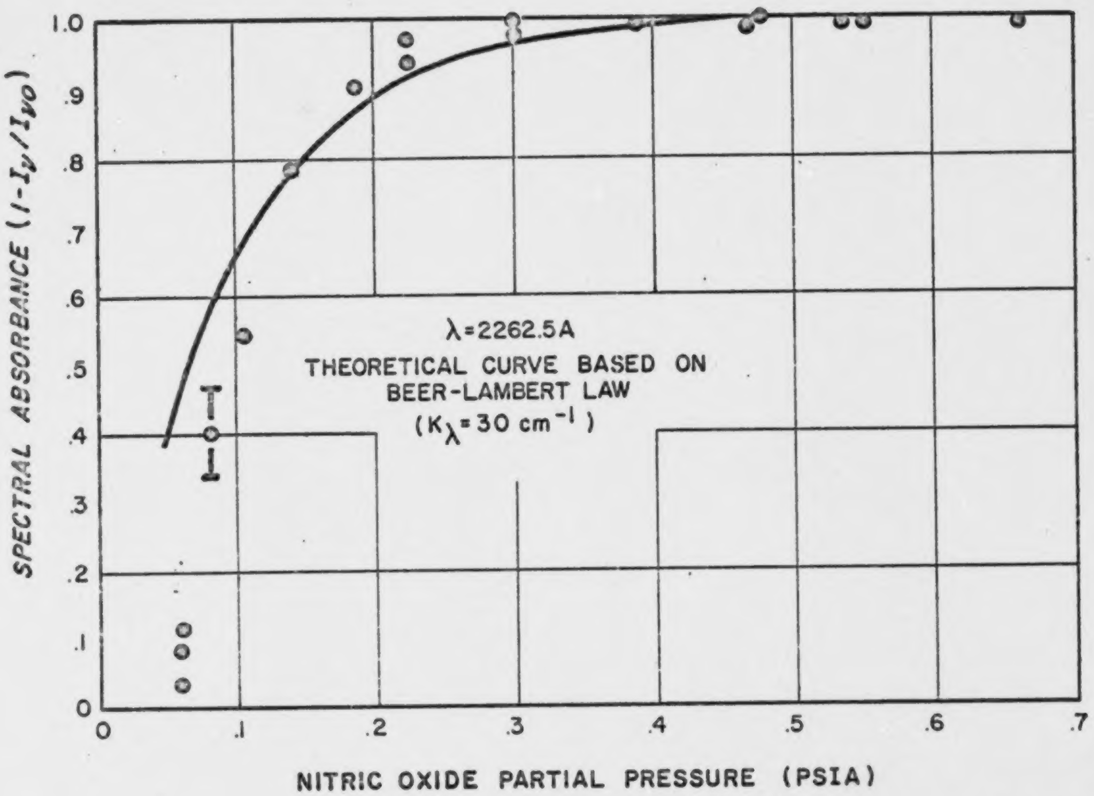

COMPARISON OF THEORETICAL AND MEASURED PEAK SPECTRAL ABSORBANCE OF THE (0,0) γ BAND OF NITRIC OXIDE

FIGURE 13

instrumental resolution is of the order of the absorption band width. Nevertheless, when the log of the measured peak spectral transmittance was plotted versus the optical density the result was a reasonably straight line (the log plot tended to suppress the instrumental errors which were observed at low optical densities) (figure 14). The absorption coefficient calculated from this curve (30 cm^{-1}) was higher than values obatined from the literature (about 6 cm^{-1}). Reported spectral absorption coefficients were, however, invariably obtained with pure nitric oxide at low total pressure, where there is no substantial overlap of rotational lines. These measurements were therefore limited by the resolution of the monitoring equipment, and were intended to be only semi-quantitative (40). Although not directly applicable to the present work (in which, it has been shown, measurements are resolution limited only at low nitric oxide partial pressure) they do provide an estimate of the order of magnitude of the actual spectral absorption coefficient, and as such agree reasonably well.

4. Depopulation of the Ground Electronic State of the NO Molecule.

The absorbance of the product gas corresponding to the (0,0) transition of the γ system of NO is actually a function of the number of the NO molecules in the ground electronic and vibrational states. If a substantial proportion of the NO molecules in the product gas are in an excited electronic or vibrational state, then the spectral absorbance does not measure the total NO population directly. At temperatures of interest, if the system is in thermodynamic equilibrium

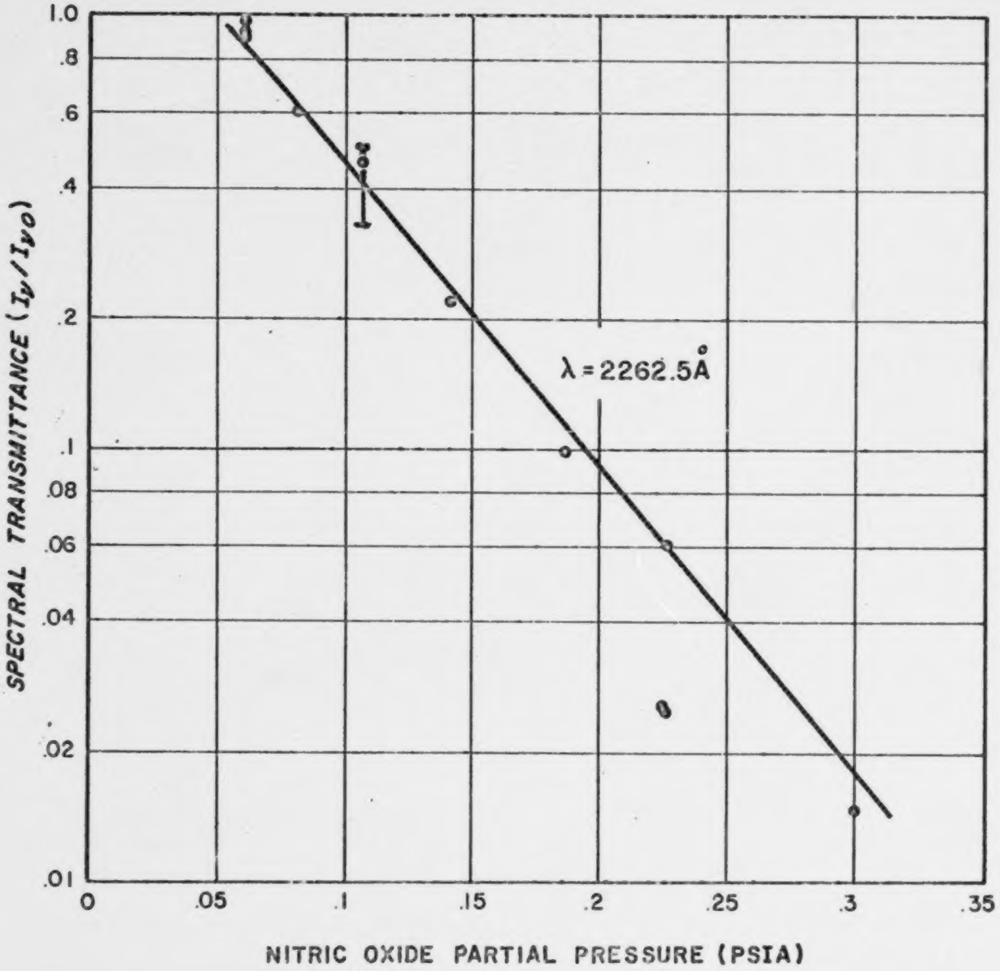

LOG OF THE PEAK MEASURED SPECTRAL TRANSMITTANCE OF THE (0,0) γ BAND OF NO AS A FUNCTION OF THE NITRIC OXIDE PARTIAL PRESSURE

FIGURE 14

all NO molecules will be in the ground vibrational state (36).

The rate of production of electronically excited nitric oxide will be a function of the photon flux into the combustion chamber. In the steady state this will be balanced, in the worst case, by the rate of spontaneous decay of excited NO. There will be, therefore, an equilibrium concentration of electronically excited NO which will depend upon the photon flux into the chamber and the decay time. That is, $\left.\frac{dNO^*}{dt}\right)_{form} = \left.\frac{dNO^*}{dt}\right)_{decay} = k\,[NO^*]$ (5)

Decay times for transitions between the first excited and ground electronic states are of the order of 2 X10^{-7} seconds, so that k is of the order of 0.5×10^{7} sec^{-1} (48). If it is assumed that all photons of proper wavelength which enter the chamber are absorbed (as would be the case for an optically thick gas), then the rate of production of excited NO is equal to the photon flux into the chamber. For the high pressure xenon arc, at 2260Å the power output of the lamp is about 30 milliwatt/100 Å ster or, for a band halfwidth of 10Å, 3mw/ster (44). The focal length of the quartz lens was 100mm., and the diameter of the collimated beam was 18mm. The solid angle which encompasses radiation entering the chamber is then

$$\theta = \frac{\pi}{4}\left(\frac{16^2}{100^2}\right) = .019 \text{ Ster}$$

and the total radiant power into the chamber within the region 2265 ± 5A is

$$P = 3(.019) = .057 \text{ mw} = 5.7 \times 10^{2} \text{ erg/sec}$$

at a wavelength of 2265Å the energy of a photon is

$$E = h\nu = h\ c/\lambda = 8.79 \times 10^{-12}\ \text{erg} \qquad (6)$$

Then the number of photons of proper wavelength entering the chamber per unit time is

$$P/E = 6.553 \times 10^{13}$$

$$\text{and}\ A\ \frac{dNO^*}{d\ t} = 6.553 \times 10^{13}\ \text{sec}^{-1}$$

where A is Avogodro's number, 6.02×10^{23} mole^{-1}

$$\text{then,}\ \frac{dNO^*}{d\ t} = 1.086 \times 10^{-10}\ \text{mole/sec} = kNO^*$$

$$\text{or}\ NO^* = 2.172 \times 10^{-17}\ \text{mole}$$

Using the perfect gas law, for $P = 80$ psia, $T = 810^\circ R$ and $X_{NO} = .004$ the total number of moles of NO in the volume of the collimated beam within the chamber, V, is

$$NO_T = 9.6 \times 10^{-6}\ \text{moles}$$

or the mole fraction of excited nitric oxide is,

$$\frac{NO^*}{NO_T} = \frac{2.172 \times 10^{-17}}{9.6 \times 10^{-6}} = 0\ [10^{-11}]$$

Equilibrium concentrations for different excited electronic states will be of the same order of magnitude since the photon flux and spontaneous decay times are similar to the present case.

One may say, therefore, that virtually all nitric oxide molecules are in the ground electronic state, and absorbance at the $(0,0)\gamma$ band will reflect total product gas concentration of nitric oxide.

E. Experimental Procedure.

1. General.

It was possible to relate combustion product gas concentration of nitric oxide a few seconds after the completion of combustion to the absorbance of the product gas at the $(0,0)\gamma$ band of nitric oxide since it was demonstrated that at low temperatures, and before the formation of NO_2, there were no species present that would interfere with absorption by NO. This was confirmed by comparing spectral scans obtained with the cell evacuated, with the reference gas added at a given pressure, and with the combustion gas present. At wavelengths where NO would not be expected to absorb there was no difference in signal levels between the evacuated, reference gas and product gas scans. Absorption band profiles of the reference gas and product gases were identical.

Since pressure broadening by inert species was determined to be negligible, spectral absorbance was an exclusive function of the partial pressure of nitric oxide, at a given temperature.

2. Calibration.

Reference gas nitric oxide absorption scans were obtained for different total gas pressures before, after and in some cases during each series of experimental runs (figure 15). Calibration curves were then constructed in which reference gas absorbance at and between each of the band heads was plotted versus the nitric oxide partial pressure (figure 16). In this manner a functional relationship was established

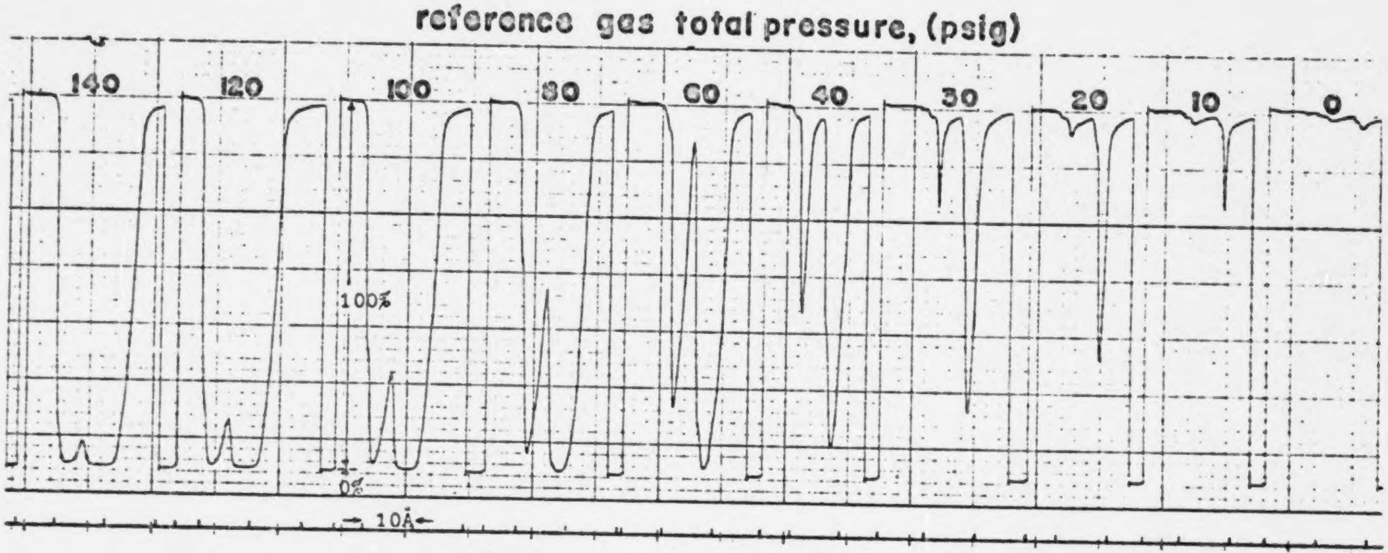

REFERENCE GAS ABSORPTION SCANS OF THE (0,0) γ BAND OF NITRIC OXIDE
FIGURE 15

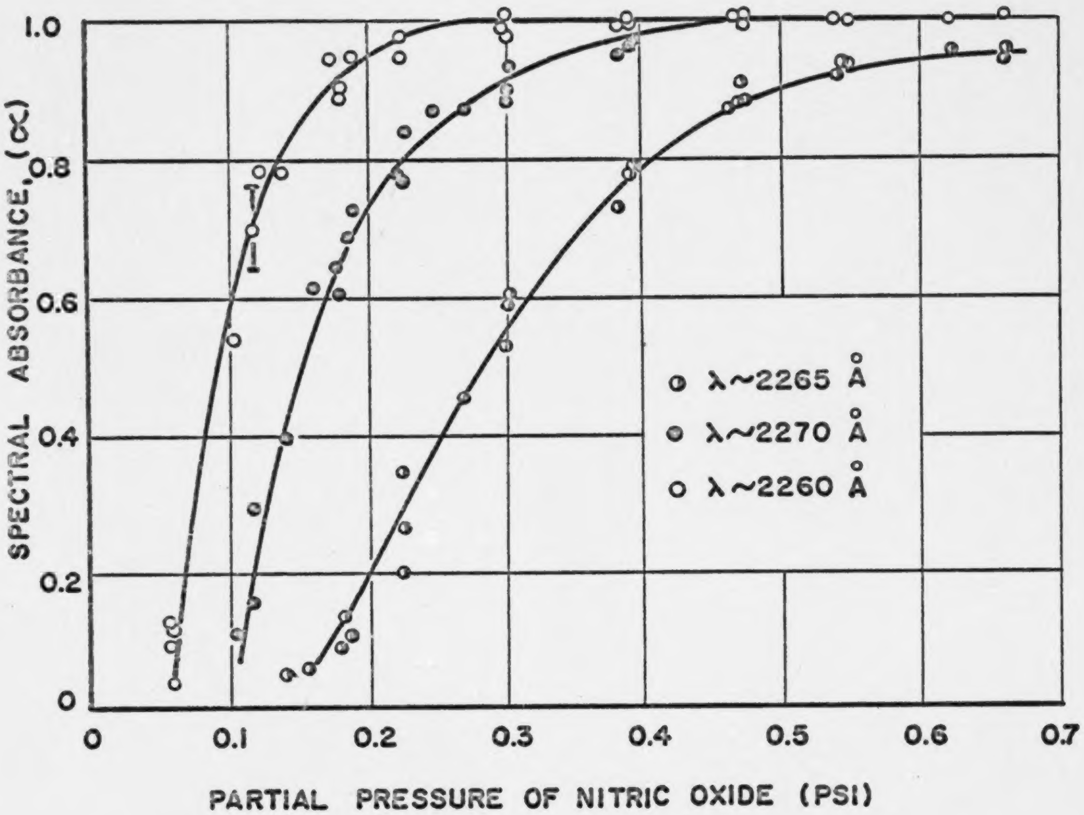

CALIBRATION CURVES FOR THE NITRIC OXIDE ULTRAVIOLET
MONITORING TECHNIQUE

FIGURE 16

between product gas absorbance and nitric oxide partial pressure. Measured product gas absorbance yielded, through the calibration curves, the nitric oxide partial pressure of the product gas. Measurements of the total pressure of the gas following combustion enabled calculation of nitric oxide concentration.

3. NO Concentration Measurements.

Product gas nitric oxide concentration was measured as a function of such parameters as initial pressure, initial temperature, equivalence ratio, and rate of expansion. Figures 17 through 21 present nitric oxide concentration as a function of equivalence ratio for initial pressures ranging (in increments of 25psia) from 25 to 125 psia. The solid curves represent theoretical NO concentrations based on calculations outlined in Appendix E. All reported data were obtained at an initial temperature of 350°F. Figure 22 presents, for stoichiometric conditions, the nitric oxide concentration as a function of initial pressure.

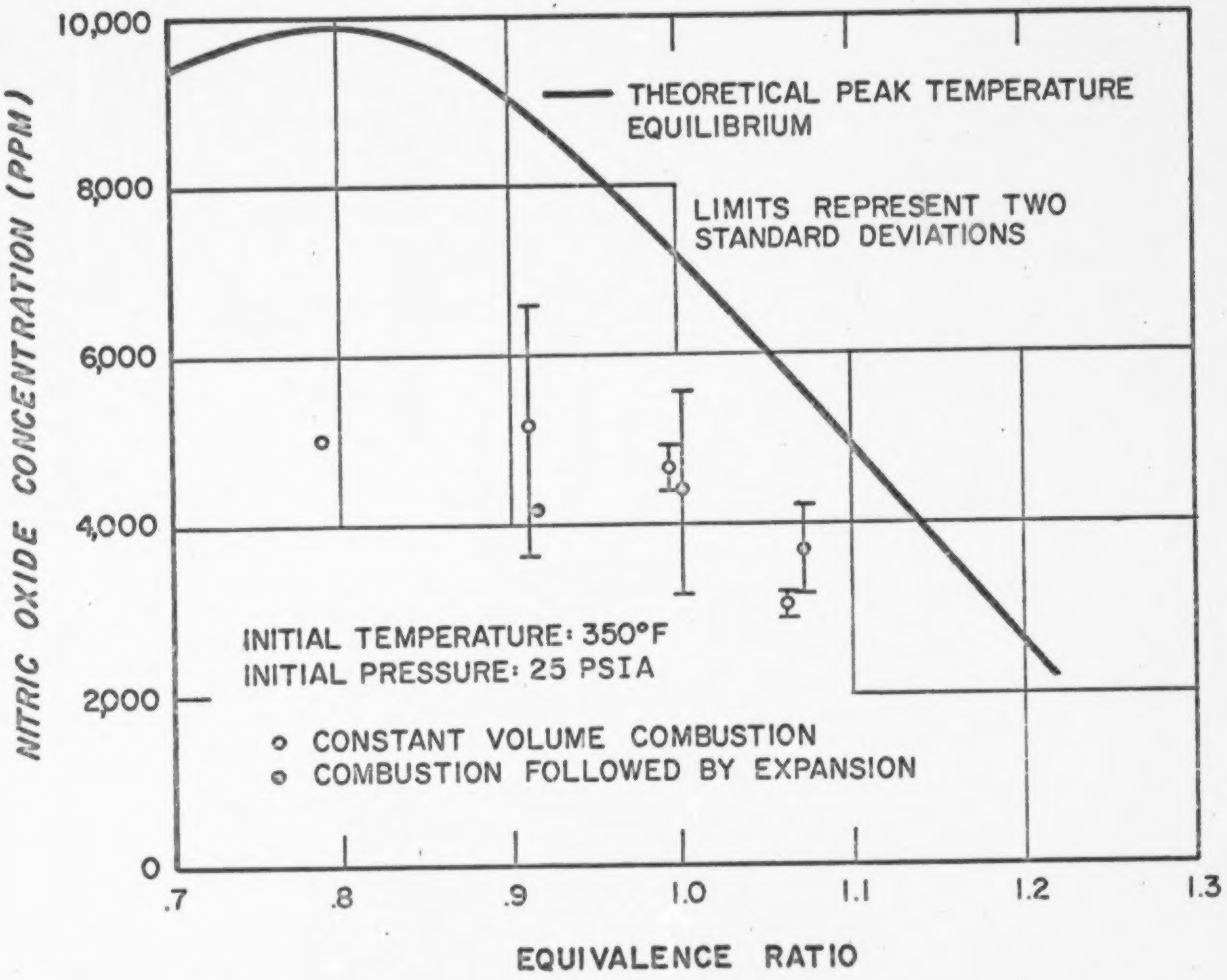

DEPENDENCE OF PRODUCT GAS NITRIC OXIDE CONCENTRATION ON EQUIVALENCE RATIO

FIGURE 17

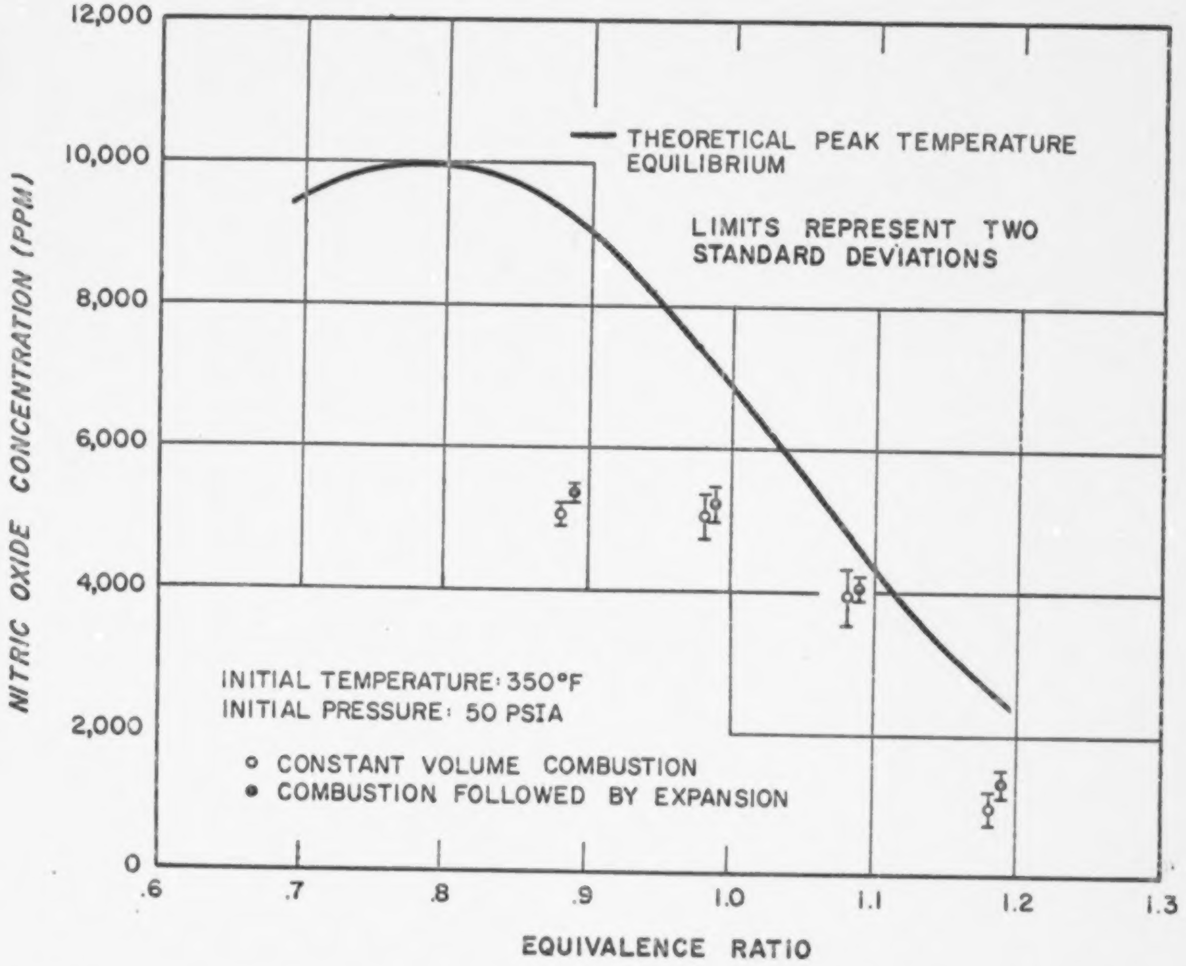

DEPENDENCE OF PRODUCT GAS NITRIC OXIDE CONCENTRATION ON EQUIVALENCE RATIO.

FIGURE 18

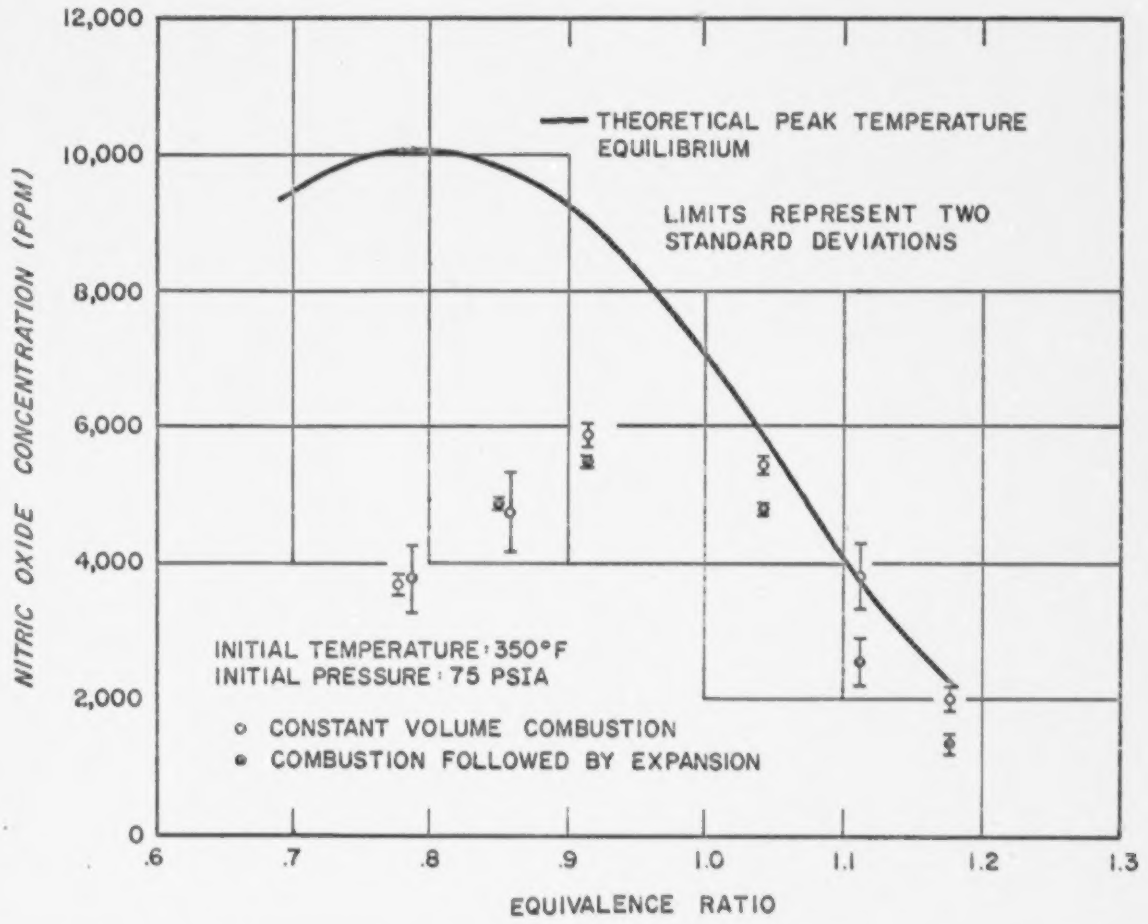

DEPENDENCE OF PRODUCT GAS NITRIC OXIDE CONCENTRATION ON EQUIVALENCE RATIO

FIGURE 19

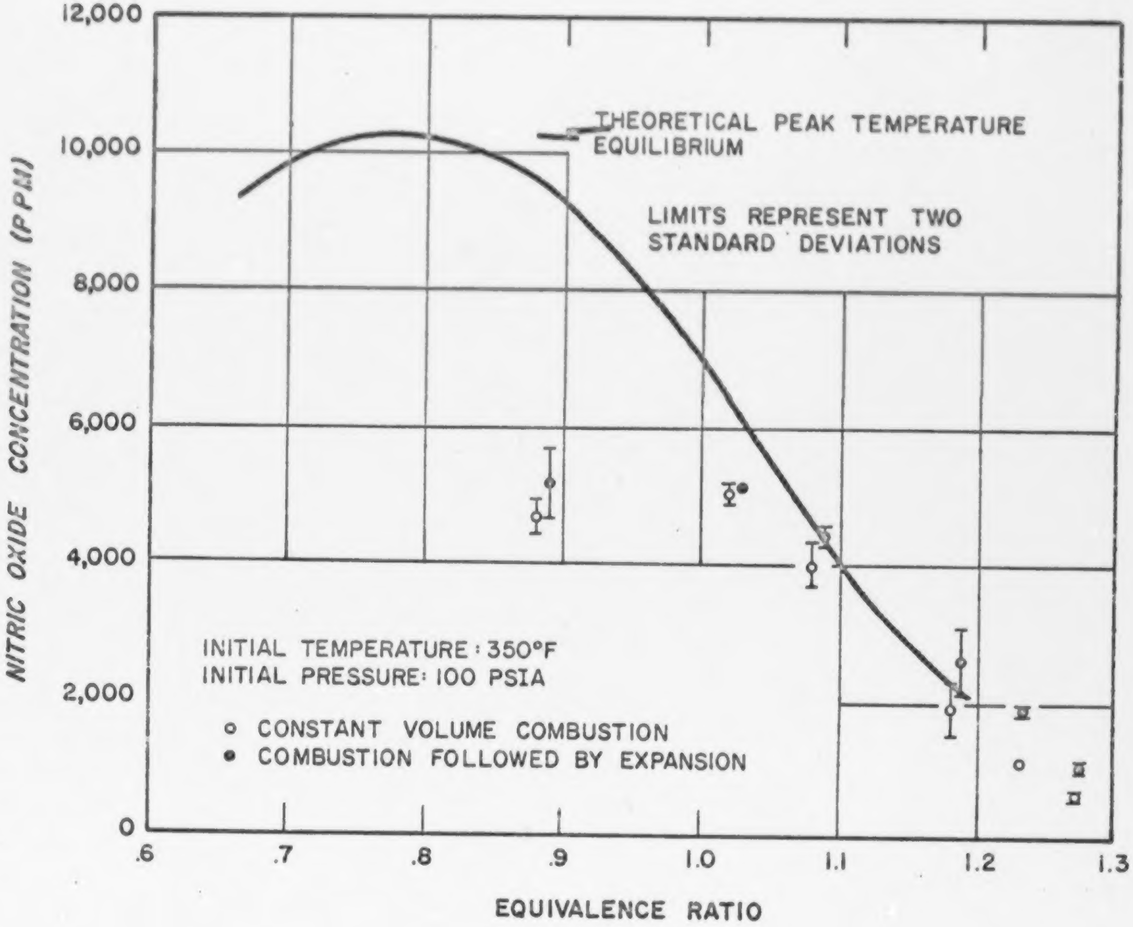

DEPENDENCE OF PRODUCT GAS NITRIC OXIDE CONCENTRATION ON EQUIVALENCE RATIO

FIGURE 20

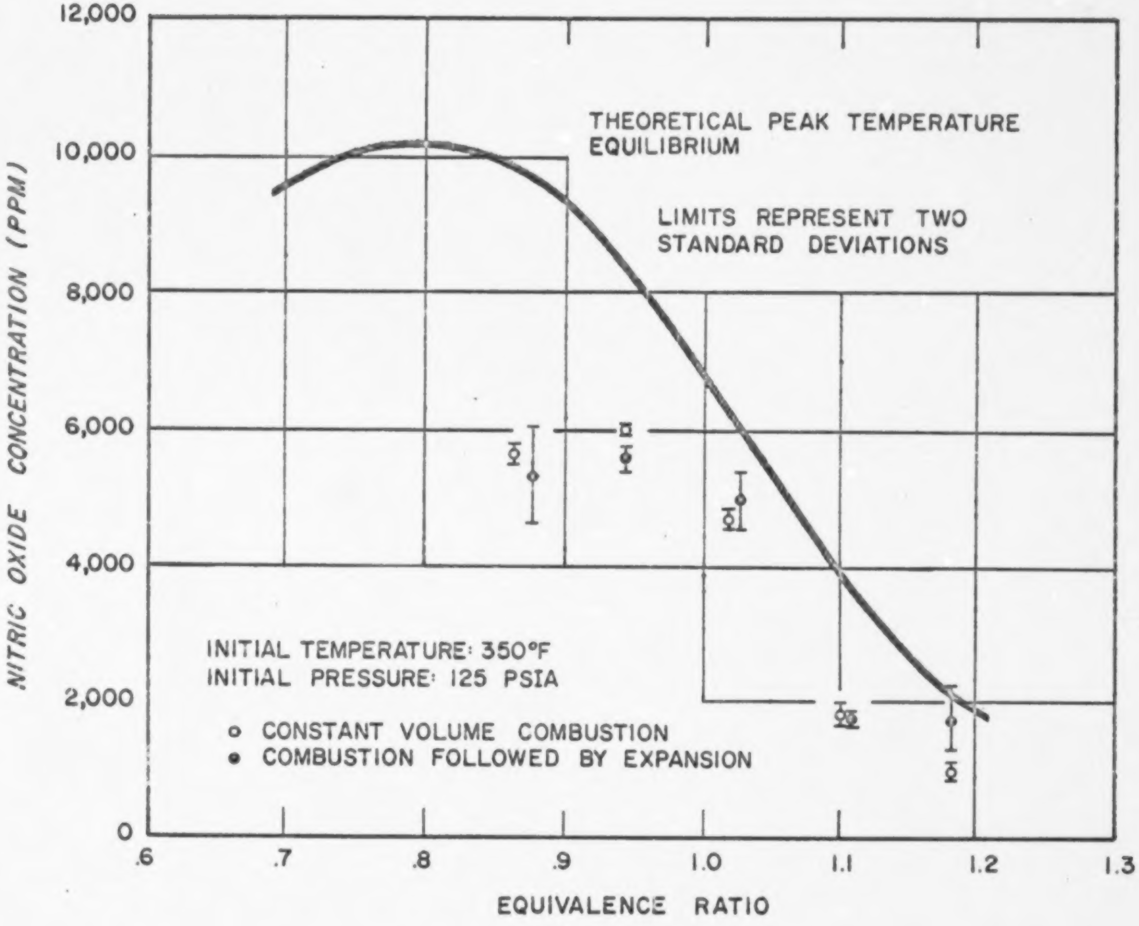

DEPENDENCE OF PRODUCT GAS NITRIC OXIDE CONCENTRATION ON EQUIVALENCE RATIO

FIGURE 21

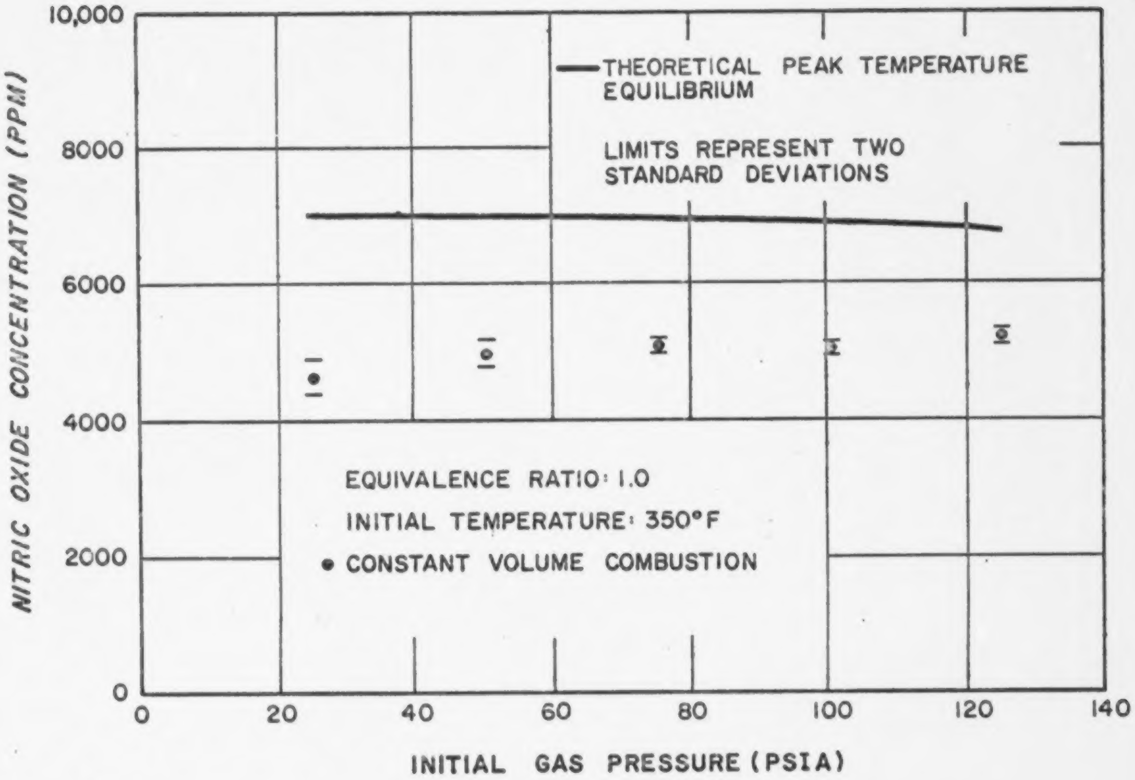

DEPENDENCE OF PRODUCT GAS NITRIC OXIDE CONCENTRATION ON INITIAL PRESSURE

FIGURE 22

4. Discussion.

As expected, NO concentration was a weak function of initial temperature and pressure, and a strong function of equivalence ratio, resulting in the familiar "inverted U" characteristic of measurements made on actual spark ignition engines (10, 11, 49).

A discussion of some of the conclusions which can be drawn from these data follow:

i.) Measured concentrations were considerably higher than would be expected in engines. This could be a real effect, or the result of an error in measurement. Evidence is available to support either (or both) conclusions. For example, in real engines the residual exhaust fraction carried over from one cycle to the next will tend to dilute the incoming charge, with a consequent reduction in peak cycle temperature and, therefore, NO concentration. This effect is consciously used to suppress NO formation in engines in the exhaust gas recycle technique (22). In the analog device, however, the residual exhaust gas fraction is zero.

The presence of moisture in the air similarly reduces peak cycle temperatures (and NO concentration) in engines. Dry air was used in all experimental runs described herein.

In engines piston ring blow-by (leakage) and piston motion will allow the gas to expand during combustion, reducing peak temperature and NO concentration. These effects will also be absent in the analog device.

Nitric oxide concentration measurements in engines are usually made at the end of the exhaust pipe or, at best, near the exhaust manifold. There is good evidence that exhaust gas nitric oxide concentration may be reduced as the product gas passes through the exhaust system (11). Measurements made at the tailpipe, or exhaust manifold of an engine would not be representative of concentrations occuring at the end of the power stroke.

There is reason to expect, therefore, that as a consequence of the absence of residual gas dilution, moisture in the air and leakage (all of which would be present in an actual engine), and allowing for the losses in nitric oxide which will occur in the exhaust system of an engine, nitric oxide concentration measured in the analog device product gas a few seconds after combustion will be higher than measurements made at the tailpipe of an S.I. engine operating under similar conditions.

There may be, however, potential sources of error in measurement which could contribute to an apparently high (fictitious) measured NO concentration.

Errors in measurement could arise from an error in setting initial pressure, temperature or stoichiometry, in measuring final pressure, final peak absorbance or in the value used for reference gas nitric oxide concentration (that is, the value used for calibrating the apparatus).

Pressure measurement is a straight-forward procedure and the pressure gage used in the experiment was frequently calibrated with a dead weight tester (the pressure transducer was calibrated by comparing output of the transducer and pressure gage). In any event, in order to account for discrepancies between theoretical and measured pressures, the initial pressure would have to be in error in a magnitude of 30%.

It was experimentally determined that variations in initial temperature up to 50°F do not have a strong influence on measured peak pressure or NO concentration. Gas temperature was monitored during normal operation using an iron-constantan thermocouple and Brush model 250 strip chart recorder. Variations in initial temperature did not exceed 10°F.

Injection of fuel into the chamber is a simple procedure, and any errors in measurement would be random.

Non-random errors in measured peak absorbance would be compensated during calibration. The only major potential source of experimental error is, therefore, the value used for the nitric oxide concentration of the reference gas. Two independent measurements of the nitric oxide reference gas concentrations revealed that the manufacturers' value of the nitric oxide concentration had not changed by more than five percent during storage. Using a NDIR technique, the NO concentration of the reference gas was found to be 3850 ppm; using the Salzman technique the NO concentration was found to be 4,200 ppm. Other workers have reported a reduction of reference gas nitric oxide concentration during transfer from storage bottle to test cell, which would result in higher than normal measured concentrations (11). However, transfer path lengths were much longer than were used in this work. On the basis of the results of the above measurements and the referenced data, a variation in the nitric oxide concentration measured in. situ. from its true value is not expected to exceed 10 - 15 percent.

ii.) Difference between measured and theoretical peak temperature equilibrium concentrations were greatest for lean mixtures.

There is both experimental and theoretical evidence available which indicate that for rich mixtures, NO decomposition half-life is high (10, 12, 14); in fact, NO formation is rate-limited and under certain conditions (a late-burning, rich mixture) freezing can occur during combustion (16). Decomposition reaction rates are higher for lean mixtures, and previous work suggests that partial decomposition of nitric oxide may occur as gas temperature falls (12, 16). It would therefore be expected that a greater difference between theoretical peak temperature equilibrium and measured values of NO concentration would occur for lean mixtures than rich mixtures. This has been observed and is consistent with other work.

iii.) For rich mixtures theoretical NO concentrations are higher, but not significantly higher than measured values. It is not clear why this should be true. Measured peak combustion pressures are considerably lower than theoretical peak pressures (figure 23), and although NO concentration is not a strong function of gas pressure, it is difficult to conceive of a physical means by which the difference in pressure would not be accompanied by a corresponding difference between theoretical and actual temperature distribution. In fact, comparison of theoretical and measured pressure histories in engines reveal similar discrepancies (51) and it has been the custom to correct (by lowering) the theoretical gas temperature to account for this. Correction techniques have assumed an isentropic relation between theoretical pressure and temperature and the measured pressure and corrected temperature (in effect attributing the differences in pressure exclusively to leakage) (52), and by adjusting the specific heat of the product gas to match theoretical and measured pressures (16). An adjustment of a few percent was all that was necessary to correlate theoretical and measured data, and it was argued that the precision with which the average specific heat of the product gas could be determined was less than the magnitude of the correction.

Although the proper procedure for adjusting theoretical peak temperatures is not yet clear there is little doubt that such correction would result in a lowering of the peak cycle temperature, with a consequent reduction in theoretical NO concentration.

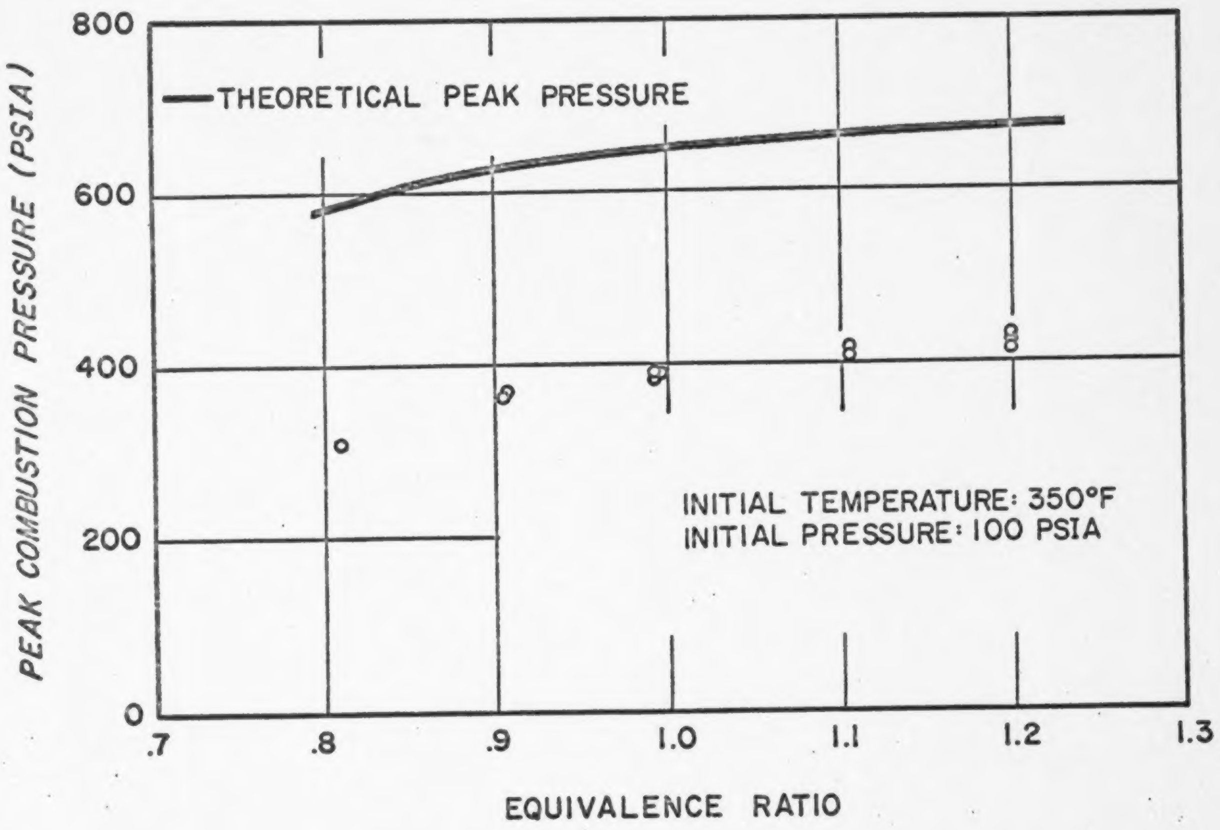

COMPARISON OF THEORETICAL AND MEASURED PEAK COMBUSTION PRESSURE

FIGURE 23

iv.) Measured nitric oxide concentrations obtained when the product gas expanded as rapidly as possible following combustion were compared with nitric oxide concentrations in the product gas after constant volume combustion and it was noted that there was no significant difference in the measured values. This would tend to imply that piston motion plays a relatively minor role in the events which lead to the freezing of nitric oxide in spark ignition engines.

Current kinetic schemes invariably assume that the only means by which a reduction in product gas temperature can be obtained is the isentropic expansion of that gas (i.e., through piston motion) (12, 16). Effects such as heat transfer to the wall, radiation, etc. are thought, quite correctly, to have only a minor influence on the bulk temperature of the gas. However, it should be noted that strong temperature gradients (up to 400°F) exist across the combustion chamber (16). Nitric oxide equilibrium concentration in the hottest part of the product gas was about six times that in the coolest part; radiation losses were 50% greater in the hottest part of the product gas. The portion of the gas mixture richest in NO is closest to the wall, where wall cooling effects would be expected to have the greatest influence. Additionally, any mixing of the hot and cool segments of the product gas could also result in freezing of the nitric oxide concentration. Apparently the "rate of expansion",or more specifically the rate at which gas pressure changes with time, is reflective only of the rate at which the average, or bulk temperature changes with time. Local cooling rates, however, would be expected to exceed the average in precisely that portion of the gas mixture richest in nitric oxide.

V. TIME-RESOLVED NITRIC OXIDE CONCENTRATION MEASUREMENTS

A. General.

An attempt was made to follow the formation of nitric oxide during combustion at constant volume. Since interference by hot oxygen and change in band shape with temperature had a significant effect on results it was necessary to obtain time-resolved spectrographs in the vicinity of the (0,0)γ band of nitric oxide, rather than monitor the monochromatic absorbance of the gas. Qualitative results were obtained at low initial gas pressure.

B. Experimental Considerations.

1. The Schumann-Runge Bands and Continuum of O_2.

The ultraviolet Schumann-Runge bands of oxygen correspond to transitions between the $^3\Sigma_g^-$ ground and $^3\Sigma_u^-$ excited electronic states of the molecule (36). At low temperatures, when virtually all molecules are in the ground electronic and vibrational states, the bands converge to a clear limit at 1759Å, followed by a continuous spectrum (41). As with the nitric oxide molecule an increase in temperature results in an increase in vibrational excitation in the ground electronic state, with a consequent shift of both bands and continuum towards longer wavelengths (54, 55). At the high temperatures characteristic of combustion absorption by the O_2 Schumann-Runge bands will interfere with absorption by NO and will introduce, if unaccounted for, a serious error in the results. It was necessary, therefore, to determine the extent of the interference by both bands and continuum.

Experimental and theoretical data are available which relate continuous Schumann-Runge absorption by O_2 to temperature, however the wavelength range over which these data are available do not extend to 2260Å (55, 56). The Sulzer-Weiland formula, on which some of the theoretical calculations are based, was used to extend the data beyond 2260Å. The results are presented in figure 24. A discussion of the range of validity of the formula in reference (56) suggests a good correlation between theoretical predictions and experimental data would be expected. On the basis of these predictions continuous absorption by O_2 at 2260Å would be no greater than that by nitric oxide, and in most cases considerably less.

Determination of the influence of Schumann-Runge band absorption is complicated not only by the effect of temperature on band shape, but also by the fact that the fine structure which comprise these bands may not be resolved with the present spectroscopic apparatus (that is, measured absorbance may depend upon instrumental resolution as well as the thermodynamic state and molecular properties of oxygen). It is possible, however, by monitoring product gas monochromatic absorbance during combustion on either side of the nitric oxide (0,0)γ band as a function of instrument resolution, to experimentally determine this

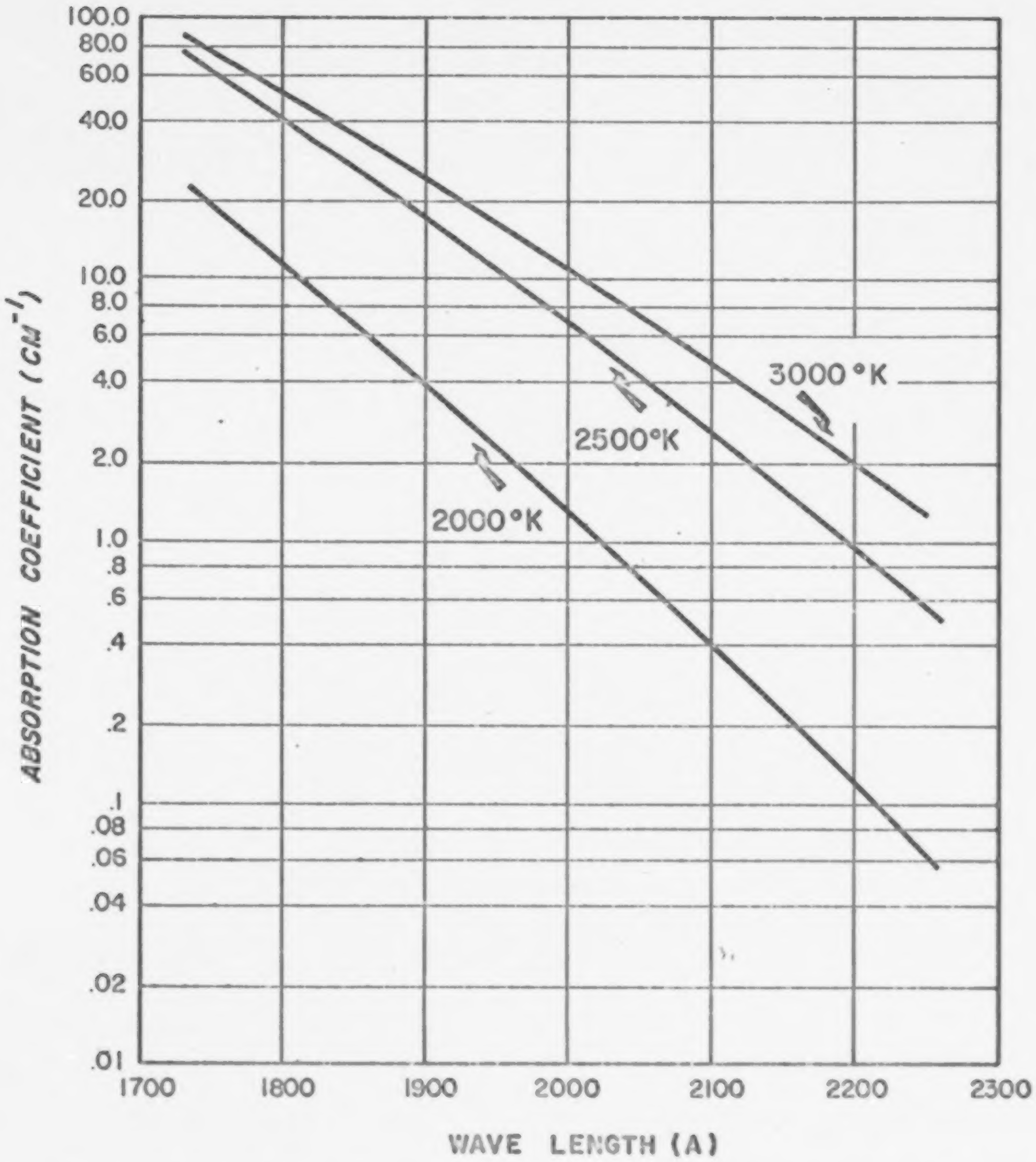

THEORETICAL SCHUMANN-RUNGE CONTINUUM ABSORPTION AT ELEVATED TEMPERATURES

FIGURE 24

effect. The background, continuous absorption should not be affected by changes in resolution. Measured band absorbance should, if resolution limited, be a strong function of the resolving power of the apparatus. In the limit, as instrument resolution deteriorates, measured band absorbance should go to zero. Inspection of absorption traces presented in figure 25 reveals that this does in fact occur. At high resolving power the gas is essentially opaque at the monitored wavelengths, whereas as resolution is decreased monitored absorbance falls accordingly.

2. Population Distribution of the NO γ Bands with Temperature.

As gas temperature increases the vibrational ground state of the nitric oxide molecule will become depopulated and, as with the Schumann-Runge bands of O_2, absorption will be observed at longer wavelengths. Measurements of absorption by NO at the (0,0) band of the γ system can be related only to the concentration of molecules in the ground vibrational state. It would be necessary to correct these measurements to account for the depopulation of that state. Calculations of the population distribution of the vibrational states of the NO molecule in the ground electronic state as a function of temperature, based on molecular constants obtained from reference (36), are presented in figure 26.

3. Vibrational Relaxation of Nitric Oxide.

As mentioned, absorbance of the (0,0)γ band of nitric oxide can

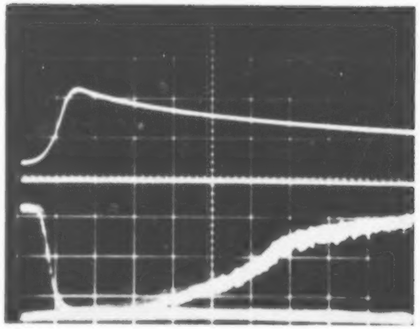

50 µ entrance slit
50 µ exit slit
resolution 1.65A

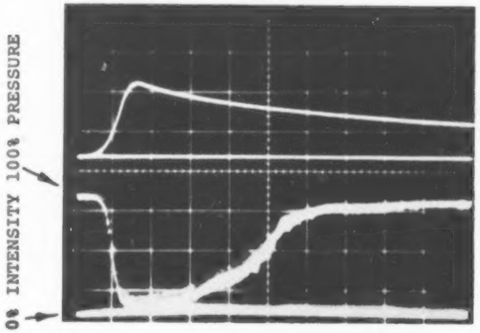

50 µ entrance slit
.0035" exit slit
resolution: 10.6A

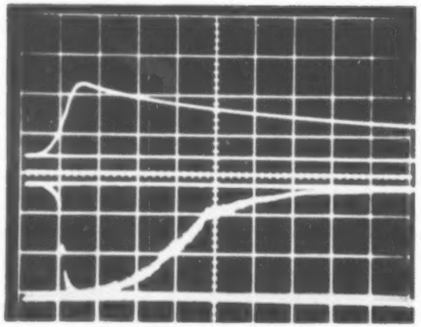

.0035″entrance slit
.0070″exit slit
resolution 23A

2275A
100 ps7/div
20 ms/div

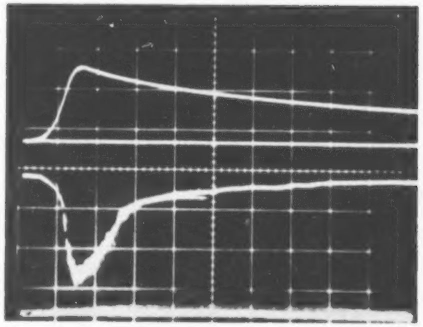

.0035″entrance slit
.0195″exit slit
resolution: 50A

INITIAL TEMPERATURE: 350°F
INITIAL PRESSURE: 50 psia
EQUIVALENCE RATIO: 1.0
CONSTANT VOLUME

EFFECT OF RESOLUTION ON PRODUCT
GAS ABSORPTION WITH TIME

FIGURE 25

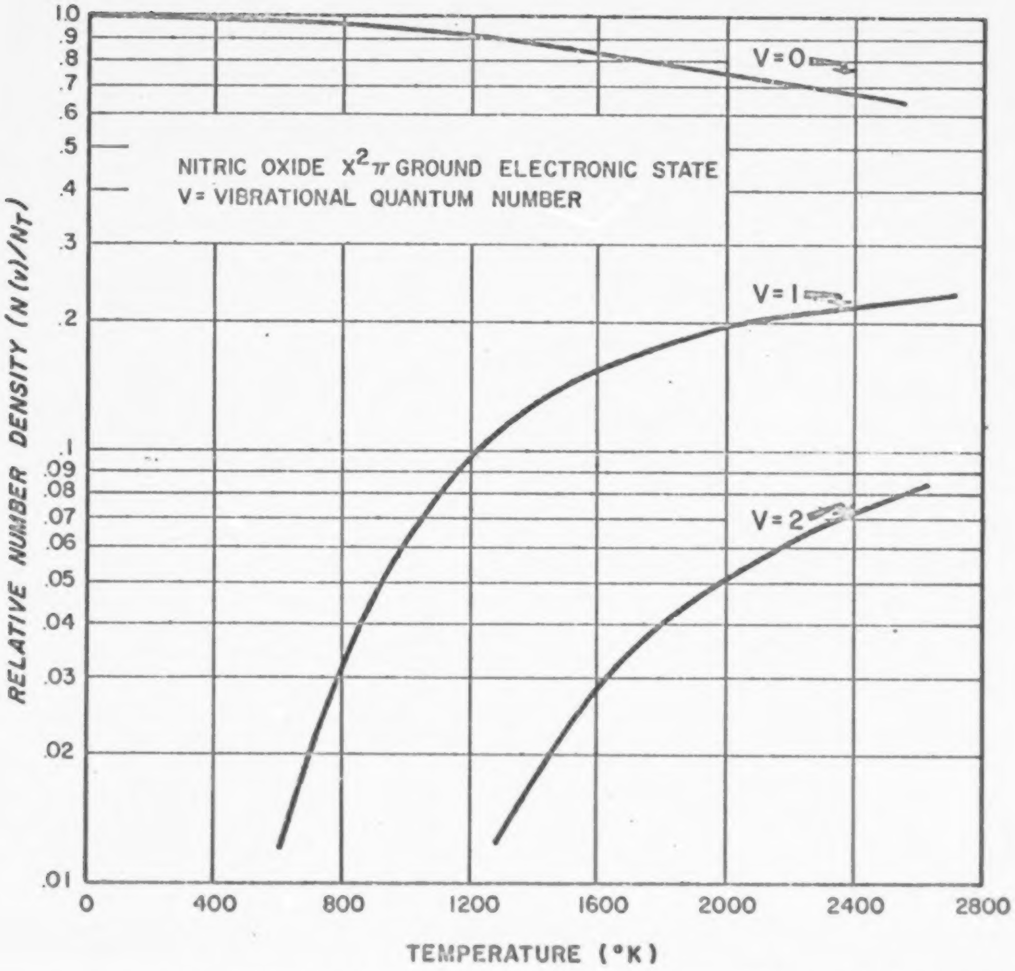

THEORETICAL POPULATION DISTRIBUTION OF VIBRATIONAL QUANTUM STATES OF NO AS A FUNCTION OF TEMPERATURE

FIGURE 26

be related only to the population of the ground vibrational state of the molecule. Corrections can be made at elevated temperatures, but these corrections assume that population of the vibrational states instantaneously readjust with changes in temperature. Significant vibrational relaxation by nitric oxide would result in an error in measurement. Vibrational relaxation times can be estimated, however (57, 58);

$$\tau^{-1} = Z\,P_{10}\,[1 - e^{-\theta/T}] \qquad (1)$$

where τ is the vibrational relaxation time

z is the number of collisions by a single molecule per second

P_{10} is the transition probability between the $v'' = 1$ and $v' = 0$ vibrational levels per molecule per collision

T is the translational (thermodynamic) temperature

θ is the characteristic vibrational temperature of nitric oxide (equal to 2688°K)

for $T = 1500^{\circ}\mathrm{K}$, $P_{10} \cong 10^{-3}$ (59)

Assuming $T = 1500^{\circ}\mathrm{K}$ and a collision diameter of 3.5A for NO-NO collisions, it can be shown that

$$Z = 1.063 \times 10^{11}\, P/T^{1/2} \qquad (2)$$

with the pressure, P, in atm and the temperature, T, in °K (59). For $P = 30$ atm and $T = 1500^{\circ}\mathrm{K}$, substituting (2) in (1),

$$\tau_{1 \rightarrow 0} \cong 1.5 \times 10^{-8} \text{ sec.}$$

Vibrational relaxation times are therefore far less than times characteristic of the combustion process, and the vibrational temperature can be assumed equivalent to the thermodynamic temperature of the system.

4. Change in Band Shape with Temperature.

As the temperature of the system is increased changes in the rotational population distribution may occur, in effect changing the shape of the bands in the system. The integrated intensity of the $(0,0)\gamma$ band will not, however, be affected by this change in shape - it will remain an exclusive function of the partial density of nitric oxide (37). For this reason it was necessary to obtain film records of the absorption spectrum of nitric oxide which could later be reduced to obtain values for the integrated intensity of the band. This was also a convenient way of accounting for the interference by the Schumann-Runge bands of O_2 and any other potential source of signal attenuation (such as a suspension of carbon particles, etc.). Absorption by NO was monitored relative to that by O_2 (which would, with the present apparatus, appear as a continuum).

C. Description of Apparatus.

1. General.

A schematic of the time-resolved experimental apparatus appears in figure 27.

An E.G. & G. model FX-11 flash tube was used as a source of pulsed U.V. radiation in conjunction with a time delay circuit which was

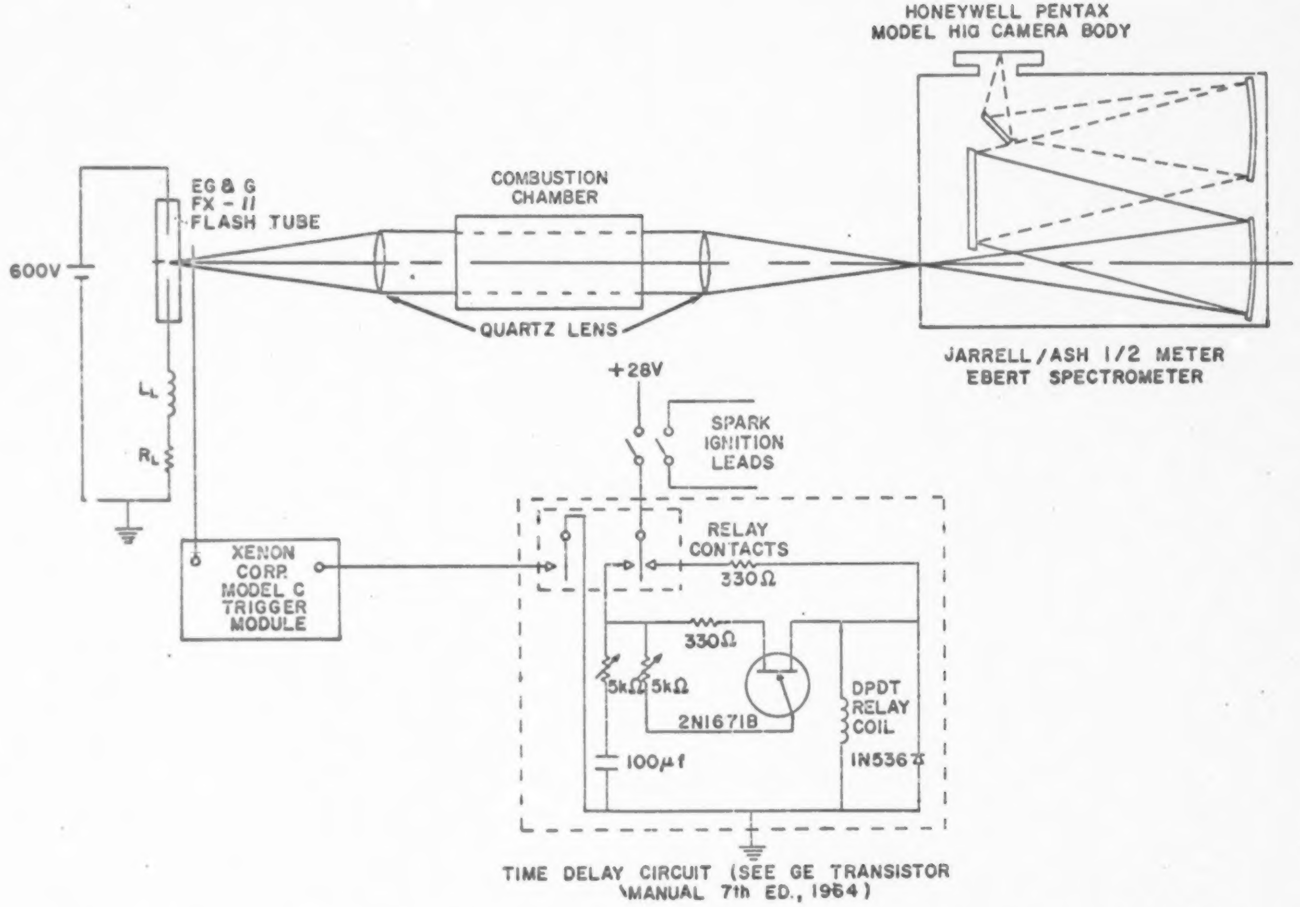
HONEYWELL PENTAX
MODEL H1G CAMERA BODY
EG & G
FX - 11
FLASH TUBE
COMBUSTION
CHAMBER
600V
QUARTZ LENS
JARRELL/ASH 1/2 METER
EBERT SPECTROMETER
L_L
R_L
+28V
SPARK
IGNITION
LEADS
XENON
CORP.
MODEL C
TRIGGER
MODULE
RELAY
CONTACTS
330Ω
330Ω
5kΩ
5kΩ
2N1671B
DPDT
RELAY
COIL
100μf
IN536
TIME DELAY CIRCUIT (SEE GE TRANSISTOR MANUAL 7th ED., 1964)

TRANSIENT ULTRAVIOLET NITRIC OXIDE CONCENTRATION MONITORING APPARATUS

FIGURE 27

triggered by the ignition spark. By adjusting the time delay circuit it was possible to trigger the flash tube (with a Xenon Corp. model C trigger module) during, or after, any stage of combustion. Time delay was reproducible within about one millisecond.

As with the steady state apparatus, radiation from the source was collimated, passed through the combustion chamber and focused upon the entrance slits of a Jarrell/Ash one half meter spectrometer. The unit, which had been used as a monochromator, was converted for the acquisition of film records of the NO absorption spectrum. An adapter was fabricated which diverted radiation from the monochromator exit slit and brought a dispersed image to focus on the focal plane of a Honeywell Pentax model H1a camera body. A low pressure mercury lamp was used to adjust the focus and calibrate the apparatus. Spectographs of of the Hg emission spectrum were obtained to determine the dispersion of the instrument (230 Å/inch).

Signal levels were much lower than would be required to expose film with one pulse of the flash tube, even with the combustion chamber empty. It was necessary to manipulate the spectrometer entrance slit width, type of film used, flash tube discharge energy and voltage, and number of flashes per run to optimize the design of the system.

2. Spectrometer Entrance Slit Width.

The xenon flash tube emission spectrum appears, in the region between 2100 and 2400 Å, as a continuum upon which are superposed distinct spectral lines. In order to maximize total radiant energy incident on the camera focal plane the entrance slit was as wide as possible. Increasing the entrance slit width will, however, result in a decrease in instrument resolution. Maximum slit width was therefore limited by the resolution required of the apparatus. A steady-state high pressure xenon lamp was used to acquire, at room temperature, the absorption spectrum of reference gas nitric oxide (4040 ppm NO, balance N_2) between 2100 and 2400 Å as a function of the entrance slit width. These spectrographs were inspected to determine the maximum slit width for which resolution of the (0,0)γ band of nitric oxide was adequate. A .007 inch entrance slit was used, unless otherwise specified, in all subsequent work. Although these data were obtained at low temperature, the conclusions will be valid at elevated temperatures since the rotational population redistribution at higher temperatures will tend to increase band half width, and peak emission for broadened rotational lines will always be lower than that of unbroadened lines (37).

3. Spectroscopic Film.

Desirable properties of spectroscopic films include high contrast (in order that low concentrations of nitric oxide can be detected), and high sensitivity. Of the conventional spectroscopic films Kodak Type 103-0 seemed best suited for use in the region between 2100-2400Å (60). Since film emulsion absorbs radiation below about 2800Å, it was necessary to sensitize the film for use in this region. Performance of the film proved inadequate (sensitivity and contrast were low), and it was used only to obtain some of the preliminary data necessary to establish the final configuration of the apparatus. Although Kodak Short Wavelength Range (type SWR) film has a very low gel content, and is exceptionally sensitive to abrasion, it is the only film available with the necessary contrast and sensitivity in the spectral region of interest. Processing of the film with available equipment was difficult, and processing variations precluded acquisition of quantitative data.

4. Flash Tube.

The peak radiant power of a flash tube is limited by thermal and physical considerations. Total radiant energy per pulse was therefore raised by increasing flash pulse width, i.e., by increasing capacitance and placing a low resistance in series with the flash tube. High total energy output was accompanied, however, by a reduction in lamp life. Final operating conditions, a compromise between lamp output energy and lifetime, were as follows: flash tube discharge voltage was 600 or 700 volts, and capacitance was 900 μ farad. No attempt was made to measure the impedance of the discharge circuit, but the flash pulse width was determined, by observing monochromatic emission oscillographs, to be about 5 ms.

D. Experimental Results.

Multiple exposures of the spectroscopic film were needed to bring film density within a useful range, even with the cell filled with dry air at room temperature. During combustion, at initial pressures typical of operating engines, the product gas was in all cases opaque, although it was possible to observe a strong NO absorption band with the product gas about 200 to 250 milliseconds after peak pressure (when gas temperature had dropped substantially). In order to obtain useful data it was necessary to reduce the optical density of the gas at high temperature. The most practical means of reducing peak temperature optical density was to reduce initial gas pressure. However, at low initial gas pressures the product gas partial density of nitric oxide, and consequently the peak spectral absorbance was low.

To define an operating regime in which the probability of successful acquisition of data was reasonable, the cell was filled with reference gas at room temperature, and spectographs were obtained over a range of total gas pressures. These spectographs were inspected to determine the minimum partial density of nitric oxide for which absorbance of the gas was adequate. It was determined that it should be possible to detect high temperature NO absorption traces for initial gas pressures between 25 and 40 psia, and an equivalence ratio equal to, or less than one.

E. Discussion.

In figure 28 are presented high temperature absorption spectrographs obtained during combustion of a fuel-air mixture at an initial pressure and temperature of 40 psia and 400°F, respectively, and an equivalence ratio equal to 0.975.

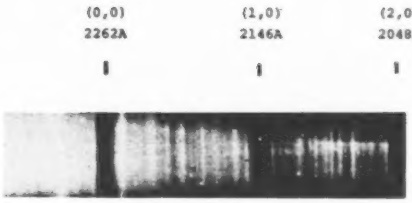

Ref. Gas; 100 psia

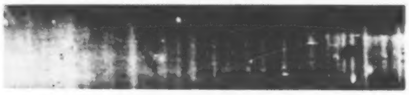

Lamp Emission

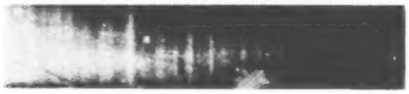

Comb. Prod. Gas; 10 ms
Before Peak Pressure

Comb. Prod. Gas; 5 ms
Before Peak Pressure

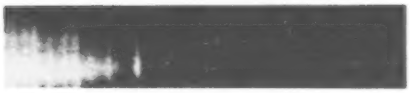

Comb. Prod. Gas, Peak
Pressure

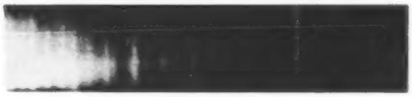

Comb. Prod. Gas; 20 ms
After Peak Pressure

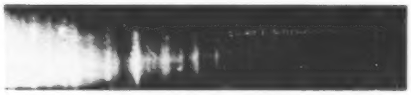

Comb. Prod. Gas; 50 ms
After Peak Pressure

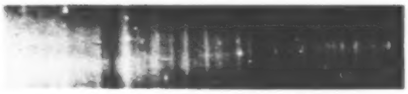

Comb. Prod. Gas; 2 sec.
After Peak Pressure

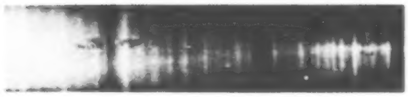

Ref. Gas; 40 psia

Reference Gas: 4040 ppm NO/
Balance, N_2, 400°F

Combustion Product Gas: 400°F
Initial Temperature, 40 psia
Initial Pressure, 0.975 Equivalence
Ratio

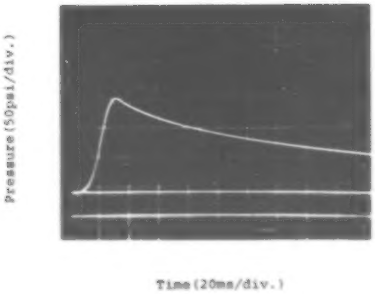

Reproduced from
best available copy.

TIME-RESOLVED NITRIC OXIDE ABSORPTION SPECTRUM

FIGURE 28

A shift in absorption by molecular oxygen to longer wavelengths at higher temperatures is clearly demonstrated. Reference gas and low temperature product gas spectographs reveal absorption by the (0,0), (0,1) and (0,2) bands of nitric oxide at 2262, 2146 and 2048 Å, respectively. At combustion temperatures the (0,1) and (0,2) bands are obscured by hot oxygen. Absorption at the (0,0)γ band of NO can be observed in spectrographs obtained 5 ms. before peak pressure, at peak pressure, and 20 to 50 ms. after peak pressure. The absorbance of the product gas increased as temperature was reduced. This would be expected since at combustion temperatures about 25 percent of the NO molecules are in excited vibrational states. No nitric oxide absorption bands were detected in the combustion gas 10 ms. before peak pressure.

In order to obtain quantitative data it will be necessary to obtain more continuous source radiation and to improve the technique of processing the spectroscopic film. However, a semiquantitative determination of product gas concentration can be made by comparing product gas absorbance at 2260Å with that of the reference gas at a total pressure of 40 psia.

VI. FUTURE WORK

A. Steady State Apparatus.

The U. V. absorption method may be a commercially useful means of monitoring nitric oxide concentration, continuously and directly, in automotive exhaust gas. Of the NO monitoring techniques described in Appendix A only the mass spectrometric and NDIR instruments offer the advantages of continuous and direct measurement (conversion to NO_2 is not required), with excellent time response. As with the NDIR apparatus, however, there is a possibility of the existence of interfering species. Iso-octane was used as a fuel in the present work, and paraffins do not absorb radiation between 2260-2270Å. Of the conglamerate of organic compounds which comprise commercial gasoline there are species present which do absorb in this region. The extent of their interference in the exhaust will have to be determined.

It is anticipated that a dual beam spectromenter, intended specifically for the steady state nitric oxide measurements, would eliminate the necessity of frequent alignment and construction of calibration curves, and would provide a direct readout of exhaust gas absorbance, which could be immediately related to nitric oxide concentration.

Relative cost of the apparatus would also need to be determined.

B. Time Resolved Apparatus.

In order to obtain quantitative time-resolved absorption spectrographs of the product gas in the region between 2100 and 2350Å it will be necessary to maintain more precise control over the processing of the spectroscopic film.

It would also be desirable to increase flash tube emissivity in the wavelength range of interest in order to increase source radiance and to suppress the wavelength dependence of emitted radiation (it is difficult to detect a small NO absorption signal against a background which is a strong function of wavelength). Optical density could be increased either by raising the operating pressure of the lamp, or increasing the effective flash tube diameter.

C. Theoretical Model.

See the discussion in Appendix E.

VII. SIGNIFICANT RESULTS OF THIS INVESTIGATION.

i. The spark ignition engine analog device provides a useful alternative, for purposes of combustion research, to the spark ignition engine. Reproducibility and flexibility of the device both exceed that possible with an engine, without sacrificing the essential combustion aspects of the problem.

ii. The nitric oxide ultra-violet absorption monitoring technique can be used to measure steady-state nitric oxide concentration following combustion. Comparison of the direct U.V. absorption technique and other methods should take account of the apparatus used for these measurements. With the present apparatus, in terms of precision and convenience the method does not compare favorably with more conventional techniques (although it does hold promise of applicability to detailed study of the non-steady processes occuring during combustion). However, apparatus designed specifically for the steady-state measurements might result in a considerably increase in the precision of measurement.

iii. The mechanism by which nitric oxide "freezes" in the product gas does not appear to depend upon piston motion, but rather depends upon instantaneous local cooling resulting from radiation or the mixing of the inhomogeneous product gases.

iv. The time-resolved nitric oxide monitoring apparatus was used to obtain limited qualitative data. High temperature spectrographs revealed absorption by nitric oxide at the (0,0)γ band during combustion. The low intensity of the ultra-violet light source, and inadequate control of the film processing technique proscribed aquisition of detailed quantitative data.

Appendix A

Methods of Monitoring Nitric Oxide in Automobile Exhaust

Many of the NO monitoring techniques, such as the Saltzman and non-dispersive ultraviolet absorption methods, actually monitor nitrogen dioxide concentration (14, 61). Nitrogen dioxide, however, is not present in significant quantities in automotive exhaust; the nitric oxide which does predominate must first be oxidized to NO_2. Oxidation is often accomplished simply by mixing the exhaust with oxygen in large containers for a period of approximately forty minutes, with the result of higher than 98 percent oxidation (14). Faster oxidation rates have been reported when 50-50 mixtures of exhaust and oxygen have been injected, under pressure, directly into a spectrophotometer cell and allowed to stand until NO_2 absorbance no longer changed with time. Oxidation rates were found to depend upon nitric oxide concentration, but even at a relatively low concentration of 150 ppm oxidation was complete after about 15 minutes (49). Rapid oxidation of nitric oxide has also been accomplished through ozonation, permitting the development of a continuous flow analyzer with a response time of about 20 seconds (62).

Some of the more common methods of determining nitric oxide or NO_x concentration in automotive exhaust are enumerated below:

(1) Phenoldisulfonic Acid Method (63). Exhaust gas is bubbled through, and nitrogen oxides are absorbed by an acid solution to form nitrous and nitric acid. The nitrous acid is then oxidized with hydrogen peroxide after which the solution is neutralized and evaporated to dryness. The resultant alkali nitrate is mixed with a solution

of sulfuric and phenoldisulfonic acid which, upon neutralization by ammonium hydroxide, forms tri-alkali nitro phenoldisulfonate. The intensity of the yellow color of this compound can be related, through the use of a colorimeter, to the concentration of the oxides of nitrogen. With this method oxidation occurs in the liquid rather than the gas phase. The oxidation step is quite long; the solution is usually allowed to stand overnight. The method has been modified through inclusion of a vapor phase oxidation step which takes no longer than 15 minutes. The technique has been used to monitor nitric oxide concentrations as low as 5 ppm.

(2) Saltzman Method (61). With this method the nitric oxide present in the exhaust gas must first be converted to nitrogen dioxide using one of the oxidation techniques outlined above. The gas is then bubbled through a reagent, which is a mixture of sulfanic acid, N-(1-napthyl)-ethylenediamene dihydrochloride and acetic acid. The intensity of color of the resulting compound can be directly related to the nitrogen oxide concentration. Sensitivity of the method extends to a few parts per billion and for this reason it is most often used to measure NO_x concentration in the atmosphere. The extent of dilution required in order to adapt the technique for exhaust gas analysis results in a reduction in the precision of measurement.

(3) Non-Dispersive Ultraviolet Method (NDUV) (14). Absorption of radiation by nitrogen dioxide extends throughout the near ultraviolet region of the spectrum. With the NDUV method the NO in the

exhaust gas must also be converted to nitrogen dioxide. Absorption of the U.V. light by NO_2 at about 3900A, as measured by a spectrophotometer, is related, after calibration with a reference gas, directly to NO_2 concentration. This technique offers a considerably advantage over previous methods in that, if a suitable oxidation step is chosen, NO_x concentration in the exhaust can be monitored continuously.

(4) Non-Dispersive Infrared (NDIR) Method (14). The NDIR method relates nitric oxide concentration in the exhaust directly to absorbance of infrared radiation at the 5.3μ fundamental band of nitric oxide. The major advantages of this technique are that no intermediate oxidation step is required, nitric oxide can be distinguished from NO_2 concentration and can be measured directly and continuously. Disadvantages include moderate signal instability and interference by carbon monoxide, carbon dioxide and, if the sample is not dried, water vapor.

(5) Mass Spectrometric Method (11). The mass spectrometer has been used to monitor, continuously and directly, the nitric oxide concentration in automotive exhaust gas. Advantages of the technique are that, like the NDIR method, NO concentration can be distinguished from NO_2, response time is sufficient to permit continuous operation and no oxidation step is required. Additionally, interference from other species present in the exhaust is negligible.

Appendix B

Spark Ignition Analog Device Engineering Drawings

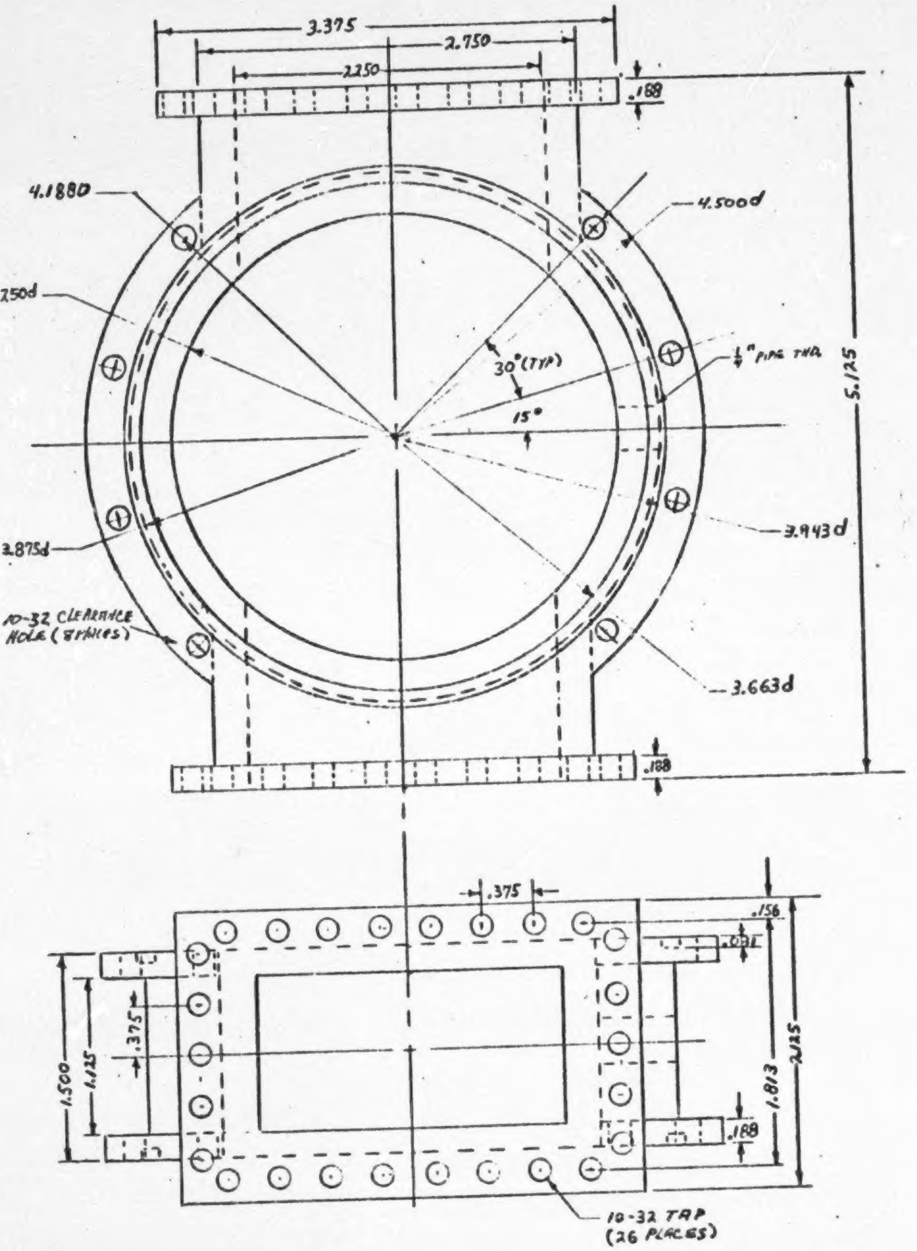
3.375
2.750
2.250
.188
4.188D
4.500d
3.250d
30°(TYP)
15°
1/4" PIPE THD
5.125
3.875d
3.943d
10-32 CLEARANCE HOLE (8 PLACES)
3.663d
.188
.375
.156
.031
1.500
1.125
.375
1.813
2.125
.188
10-32 TAP (26 PLACES)

COMBUSTION CHAMBER BODY

FIGURE 29

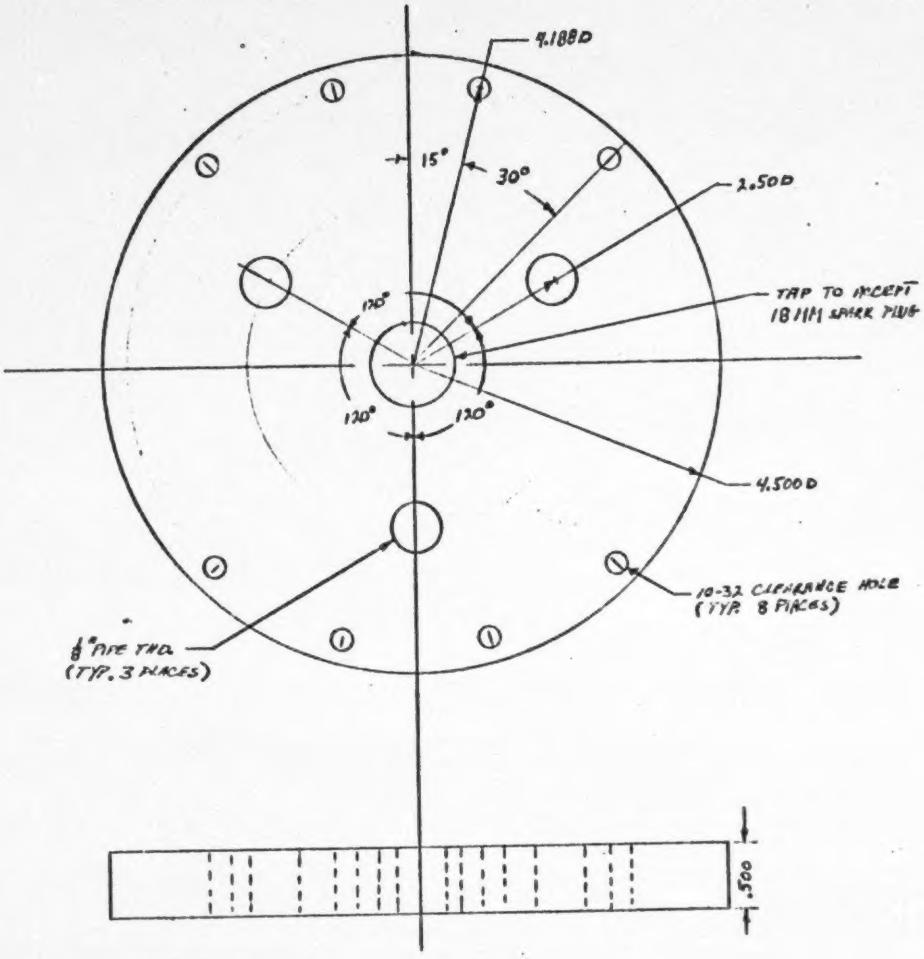
4.188D
15°
30°
2.50D
TAP TO ACCEPT
18 MM SPARK PLUG
120°
120°
120°
4.500D
10-32 CLEARANCE HOLE
(TYP. 8 PLACES)
1/8" PIPE THD.
(TYP. 3 PLACES)
.500

COMBUSTION CHAMBER COVER-TOP

FIGURE 30

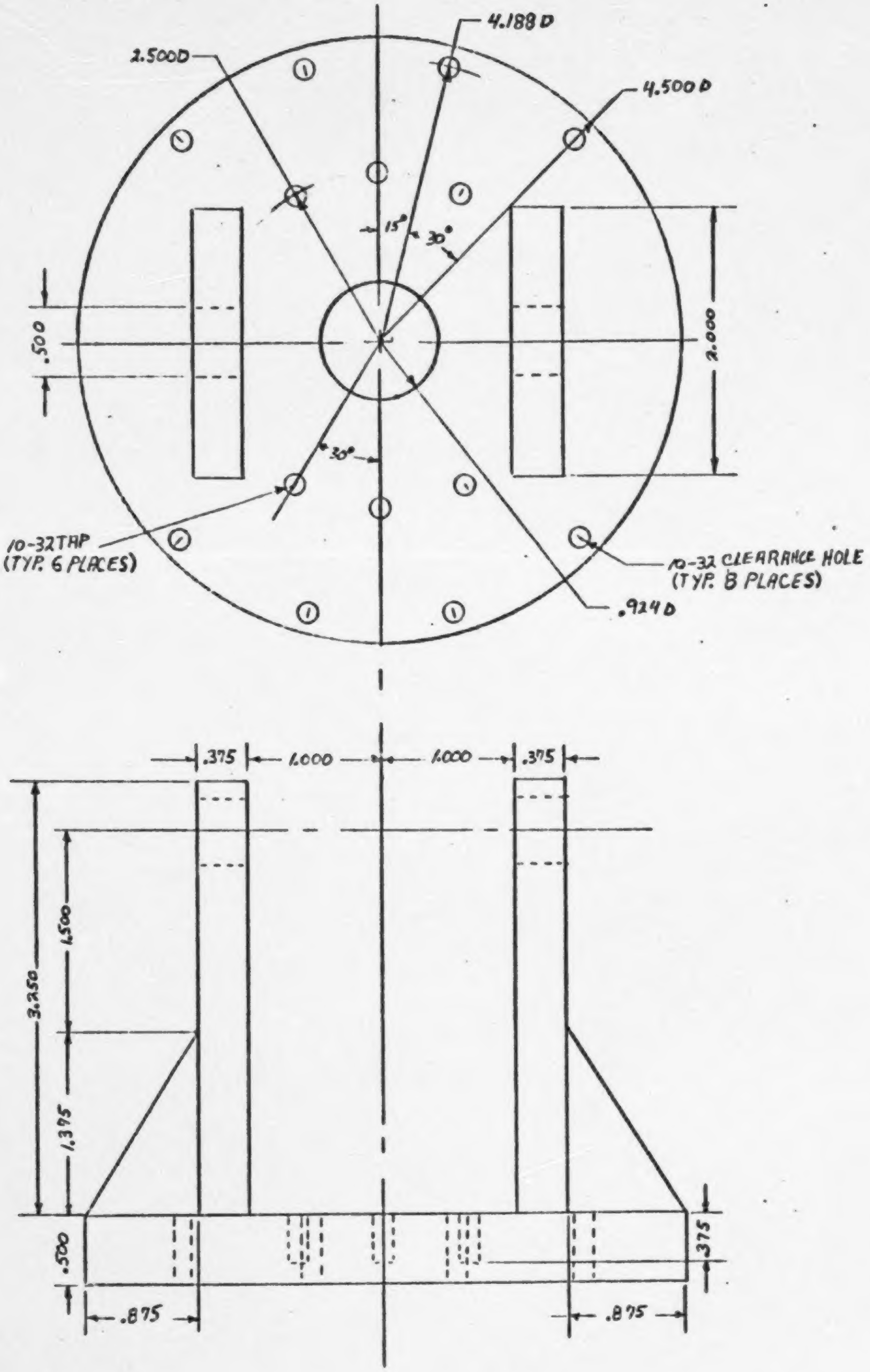
4.188 D
2.500D
4.500 D
15°
30°
.500
2.000
30°
10-32 TAP
(TYP. 6 PLACES)
10-32 CLEARANCE HOLE
(TYP. 8 PLACES)
.924 D
.375
1.000
1.000
.375
3.250
1.500
1.375
.500
.375
.875
.875

COMBUSTION CHAMBER COVER-BOTTOM

FIGURE 31

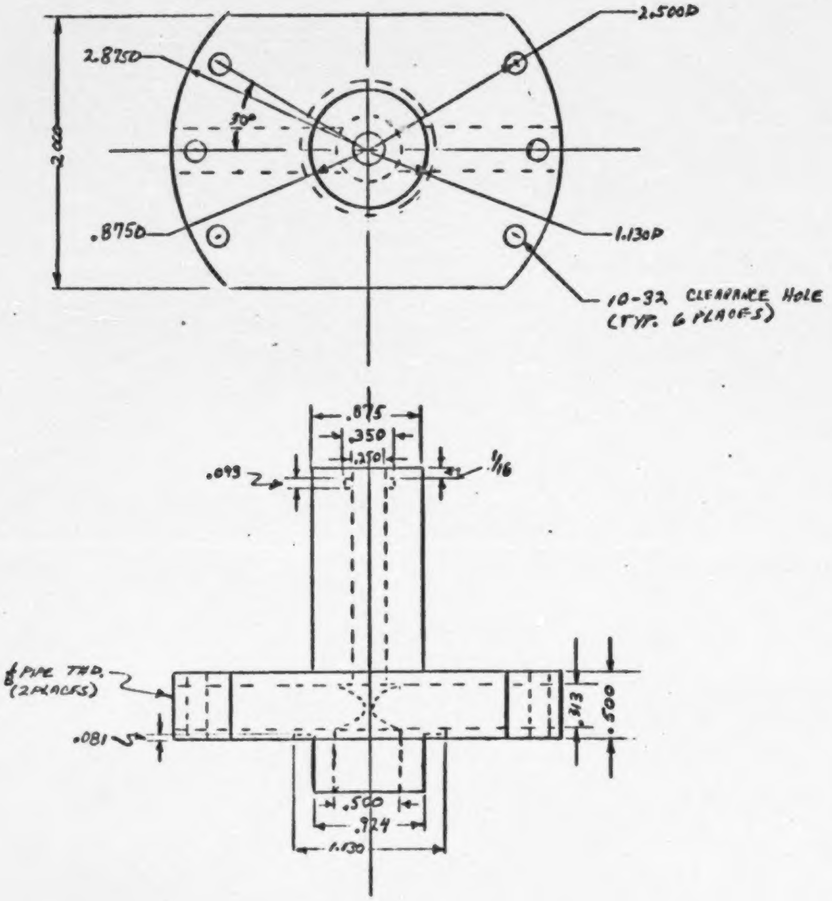
2.500D
2.875D
30°
2.000
.875D
1.130D
10-32 CLEARANCE HOLE
(TYP. 6 PLACES)
.875
.350
.250
.093
1/16
1/8 PIPE THD.
(2 PLACES)
.081
.313
.500
.500
.924
1.130

VALVE HOUSING ASSEMBLY

FIGURE 32

Appendix C

Poppet Valve-Cam Assembly Design

Valve lift was determined as a function of the rate of change of gas pressure with time by coupling the equations for choked flow and isentropic expansion with the perfect gas law. That is, the product gas within the combustion chamber at any instant of time was assumed to have expanded isentropically in the process of expelling a portion of gas from the chamber. The isentropic, or polytropic, exponent was assumed constant, independent of changes in temperature and composition. The state of the gas was assumed to be adequately characterized by the perfect gas law. Changes in composition were assumed to have no effect on the gas constant R. Steady flow, one dimensional gas dynamical relations for choked flow were assumed applicable. The discharge coefficient was assumed constant and equal to unity.

Then,

$$\omega/A = \left[kg/R \left(\frac{2}{k+1}\right)^{\frac{k+1}{k-1}}\right]^{1/2} \frac{P_o}{\sqrt{T_o}} \quad \text{(reference 64)} \qquad (1)$$

$$T_o/T_o' = (P_o/P_o')^{\frac{k-1}{k}} \qquad (2)$$

$$P_oV_o = mRT_o \qquad (3)$$

$$m = \frac{P_oV_o}{RT_o} = \left(\frac{V_o}{R} \frac{P_o'^{\frac{k-1}{k}}}{T_o'}\right) (P_o^{1/k}) \qquad (4)$$

$$\frac{dm}{dt} = \omega = \left(\frac{V_o}{Rk} \frac{P_o'^{\frac{k-1}{k}}}{T_o'}\right) P_o^{\frac{1-k}{k}} \frac{dP_o}{dt} \qquad (5)$$

combining (1) and (5)

$$\left(\frac{V_o}{Rk}\,\frac{P_o'^{\frac{k-1}{k}}}{T_o'}\right)\left(P_o^{\frac{1-k}{k}}\right)\frac{dP_o}{dt} = A\left(\frac{kg}{R}\left(\frac{2}{k+1}\right)^{\frac{k+1}{k-1}}\right)^{1/2}\frac{P_o}{\sqrt{T_o}} \qquad (6)$$

$$\sqrt{T_o} = \sqrt{T_o'}\left(\frac{P_o}{P_o'}\right)^{\frac{k-1}{2k}} \qquad (7)$$

$$\frac{\left(\frac{V_o}{Rk}\,\frac{P_o'^{\frac{k-1}{k}}}{T_o'}\right)\sqrt{T_o'}}{A\left[\frac{kg}{R}\left(\frac{2}{k+1}\right)^{\frac{k+1}{k-1}}\right]^{1/2}\left(P_o'^{\frac{k-1}{2k}}\right)}\;\frac{dP_o}{dt} = \frac{P_o}{P_o^{\frac{k-1}{2k}}}\;\frac{1}{P_o^{\frac{1-k}{k}}} \qquad (8)$$

and rearranging,

$$A = \left[\frac{V_o}{k\sqrt{kRgT_o'}\left(\frac{2}{k+1}\right)^{\frac{k+1}{k-1}}}\right]\frac{\frac{d\left(P_o/P_o'\right)}{dt}}{\left(P_o/P_o'\right)^{\frac{3k-1}{2k}}} \qquad (9)$$

where W = exit mass flow

A = poppet valve throat area

k = polytropic exponent

g = gravitational constant

R = gas constant

P_o = combustion chamber pressure

T_o = combustion chamber temperature

V_o = combustion chamber volume

m = mass of product gas in chamber

primed symbols refer to initial conditions

Valve throat area, A, the surface area of the conical frustrum of slant height, t, was related to valve lift and configuration as follows (see figure 33);

$$A = \pi\ (r+r')\ [(r-r')^2 + h^2]^{1/2} \qquad (10)$$

$$t = s \sin \alpha \qquad (11)$$

$$h = t \sin \alpha = s \sin^2\alpha \qquad (12)$$

$$r = d/2 \qquad (13)$$

$$r' = d/2 - t \cos\alpha = d/2 - s \sin\alpha \cos\alpha \qquad (14)$$

$$A = \pi\ (\frac{d}{2} - s \sin\alpha \cos\alpha + d/2)\ (s^2 \sin^2\alpha \cos^2\alpha + s^2 \sin^2\alpha)^{1/2} \quad (15)$$

$$A = \pi\ s \sin\alpha\ (d - s \sin\alpha \cos\alpha) \sqrt{\cos^2\alpha + 1} \qquad (16)$$

combining equations (9) and (16)

$$s(d - s\sin\alpha \cos\alpha) = \frac{1}{\pi \sin\alpha \sqrt{1+\cos^2\alpha}}\ \frac{V_o}{k\sqrt{kRgT_o'}\ (2/k+1)^{\frac{k+1}{2(k-1)}}}\ \frac{\frac{d\ (P_o/P_o')}{dt}}{\frac{P_o}{P_o'}^{\frac{3k-1}{2k}}} \quad (17)$$

Values for α, the valve cam angle, d, the valve seat diameter and s, the poppet valve lift were manipulated to provide, through the requisite area-time relation, a desired rate of expansion. A practical limit on the range of s_m, the maximum poppet valve lift, was dictated by the necessity of minimizing both inertial forces in the valve train and those errors resulting from imprecision in fabrication and adjustment of the apparatus. Solutions for these equations were acquired through use of a digital computer. A printout of the program appears at the end of this appendix.

Results of the optimization procedure indicated that changes in α

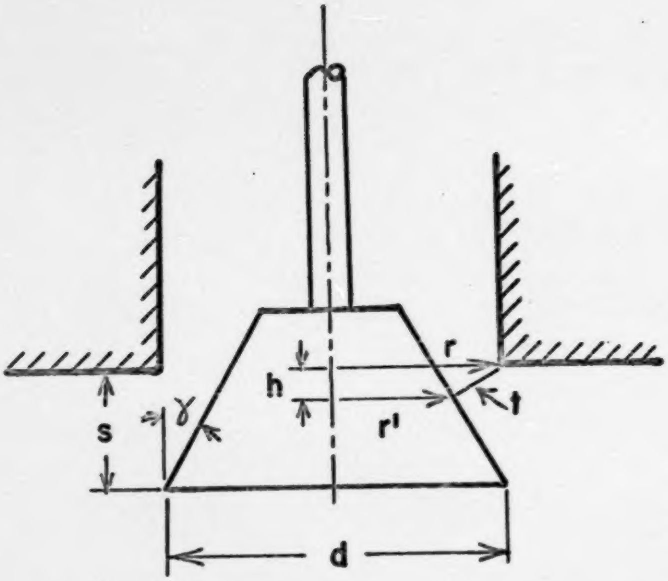

POPPET VALVE DIMENSIONS
FIGURE 33

had a much greater influence on s_m than changes in d. Two basic configurations were finally selected; a valve housing assembly with d equal to .410 inches and α equal to 10 degrees for lower rates of expansion, and an assembly with d = .550 inches and α equal to 15 degrees for higher rates of expansion. A series of cams providing a range of expansion rates were fabricated for each of the assemblies. Nominal expansion rates (with assumed discharge coefficient equal to one) ranged from 25 to 70 $\sec^{-1}$. Higher rates of expansion were prohibited by the excessive valve train forces incurred when the poppet valve opened abruptly at the initial stage of expansion.

The process of valve dimension optimization required that the valve lift function S (θ) (where θ is the relative camshaft angle) be calculated for many different values of α and d, and for various expansion rates, a procedure well suited to the use of a digital computer. Additionally, once a configuration had been selected and the valve lift function S(θ) calculated, it was necessary to correct that function, since a flat face follower-cam arrangement was used, to obtain the required cam profile (65). Conventional graphical correction techniques lacked the required accuracy, and so an algebraic analog of the usual graphical method was developed, programmed and incorporated into the previous program. The basis for the correction program follows.

The valve lift function S (θ (I)) was considered the first column in an N by N + 1 matrix. Each element, S (I,1), in the first column defined subsequent terms in the I^{th} row of the matrix. The elements in each row corresponded, geometrically, to points on a straight line passing through S(I,1) and normal to the line connecting S (I,1) and the origin. (see figure 34). Each column of the matrix, with the exception of the first, will correspond to a given camshaft angle θ (J-1), forming a set with the parent element in the first column S(J,1), one term of which will equal the cam radius at the angle θ(J-1). Inspection of figure 34 will reveal that it is the smallest term in this set which equals the appropriate cam radius.

The basic program was also modified slightly to determine performance at off-design conditions, specifically at motor speeds different from the normal rpm.

The method of fabricating the poppet valve cams involved first mounting a cam blank in a precision machinists' turntable which was, in turn, mounted on the bed of a vertical milling machine. The axes of symmetry of the cam blank, the turntable and the milling machine were all coincident. The transverse feed of the miller was then used to position the part relative to the cutter so that the edge of the cutter coincided with the required cam radius at an initial angle θ_o. Excess material was machined off, after which the turntable was moved two degrees and the transverse feed adjusted to coincide with a new cam radius (specified by the computer program). Additional material was removed, and the process was repeated until the desired cam profile had been generated. The small ridges formed as a consequence of the finite

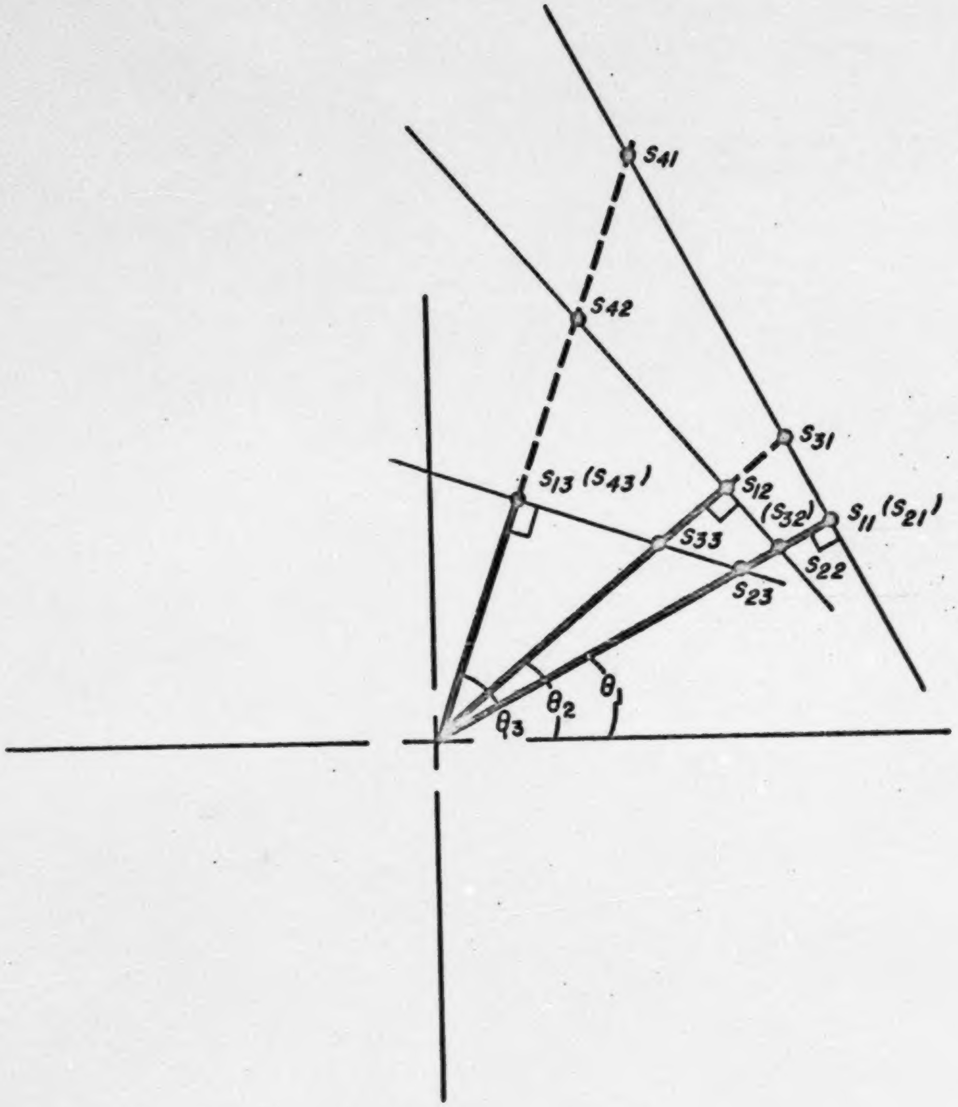
S_{41}
S_{42}
S_{31}
S_{13} (S_{43})
S_{12}
(S_{32})
S_{11} (S_{21})
S_{33}
S_{22}
S_{23}
θ_1
θ_2
θ_3

CAM PROFILE GENERATION

FIGURE 34

number of machining operations were removed using a hand file. A cam profile was generated in this manner which was accurate within 1.001 inches of the nominal profile.

```
$JOB HODGES, 20 30 112,206
NO
$F4
      INTEGER C,B,BI
      DIMENSION S(100,100),R(100),THETA(100),XR(100)
      DATA S/10000*2.0/
      READ(5,1) D,VO,TOIN,GAMMA,RX,GEE,ALPHA
      READ (5,2) OMEGA,DANG,DPONDT
      READ(5,7) BASE
      WRITE(6,3) D,VO,TOIN,GAMMA,RX,GEE,ALPHA
      WRITE(6,4) OMEGA,DANG,DPONDT
      WRITE(6,9) BASE
      WRITE(6,9)
      OMEGA=6.2832/60.*OMEGA
      DANG=3.1416/180.*DANG
      XK1=VO/(GAMMA*(SQRT(GAMMA*RX*GEE))*(2./(GAMMA+1.))**((GAMMA+1.)/
     1(2.*(GAMMA-1.))))
      XK2=D/SIN(ALPHA)/COS(ALPHA)
      XK3=3.1416*(SIN(ALPHA))**2*COS(ALPHA)*SQRT((COS(ALPHA))**2+1.)
      XAREA=XK1/SQRT(TOIN)*DPONDT
      SINIT=.5*(XK2-SQRT((XK2**2-4.*XAREA/XK3)))
      TOTIME=.5/DPONDT
      DTHETA=OMEGA*TOTIME
      IF(DTHETA-.5233) 10,20,20
 10   DTHETA=.5233
 20   XITHET =.2*DTHETA
      IF(XITHET -.1744)30,40,40
 30   XITHET =.1744
 40   B=XITHET /DANG
      DS=SINIT/B
      C=DTHETA/DANG+B
      BI=B+1
      DTIME=TOTIME/(C-B)
      J=1
      DO 90 I=1,B
      S(I,J)=DS*(I-1)
      THETA(I)=DANG*(I-1)
 90   CONTINUE
      TIME=0.0
      DO 100 I=BI,C
      PONM=1.-TIME*DPONDT
      AREA=XK1/SQRT(TOIN)*DPONDT/PONM**((3.*GAMMA-1.)/(2.*GAMMA))
      S(I,J)=.5*(XK2-SQRT((XK2**2-4.*AREA/XK3)))
      THETA(I)=DANG*(I-1)
      TIME=TIME+DTIME
 100  CONTINUE
      DO 50 I=1,C
      S(I,J)=S(I,J)+BASE
 50   CONTINUE
      DO 110 I=1,C
      Z=SIN(THETA(I))
      IF(Z) 120,130,120
 130  CONTINUE
      KK=C+1
      DO 65 J=2,KK
      THETA(J)=DANG*(J-2)
      S(I,J)=S(I,1)/COS(THETA(J))
      IF (S(I,J)-1.) 83,84,84
 84   S(I,J)=1.
 83   CONTINUE
```

```
65    CONTINUE
      GO TO 70
120   XM=-COS(THETA(I))/SIN(THETA(I))
      XINT=S(I,1)/SIN(THETA(I))
      KK=C+1
      DO 60 J=2,KK
      THETA(J)=DANG*(J-2)
      IF(SIN(THETA(J))) 161,162,161
162   S(I,J)=S(I,1)/COS(THETA(I))
      GO TO 163
161   CONTINUE
      S(I,J)=XINT/(SIN(THETA(J))-XM*COS(THETA(J)))
163   CONTINUE
      IF(S(I,J)-1.) 81,82,82
82    S(I,J)=1.
81    CONTINUE
60    CONTINUE
70    CONTINUE
110    CONTINUE
      KK=C+1
      DO 80 J=2,KK
      R(1)=S(1,J)
      DO 140 I=1,C
      R(I+1)=AMIN1(R(I),S(I,J))
140   CONTINUE
      XR(J)=R(KK)
80    CONTINUE
      DO 180 J=1,C
      THETA(J)=57.2956*THETA(J)
180   CONTINUE
      WRITE(6,5)
      XR(1)=BASE
      DO 150 J=2,C
      DELTS=XR(J)-XR(J-1)
      WRITE(6,6) S(J,1),XR(J),THETA(J),DELTS
150   CONTINUE
1     FORMAT(7F9.3)
2     FORMAT(3F8.4)
3     FORMAT('1D=',F10.3,5X,'VO=',F10.3,5X,'TOIN=',F10.3,5X,'GAMMA=',
     1F10.3,5X,'R=',F10.3,5X,'GEE=',F10.3,5X,'ALPHA=',F10.3)
4     FORMAT(1X,'OMEGA=',F8.4,'   DANG=',F8.4,'   DPONDT=',F8.4)
5     FORMAT(1X,' FOLLOWER        CAM            THETA      DIFFERENCE')
6     FORMAT(1X,F8.4,5X,F8.4,5X,F8.4,5X,F8.4)
7     FORMAT(F9.5)
8     FORMAT(1X,'THE BASE LINE RADIUS IS',F9.5)
9     FORMAT(1X,'CAM NUMBER 70A100')
      STOP
      END
$EOF
.500     12.901   4400.    1.33     639.6    386.4    .3480
600.     1.        100.
.410
$EOJ
T
T
```

Appendix D

Spectroscopic Apparatus Description, Testing and Alignment

A. General.

The optical system of the spectroscopic monitoring apparatus is quite simple (figure 11). Radiant emission from a Jarrell/Ash high pressure xenon arc lamp was collimated, passed through the combustion chamber (in which were mounted U.V. grade sapphire windows) and imaged upon the entrance slits of a Jarrell/Ash 1/2 meter Ebert monochromator. Monochromatic radiant intensity was detected with an EMI model 6256B photomultiplier, used with a Brandenburg model 500 power supply. A circuit diagram of the photomultiplier assembly is presented in figure 35.

The bi-convex collimating and decollimating spherical lenses were of U.V. grade quartz, with a focal length of 10.2 cm., and a diameter of 51 mm. Diameter of the collimated beam was 18 mm., the effective diameter of the sapphire windows. The f-number of the optical train, therefore, was f/5.7, and the limiting f-number was that of the monochromator, f/8.6.

B. Window Design.

Thickness of the sapphire window was based on anticipated peak cylinder pressures. The diameter of the windows were chosen so that the limiting f-number of the system was not that of the optical train. An effective diameter of about 18 mm. was convenient, which led to an overall window diameter, allowing for support, of 1 inch. An empirical relation between peak pressure and the window thickness-diameter ratio

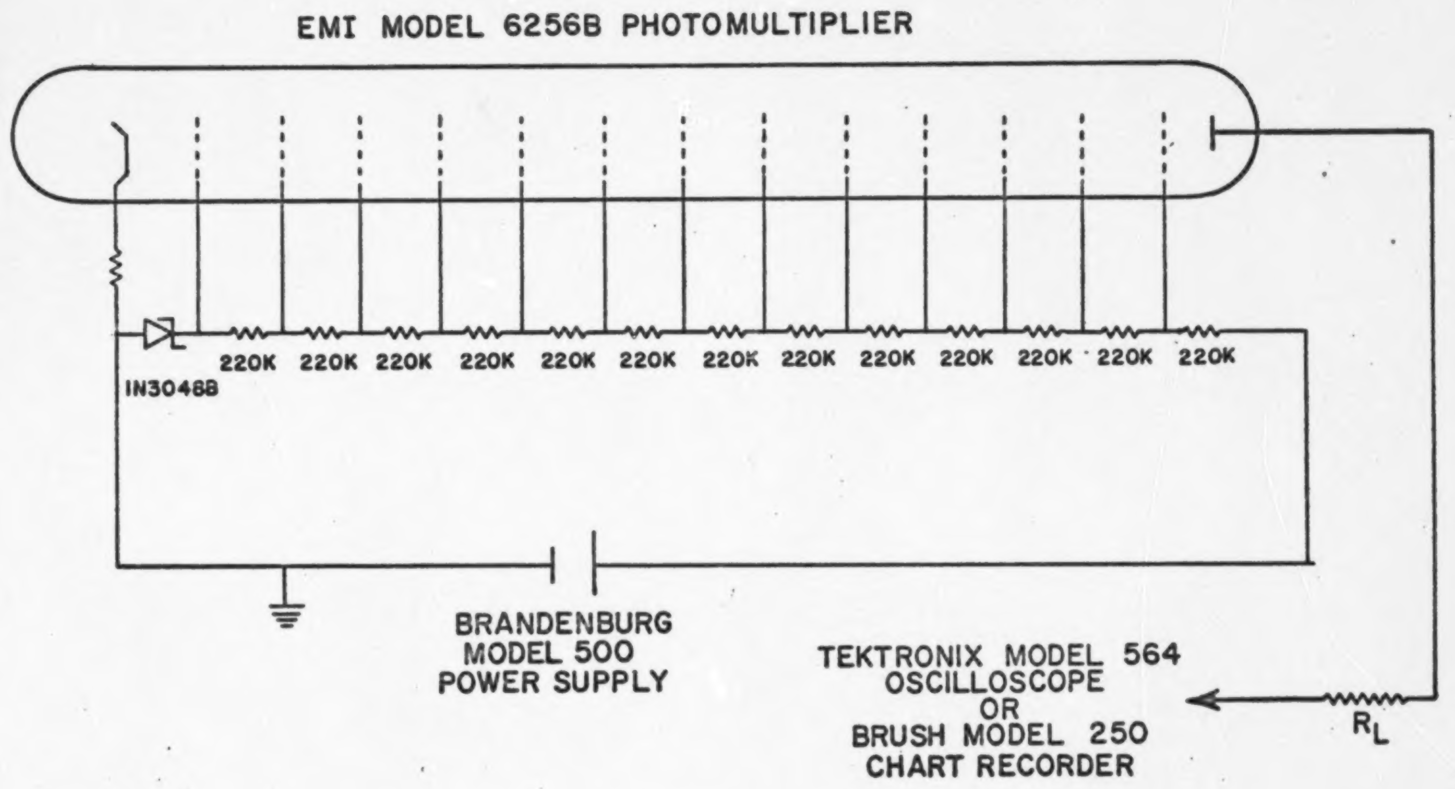
EMI MODEL 6256B PHOTOMULTIPLIER
220K
220K
220K
220K
220K
220K
220K
220K
220K
220K
220K
220K
220K
IN3046B
BRANDENBURG MODEL 500 POWER SUPPLY
TEKTRONIX MODEL 564 OSCILLOSCOPE OR BRUSH MODEL 250 CHART RECORDER
R_L

PHOTOMULTIPLIER CIRCUIT DIAGRAM

FIGURE 35

has been developed by Linde for simply supported thin plates of sapphire (thickness-diameter ratio between 0.1 and 1.0)(43). That is,

$$P \frac{d}{h}^{2} = 180,000$$

with P in psia

If P = 1500 psia and d = 1.000 inches window thickness (h) should be in excess of .091 in. A standard window, of 1.000 inch diameter and 0.125 inches thickness was selected.

C. Optical Alignment.

A University Laboratories model 200 helium-neon gas laser was used to align the optical system. The laser emitted an unpolarized, collimated, 1.4 mm diameter beam of radiation at 6328 Å. An advantage of the laser as an alignment tool is that reflections from the front and rear surfaces of the windows and lenses, and from the monochromator slits, are clearly visible. By adjusting the combustion chamber and the quartz lenses so that reflections from the window and lenses fall back upon the source it is possible to align components not only in the vertical and horizontal directions, but in rotation (about a vertical axis) as well.

Alignment proceeded as follows: the laser was first positioned so that the collimated beam passed through the centers of both combustion chamber windows. The quartz collimating lenses were properly located and aligned, and the monochromator was moved into position with the top cover removed so that the optical path within the monochromator could be observed. The monochromator was then aligned so that, with the wavelength drum of the monochromator set at 6328A, the light which entered the entrance slit illuminated the exit slit of the monochromator. Subsequently the laser was removed and replaced with the xenon arc lamp. The lamp was positioned to provide a uniform, homogeneous collimated beam. Alignment of the lamp was less precise than that of the optical train,however. Because of the strong temperature gradients within the arc, wavelength dependence of recorded output emission will depend upon the portion of the arc that is imaged upon the monochromator. No facilities were available to obtain iso-radiance contours for the arc, and so a procedure of trial and error was used to select a portion of the arc image for which, in the region of the spectrum used in this work, the lamp output was not a strong function of the wavelength. The criteria for the proper focus was the maximization of the resolution of the instrument, as determined by inspection of nitric oxide absorption bands at very low pressure.

D. Calibration.

The monochromator was calibrated by scanning the spectrum of a low pressure mercury lamp and comparing the wavelengths of known emission lines with the dial setting on the monochromator. The instrument was adjusted to minimize the error at the 2537Å line of mercury. Over the range of calibration the error did not exceed 2 Å.

E. Resolution Check.

The resolution of the apparatus was determined for a variety of entrance-exit slit combinations by slowly scanning the 2537Å mercury line, which is sufficiently narrow to ensure that any observable line width can be attributed to instrumental error. Results are presented in figure 36. All nitric oxide absorption data were acquired with 50μ entrance and exit slits, the slit combination which provided the greatest resolution.

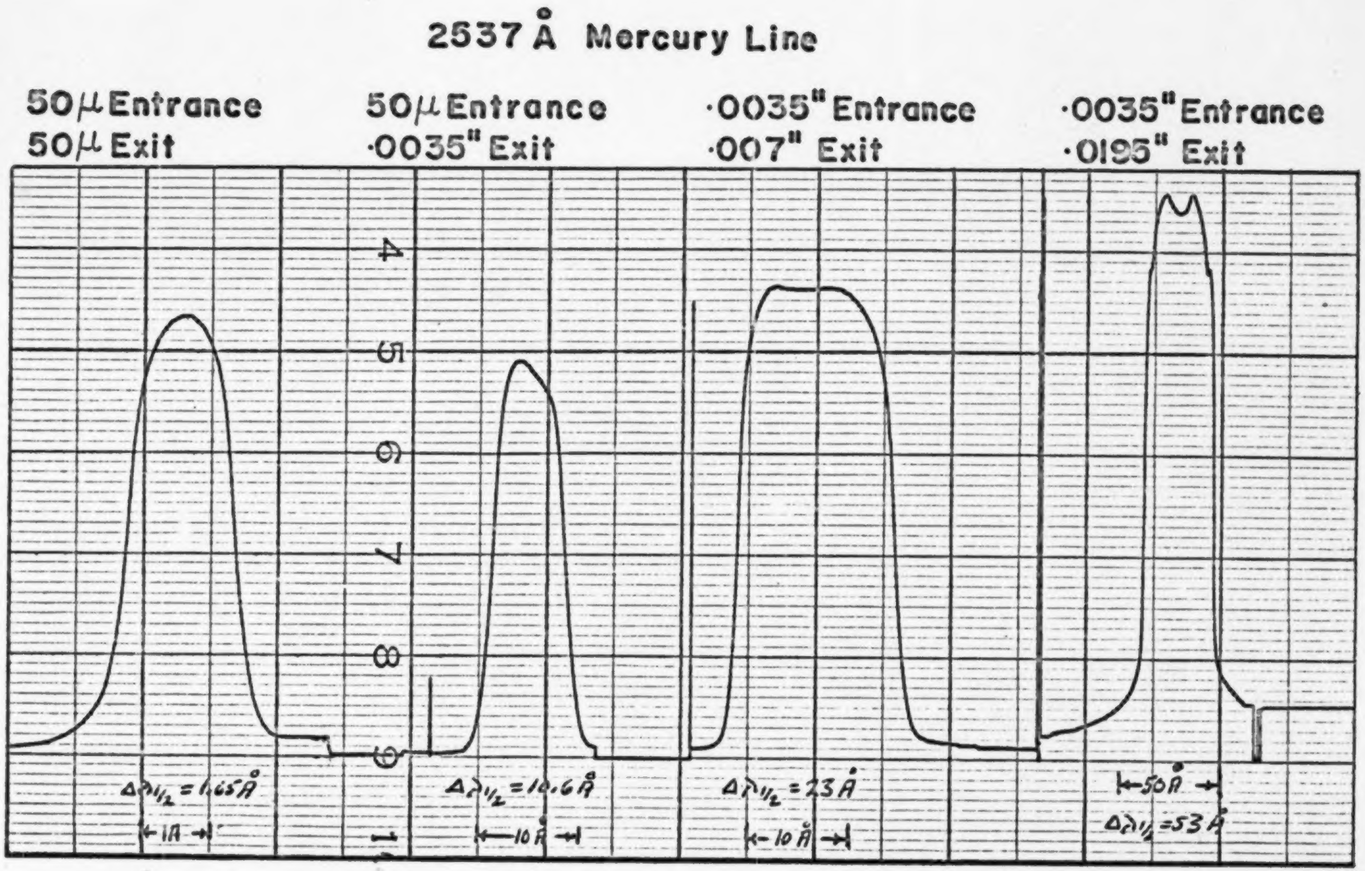

2537 Å Hg LINE AS A FUNCTION OF SPECTROMETER ENTRANCE AND EXIT SLIT WIDTH

FIGURE 36

Appendix E

Theoretical Equilibrium Nitric Oxide Concentration

A. General.

A computer program was developed to calculate the theoretical peak combustion temperature distribution within the combustion chamber assuming no mixing of, or heat transfer between, adjacent gas elements. The equilibrium concentrations of ten chemical species, including nitric oxide, corresponding to these temperature distributions were also determined. No attempt was made to introduce a kinetic scheme since the gross kinetics of nitric oxide formation and decomposition are fairly well established (26, 27), and specific knowledge of the mechanism by which the local thermodynamic state of the gas changes with time is a prerequisite to a more detailed kinetic model.

B. Theoretical Model.

The combustion chamber reactant gas was divided into N sections of equal mass. The walls of the control volumes surrounding and defining each section, or "shell", were assumed adiabatic and impermeable. Chamber pressure equilibration was assumed instantaneous, and the state of the gas was assumed adequately described by the perfect gas law. Applying an energy balance to an arbitrary shell,

$$\delta q = dH - VdP = 0 \qquad (1)$$

$$\Delta H = \int_i^f VdP \qquad (2)$$

$$H_f^o\text{prod} + \int_o^{T_i} \overline{C}_{p\ \text{prod}} dT + \int_{T_i}^{T_f} \overline{C}_{p\ \text{prod}} dT - H^o_{f\text{reac}} - \int_o^{T_i} \overline{C}_{p\ \text{reac}} dT = \int_i^f vdP \qquad (3)$$

or,

$$\Delta H_f^o + \int_o^{T_i} \Delta\overline{C}_p dT = \int_{T_i}^{T_f} \overline{C}_{p\text{prod}} dT + \int_i^f vdP \quad . \qquad (4)$$

where H is the gas enthalpy (cal/mole°K)

V is the shell volume (liter)

p is the chamber pressure (atm)

H_f^o is the standard heat of formation (cal/mole°K)

Cp is the average specific heat of the mixture (cal/mole°K)

T is the shell temperature (°K)

The specific heats and heats of formation of products and reactants were assumed exclusive functions of temperature. Standard heats of formation were obtained from references (66) and (69). When needed, power series expansions of Cp(T) were obtained from reference (68). Reference (69) was used as the source of the thermodynamic properties of iso-octane fuel (2,2,4-tri-methyl pentane).

The change in the heats of formation and average specific heat of the gas mixture will, in general, be a function of the gas composition. The reactant gas composition was assumed constant with "time" (which does not, of course, appear explicitly in the analysis). The product gas composition shift with temperature and pressure was assumed in conformance with the following set of equilibrium equations.

$$H_2 + \frac{1}{2}O_2 \rightleftarrows H_2O \qquad (5)$$

$$H_2 + CO_2 \rightleftarrows H_2O + CO \qquad (6)$$

$$2OH + H_2 \rightleftarrows 2H_2O \qquad (7)$$

$$H_2 + NO \rightleftarrows H_2O + \frac{1}{2}N_2 \qquad (8)$$

$H_2 \rightleftarrows 2H$ (9)

$O_2 \rightleftarrows 2O$ (10)

The solution of these equations (and the pertinent mass balances) for a given temperature and pressure appears as a subroutine in the main program. The subroutine is based loosely on the work of Vickland, Stange, Bell and Starkman, and the validity of the program was verified by comparing the results of the two routines. (53).

The system can be conveniently divided into three regimes containing unburned, burning and fully burned gas. It should be noted, however, that implicit in this distinction is the assumption that the combustion reaction rates are infinite, and combustion is complete in a given shell prior to the initiation of combustion in the next shell. This is not true; photographs of operating S.I. engines indicate that, in certain cases, combustion (as evidenced by the emission of light) is still proceeding in the first "shell" after the flame has propogated throughout the chamber (70). The result of this effect would be to suppress temperature gradients. Experimental evidence indicates, however, that the assumption does not introduce a serious error.

Equation (4) applies equally to all regimes, the only differences are the relative importance of the terms in the equation. For example, in the unburned gas ΔH_f^o and $\int_{T_o}^{T_i} \overline{C}p\,dT$ are zero. In the burning shell ΔH_f^o and $\int_{T_i}^{T_f} \overline{C}p\,dT$ are the major terms; $\int_i^f v\,dP$ and $\int_o^{T_i} \Delta\overline{C}p_{prod}\,dT$ are minor corrections. In the burned shell ΔH_f^o, $\int_{T_i}^{T_f} \overline{C}p_{prod}\,dT$ and $\int_i^f v\,dP$ are all significant.

All the partitions, or "shells", within the system are coupled through the requirements that the pressure within the chamber is uniform, and the total volume of the system is constant.

Then $Pv_j = n_j(T_j,P)\ R\ T_j$ (11)

$\Delta H_j\ (T_j,P) = \int_i^f v_j dP$ (12)

and $\Sigma v_j = V_T$ (13)

Where n is the number of moles in a shell and the subscript j can refer to either an unburned, burning or fully burned shell. In this set of seven equations there are seven unknowns (P,Vu, Vs, Vb, Tu, Ts, Tb), providing a fully specified problem. Note that for the unburned gas equations (11) and (12) can be combined to form Pv^k=const. It was convenient, however, to keep the equations for all shells in the same form.

C. Solution of Equations (see figure 37).

For an arbitrary burning shell initial conditions, consisting of an initial pressure, and a temperature and shell volume distribution, were specified. Then the change in heat of formation of the burning shell at initial burning shell temperature, T_{si}, was calculated. The burning shell temperature was incremented by a given amount and estimates of the corresponding temperature increments of the other shells were made. With this temperature distribution (and an approximation to

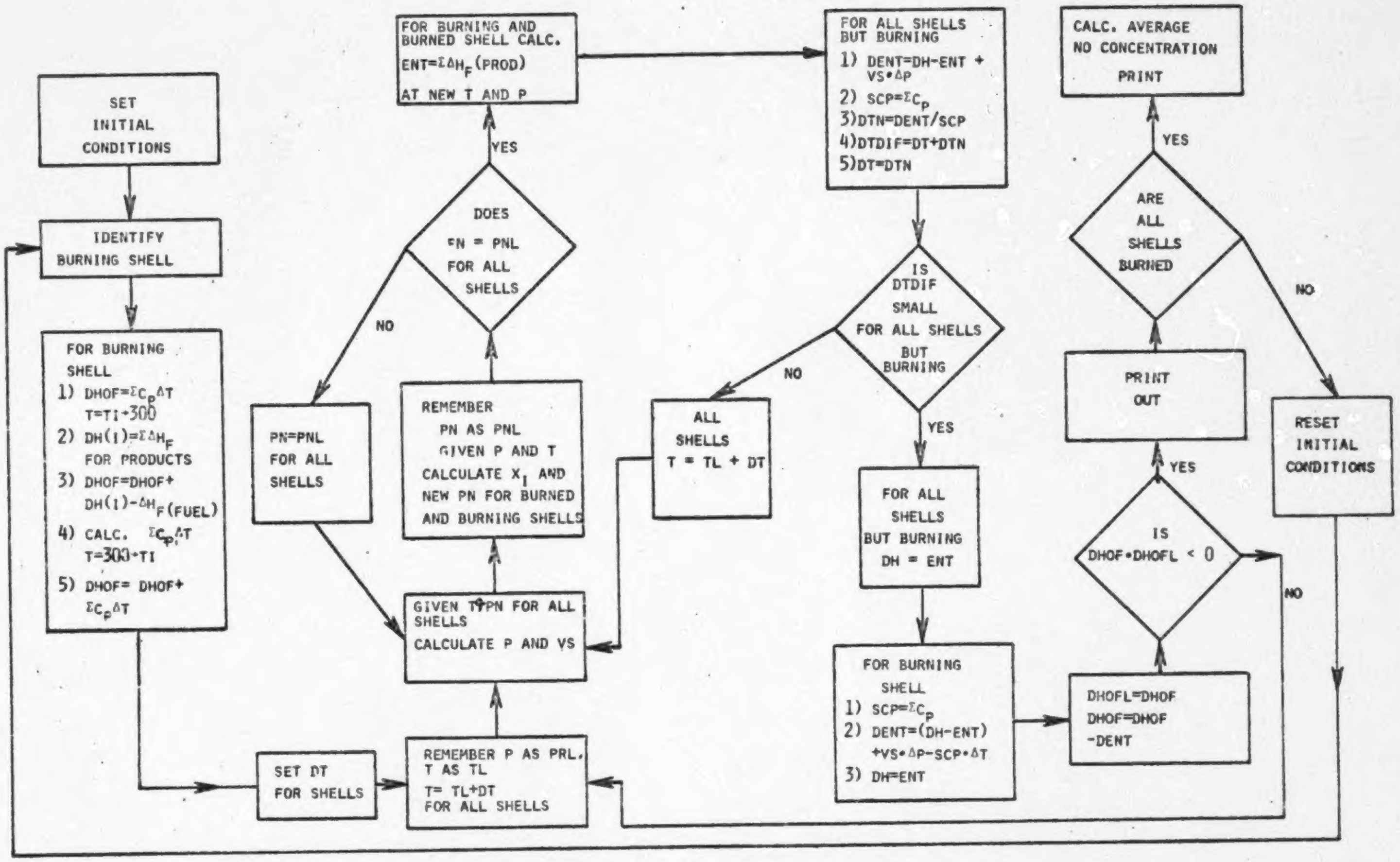
SET INITIAL CONDITIONS
IDENTIFY BURNING SHELL
FOR BURNING SHELL
1) DHOF=ΣCpΔT T=TI+300
2) DH(I)=ΣΔHF FOR PRODUCTS
3) DHOF=DHOF+ DH(I)-ΔHF(FUEL)
4) CALC. ΣCpΔT T=300+TI
5) DHOF= DHOF+ ΣCpΔT
SET DT FOR SHELLS
REMEMBER P AS PRL, T AS TL T= TL+DT FOR ALL SHELLS
GIVEN T+PN FOR ALL SHELLS CALCULATE P AND VS
REMEMBER PN AS PNL GIVEN P AND T CALCULATE XI AND NEW PN FOR BURNED AND BURNING SHELLS
DOES PN = PNL FOR ALL SHELLS
NO
PN=PNL FOR ALL SHELLS
YES
FOR BURNING AND BURNED SHELL CALC. ENT=ΣΔHF(PROD) AT NEW T AND P
FOR ALL SHELLS BUT BURNING
1) DENT=DH-ENT + VS•ΔP
2) SCP=ΣCp
3)DTN=DENT/SCP
4)DTDIF=DT+DTN
5)DT=DTN
IS DTDIF SMALL FOR ALL SHELLS BUT BURNING
NO
ALL SHELLS T = TL + DT
YES
FOR ALL SHELLS BUT BURNING DH = ENT
FOR BURNING SHELL
1) SCP=ΣCp
2) DENT=(DH-ENT) +VS•ΔP-SCP•ΔT
3) DH=ENT
DHOFL=DHOF DHOF=DHOF -DENT
IS DHOF•DHOFL < 0
YES
NO
PRINT OUT
ARE ALL SHELLS BURNED
YES
CALC. AVERAGE NO CONCENTRATION PRINT
NO
RESET INITIAL CONDITIONS

THEORETICAL FLAME TEMPERATURE AND PEAK EQUILIBRIUM NITRIC OXIDE CONCENTRATION COMPUTER PROGRAM FLOW CHART

FIGURE 37

the number of moles), new pressure and shell volume distributions were calculated. A new gas composition and number of moles were then computed, and these values were recycled to calculate another pressure and shell volume distribution. The procedure continued until the difference in the number of moles calculated from one cycle to the next was arbitrarily small. The change in the heat of formation of products in the burned shells was then determined, and the information was used, in conjunction with equation (4), to acquire a better estimate of the change in burned gas temperature as a consequence of the increase in pressure due to combustion. This process continued to convergance, after which the state of the burned gas was known for a given increment in the temperature of the burning gas. The enthapy of the burning shell was compared with the enthalpy change required for complete combustion of the shell. If the enthalpy of the burning shell was too small, the temperature of the burning gas was re-incremented and the computation continued. If the enthalpy was equal to or higher than that required, calculations terminated on the given shell and proceeded for the next shell.

A program listing is included at the end of this appendix with a typical printout.

D. Discussion.

The shape, or dimension of a shell does not appear explicitly in the mathematical model of the system. A shell is characterized by a fixed and unique mass and, providing no mixing or heat transfer occurs between shells, it is free to move throughout the combustion chamber during and after combustion without violating any of the precepts upon which the model is based.

If "freezing" of nitric oxide always occurred at peak chamber temperatures, then such mixture motion as would occur inadvertantly (or consciously, through the inducement of mixture "swirl" prior to ignition) would have no effect on the average value of the product gas concentration of nitric oxide after combustion, except indirectly, as it increases mixing and heat transfer rates during combustion.

Most of the assumptions upon which the theoretical model are based tend to result in temperatures gradients and peak pressures in excess of the actual values. For example, peak pressures based on a real gas law would be lower that those calculated from the perfect gas law used in this analysis. Incorporation of a real equation of state would be a simple matter, requiring only an adjustment in equation (11).

Introducing the effect of mixing, radiant heat transfer, heat transfer to the wall, and leakage would, of necessity, be semi-empirical.

If account were taken of finite combustion rates the effect would also be a reduction in the temperature gradient across the combustion chamber. In fact, even though time does not appear explicitly in the present treatment the model, where finite flame velocity and infinite combustion rate are implied, may be viewed as a bound of the true physical situation. The other extreme would be the isothermal case where flame velocity is assumed infinite and combustion rate finite. A better approximation to the actual values may be obtained, taking account of finite combustion rates, by introducing the concept of a "partially burned" shell. That is, the enthalpy of a given shell would be increased at a certain "rate", which would be based on experimental data. Once the enthalpy of a given shell exceeded that required for complete combustion, addition of heat would cease and the shell would subsequently be treated as a "fully burned" shell, as in the present analysis. Simultaneously, the total number of partially and fully burned shells would also be increased at a certain rate, based on observed flame propogation velocities. Time need not appear explicitly in the analysis if the combustion rate is expressed as a function of the flame velocity. In this manner it is possible to apply, to good approximation, an homogeneous analysis to an essentially heterogeneous problem.

```
      DIMENSION VS(50),T(50),TL(50),PN(50),DTN(50),DT(50),DH(50),
     1 ENT(50),DENT(50),XH2O(50),XH2(50),XH1(50),XOH(50),XCO2(50),
     2 XCO(50),XN2(50),XNO(50),XO2(50),XO1(50),PNL(50)
C     INPUT INITIAL CONDITIONS
      READ 1000,PHI,NS,VT,P,TI
1000  FORMAT(F,I,3F)
200   FORMAT('1',5X,'TEMPERATURE= ',F6.1,' DEGREES KELVIN'/5X,
     8 'PRESSURE= ',F6.2,' ATMOSPHERES'/5X,'PHI= ',F4.2)
500   FORMAT(///5X,'SHELL',5X,'TEMP',5X,'PRESSURE',5X,'VOLUME',5X,
     7 'NO CONCENTRATION'//)
      TYPE 200,TI,P,PHI
      TYPE 500
      RNS=NS
      TN=P*VT/(RG*TI)
      FN=(TN/RNS)*PHI/(PHI+12.5*4.76)
      DO 100 I=1,NS
      VS(I)=VT/RNS
      T(I)=TI
      PN(I)=TN/RNS
      XN2(I)=47./PHI*FN
      XO2(I)=12.5/PHI*FN
      DT(I)=.50
      DH(I)=0.00
100   ENT(I)=0.00
      XO2(0)=XO2(1)
      XH2O(0)=8.*FN
      XCO2(0)=6.*FN
      DO 101 I=1,NS
      DTN(I)=10.
      DHOFL=0.00
      TI=T(I)
C     CALCULATE THE HEAT OF COMBUSTION IN BURNING SHELL
      DHOF=0.00
102   T(I)=T(I)-25.
      CALL CAPAC(T(I),CH2O,CH2,CH1,COH,CCO2,CCO,CN2,CNO,CO2,CO1)
      CF=FN*(25.+(T(I)-300.)*3./50.)
      CN2=XN2(I)*CN2
      CO2=XO2(I)*CO2
      DHOF=DHOF-25.*(CF+CN2+CO2)
      IF(T(I).GT.300)GO TO 102
      XO2(I)=XO2(I-1)
      XH2O(I)=XH2O(I-1)
      XCO2(I)=XCO2(I-1)
      CALL CONC(T(I),P,PHI,PN(I),FN,XH2O(I),XH2(I),XH1(I),XOH(I),
     3 XCO2(I),XCO(I),XN2(I),XNO(I),XO2(I),XO1(I))
      DHH2O=XH2O(I)*(-57797.9)
      DHCO2=XCO2(I)*(-94051.8)
      DHCO=XCO(I)*(-26415.7)
      DHF=FN*(-53570.)
      DH(I)=DHCO2+DHCO+DHH2O
      DHOF=DHOF+DH(I)-DHF
103   T(I)=T(I)+25.
      CALL CAPAC(T(I),CH2O,CH2,CH1,COH,CCO2,CCO,CN2,CNO,CO2,CO1)
      CO2=XO2(I)*CO2
      CN2=XN2(I)*CN2
      CCO2=XCO2(I)*CCO2
      CH2O=XH2O(I)*CH2O
      CCO=XCO(I)*CCO
      CH2=XH2(I)*CH2
      DHOF=DHOF+25.*(CN2+CCO2+CH2O+CCO+CH2)
      IF(T(I).LT.TI)GO TO 103
```

```
C       CALCULATE THE STATE OF THE GAS AFTER BURNING IS COMPLETE
        DT(I-1)=.50
        DT(I)=10.
115     PRL=P
        DO 104 J=1,NS
        TL(J)=T(J)
104     T(J)=TL(J)+DT(J)
107     CALL SOLVE(VT,NS,PN,T,P,VS)
        DO 105 J=1,I
        PNL(J)=PN(J)
105     CALL CONC(T(J),P,PHI,PN(J),FN,XH2O(J),XH2(J),XH1(J),XOH(J),
     4  XCO2(J),XCO(J),XN2(J),XNO(J),XO2(J),XO1(J))
        DO 106 J=1,I
        IF(ABS(PN(J)-PNL(J)).GT.1.E-07)GO TO 107
106     CONTINUE
        DO 108 J=1,I
        DHH2O=XH2O(J)*(-57797.9)
        DHH1=XH1(J)*52089.
        DHOH=XOH(J)*10060.
        DHNO=XNO(J)*21600.
        DHO1=XO1(J)*59159.
        DHCO2=XCO2(J)*(-94051.8)
        DHCO=XCO(J)*(-26415.7)
108     ENT(J)=DHH2O+DHH1+DHOH+DHNO+DHO1+DHCO2+DHCO
        DO 109 J=1,NS
        IF(J.EQ.I)GO TO 109
        DENT(J)=(DH(J)-ENT(J))+VS(J)*(P-PRL)*24.206
        CALL CAPAC(T(J),CH2O,CH2,CH1,COH,CCO2,CCO,CN2,CNO,CO2,CO1)
        CH2O=XH2O(J)*CH2O
        CH2=XH2(J)*CH2
        CH1=XH1(J)*CH1
        COH=XOH(J)*COH
        CCO2=XCO2(J)*CCO2
        CCO=XCO(J)*CCO
        CN2=XN2(J)*CN2
        CNO=XNO(J)*CNO
        CO2=XO2(J)*CO2
        CO1=XO1(J)*CO1
        CF=FN*(25.+(T(I)-300.)*3./50.)
        IF(J.GT.I)GO TO 117
        SCP=CH2O+CH2+CH1+COH+CCO2+CCO+CN2+CNO+CO2+CO1
        GO TO 118
117     SCP=CN2+CO2+CF
118     DTN(J)=DENT(J)/SCP
        DTDIF=ABS(DT(J)-DTN(J))
109     DT(J)=DTN(J)
        DO 119 J=1,NS
        IF(J.EQ.I)GO TO 119
        IF(DTDIF.GT.1.E-02)GO TO 110
119     CONTINUE
        GO TO 112
110     DO 113 J=1,NS
113     T(J)=TL(J)+DT(J)
        GO TO 107
112     DO 111 J=1,NS
        IF(J.EQ.I)GO TO 111
        DH(J)=ENT(J)
111     CONTINUE
```

```
      CALL CAPAC(T(I),CH2O,CH2,CH1,COH,CCO2,CCO,CN2,CNO,CO2,CO1)
      CH2O=XH2O(I)*CH2O
      CH2=XH2(I)*CH2
      CH1=XH1(I)*CH1
      COH=XOH(I)*COH
      CCO2=XCO2(I)*CCO2
      CCO=XCO(I)*CCO
      CN2=XN2(I)*CN2
      CNO=XNO(I)*CNO
      CO2=XO2(I)*CO2
      CO1=XO1(I)*CO1
      SCP=CH2O+CH2+CH1+COH+CCO2+CCO+CN2+CNO+CO2+CO1
      DENT(I)=(DH(I)-ENT(I))+VS(I)*(P-PRL)*24.206-SCP*DT(I)
      DH(I)=ENT(I)
      DHOFL=DHOF
      DHOF=DHOF-DENT(I)
      IF(DHOFL*DHOF)114,115,115
114   DO 121 J=1,I
121   XNO(J)=XNO(J)/PN(J)
      TYPE 116,(J,T(J),P,VS(J),XNO(J),J=1,I)
116   FORMAT(6X,I2,6X,F6.1,4X,F6.2,7X,F6.4,8X,F9.7)
120   FORMAT(//)
101   TYPE 120
      SNO=0.0
      DO 122 J=1,NS
122   SNO=SNO+XNO(J)
      AVNO=SNO/RNS
      TYPE 123,AVNO
123   FORMAT(//5X,'AVERAGE NITIC OXIDE CONCENTRATION= ',
     5 F9.7//)
      STOP
      END
      SUBROUTINE CONC(T,P,PHI,PN,FN,H2O,H2,H1,OH,CO2,CO,RN2,RNO,O2,O1)

      TT=T
      IF(T-1250.)106,1,1
106   T=1250.
1     PNL=PN
      DET1=2.
      DET2=2.
      CDIF=0.0
      ODIF=0.0
      HDIF=0.0
      CON=P/PN
      RK1=8.229649E-04*EXP(3.04641926E04/T)/CON**(-.5)
      RK2=1.813941429E01*EXP(-2.7249693E03/T)
      RK3=(1.605606E-04*EXP(3.521466370E04/T))**2/CON**(-1)
      RK4=1.793050E-04*EXP(4.135447530E04/T)/CON**(-.5)
      RK5=(1.431885036E03*EXP(-2.738008250E04/T))**2/CON
      RK6=(3.165194272E03*EXP(-3.055530540E04/T))**2/CON
      RN=FN*94./PHI
      O=FN*25./PHI
      C=FN*8.
      H=FN*18.
```

```
C       H2O ADJUSTMENT BEGINS
        IF(PHI.GE.1.0)GO TO 2
303     CO2=C*O2**.5*RK1/(RK2+O2**.5*RK1)
2       H2=(C-CO2)*H2O/(RK2*CO2)
        IF(H2-1.E-08)3,4,4
3       H2=0.00
4       H1=(RK5*(C-CO2)*H2O/(RK2*CO2))**(.5)
        IF(H1-1.E-08)5,6,6
5       H1=0.00
6       OH=(RK2*CO2*H2O/(RK3*(C-CO2)))**(.5)
        IF(OH-1.E-08)7,8,8
7       OH=0.00
8       HN=2.*H2O+2.*H2+H1+OH
        H2OL=H2O
        H2O=H2O-(HN-H)/DET1
        HDIFL=HDIF
        HDIF=ABS(H2O-H2OL)
        IF(HDIF-HDIFL)22,23,23
23      DET1=DET1+2.
22      IF(ABS(H2O-H2OL)-5.E-09)9,9,2
C       CO2 OR O2 ADJUSTMENT BEGINS
9       OH=(RK2*CO2*H2O/(RK3*(C-CO2)))**(.5)
        IF(OH-1.E-08)10,11,11
10      OH=0.00
11      CO=C-CO2
        IF(CO-1.E-08)12,13,13
12      CO=0.00
13      RNO=RK2*CO2*RN2**(.5)/(RK4*(C-CO2))
        IF(RNO-1.E-08)14,15,15
14      RNO=0.00
15      IF(PHI.LT.1.0)GO TO 17
        O2=(RK2*CO2/(RK1*(C-CO2)))**2
        IF(O2-1.E-08)16,17,17
16      O2=0.00
17      O1=RK6**(.5)*RK2*CO2/(RK1*(C-CO2))
        IF(O1-1.E-08)18,19,19
18      O1=0.00
19      ON=2.*CO2+CO+H2O+OH+RNO+2.*O2+O1
        IF(PHI.LT.1.0)GO TO 300
        CO2L=CO2
        CO2=CO2-(ON-O)/DET2
        CDIFL=CDIF
        CDIF=ABS(CO2-CO2L)
        IF(CDIF-CDIFL)24,25,25
25      DET2=DET2+2.
24      IF(ABS(CO2-CO2L)-5.E-09)20,20,9
300     O2L=O2
        O2=O2-(ON-O)/DET2
        ODIFL=ODIF
        ODIF=ABS(O2-O2L)
        IF(ODIF-ODIFL)301,302,302
302     DET2=DET2+2.
301     IF(ABS(O2-O2L)-5.E-09)20,20,303
20      RN2=(RN-RNO)/2.
C       TEST FOR CONVERGENCE
        PN=H2O+H2+H1+OH+CO2+CO+RN2+RNO+O2+O1
        IF(ABS(PN-PNL)-1.E-07)21,21,1
21      T=TT
        RETURN
        END
```

```
          SUBROUTINE SOLVE(VT,N,PN,T,P,VS)
          DIMENSION AC(50),PN(50),T(50),VS(50)
C         CALCULATE PRESSURE AS A FUNCTION OF TEMPERATURE DISTRIBUTION
          ACT=0.00
          R=.082
          DO 57 I=1,N
          AC(I)=PN(I)*R*T(I)
57        ACT=ACT+AC(I)
28        YC=ACT*P**(-1)-VT
          YP=-ACT*P**(-2)
          PC=P-YC/YP
          IF(ABS(PC-P)-1.E-05)26,26,27
27        P=PC
          GO TO 28
26        P=PC
          DO 58 I=1,N
58        VS(I)=PN(I)*R*T(I)/P
          RETURN
          END
          SUBROUTINE CAPAC(T,H2O,H2,H1,OH,CO2,CO,RN2,RNO,O2,O1)
          Z(T,A,B,C,D,E)=1.9869*(A+B*T+C*T**2+D*T**3+E*T**4)
          IF(T-1000.)29,29,30
29        H2O=Z(T,4.15650,-1.72443E-3,5.69823E-6,-4.5930E-9,1.42337E-12)
          CO2=Z(T,2.19744,1.01630E-2,-1.01649E-5,5.72467E-9,-1.38809E-12)

          CO=Z(T,3.79299,-2.21569E-3,5.19391E-6,-3.60352E-9,8.22622E-13)
          H2=Z(T,2.86121,4.06328E-3,-9.1926E-6,8.94899E-9,-3.05132E-12)
          O2=Z(T,3.71899,-2.5167E-3,8.58373E-6,-8.29987E-9,2.70822E-12)
          RN2=Z(T,3.69274,-1.3420E-3,2.66933E-6,-9.95596E-10,-9.32767E-14)

          RNO=Z(T,4.21388,-4.62221E-3,1.10113E-5,-9.29946E-9,2.78539E-12)

          OH=Z(T,3.84242,-1.26684E-3,1.65049E-6,-6.67689E-10,1.30677E-13)

          H1=Z(T,2.49482,3.88457E-5,-1.0089E-7,1.08807E-10,-4.16151E-14)
          O1=Z(T,3.02189,-2.17372E-3,3.75422E-6,-2.99472E-9,9.07775E-13)
          GO TO 31
30        CO2=Z(T,4.40090,3.21639E-3,-1.31347E-6,2.45482E-10,-1.70946E-14)

          CO=Z(T,2.95372,1.54768E-3,-6.16038E-7,1.12728E-10,-7.72089E-15)

          H2O=Z(T,2.67075,3.03171E-3,-8.53516E-7,1.17909E-10,-6.19736E-15)

          H2=Z(T,3.07987,5.42166E-4,3.84876E-8,-3.46339E-11,3.67190E-15)
          O2=Z(T,3.56810,7.78057E-4,-2.23375E-7,4.23966E-11,-3.34190E-15)

          RN2=Z(T,2.86095,1.58518E-3,-6.17799E-7,1.11194E-10,-7.52106E-15)

          RNO=Z(T,3.15518,1.40486E-3,-5.69891E-7,1.06151E-10,-7.36590E-15)

          OH=Z(T,2.90295,9.73459E-4,-2.03210E-7,1.59116E-11,-5.16739E-17)

          H1=Z(T,2.50265,-5.25974E-6,3.33198E-9,-8.32728E-13,7.14625E-17)

          O1=Z(T,2.53726,-1.84222E-5,-8.80179E-9,5.96436E-12,-5.57436E-16)

31        RETURN
          END
```

```
 TEMPERATURE=  450.0 DEGREES KELVIN
PRESSURE=   5.10 ATMOSPHERES
PHI= 0.90


SHELL      TEMP      PRESSURE      VOLUME      NO CONCENTRATION


  1       2400.0       7.98        0.0761          0.0058255


  1       2512.4      10.76        0.0592          0.0072507
  2       2401.1      10.76        0.0564          0.0057911


  1       2596.7      13.49        0.0489          0.0084691
  2       2488.2      13.49        0.0467          0.0068526
  3       2418.0      13.49        0.0453          0.0059573


  1       2664.1      16.19        0.0419          0.0095383
  2       2557.7      16.19        0.0401          0.0077935
  3       2488.8      16.19        0.0389          0.0068193
  4       2427.3      16.19        0.0379          0.0060418


  1       2720.6      18.86        0.0368          0.0104985
  2       2615.7      18.86        0.0352          0.0086454
  3       2547.9      18.86        0.0343          0.0076034
  4       2487.4      18.86        0.0334          0.0067682
  5       2441.9      18.86        0.0328          0.0061940


  1       2769.1      21.50        0.0329          0.0113673
  2       2665.4      21.50        0.0315          0.0094240
  3       2598.6      21.50        0.0307          0.0083239
  4       2538.9      21.50        0.0299          0.0074382
  5       2494.0      21.50        0.0294          0.0068276
  6       2453.2      21.50        0.0289          0.0063106
```

```
SHELL     TEMP      PRESSURE      VOLUME      NO CONCENTRATION


  1      2812.1      24.13       0.0298         0.0121716
  2      2709.2      24.13       0.0286         0.0101456
  3      2643.0      24.13       0.0278         0.0089929
  4      2583.9      24.13       0.0272         0.0080616
  5      2539.5      24.13       0.0267         0.0074178
  6      2499.1      24.13       0.0262         0.0068717
  7      2462.0      24.13       0.0258         0.0064004


  1      2850.5      26.74       0.0273         0.0129166
  2      2748.2      26.74       0.0262         0.0108172
  3      2682.5      26.74       0.0255         0.0096175
  4      2624.0      26.74       0.0249         0.0086452
  5      2580.0      26.74       0.0245         0.0079714
  6      2540.0      26.74       0.0241         0.0073987
  7      2503.2      26.74       0.0237         0.0069037
  8      2468.9      26.74       0.0233         0.0064688


  1      2885.3      29.34       0.0252         0.0136113
  2      2783.4      29.34       0.0242         0.0114459
  3      2718.1      29.34       0.0236         0.0102038
  4      2660.1      29.34       0.0230         0.0091943
  5      2616.4      29.34       0.0226         0.0084930
  6      2576.7      29.34       0.0223         0.0078961
  7      2540.2      29.34       0.0219         0.0073794
  8      2506.2      29.34       0.0216         0.0069248
  9      2474.2      29.34       0.0213         0.0065201


  1      2917.3      31.93       0.0235         0.0142669
  2      2815.7      31.93       0.0225         0.0120408
  3      2750.7      31.93       0.0220         0.0107598
  4      2693.0      31.93       0.0215         0.0097160
  5      2649.7      31.93       0.0211         0.0089894
  6      2610.3      31.93       0.0207         0.0083700
  7      2574.0      31.93       0.0204         0.0078331
  8      2540.2      31.93       0.0201         0.0073602
  9      2508.5      31.93       0.0199         0.0069388
 10      2488.3      31.93       0.0197         0.0066815



AVERAGE NITIC OXIDE CONCENTRATION= 0.0092957
```

BIBLIOGRAPHY

1. Myers, P., "Automobile Emissions - A Study of Environmental Benefits Versus Technological Costs", SAE Paper NO. 700182 (1970).

2. Caplan, J., "Smog Chemistry Points the Way to Rational Vehicle Emission Control", SAE Transactions, Vol. 74 (1966).

3. "The Automobile and Air Pollution; A Program for Progress", Part 1 Report of the Panel on Electrically Powered Vehicles, (October, 1967).

4. Mueller, P., and Hitchcock, M. "Air Quality Criteria - Toxicological Appraisal for Oxidants, Nitrogen Oxides and Hydrocarbons", Journal of the Air Pollution Control Association, Vol. 19, No. 9, (September 1969).

5. Sax, N., "Dangerous Properties of Industrial Materials", Reinhold Publishing Co., (1957)

6. Eschenroeder, A., and Martinez, J., "Mathematical Modeling of Photochemical Smog", AIAA Paper No. 70-116, (January, 1970).

7. Heicklen, J. and Cohen, N., "The Role of Nitric Oxide in Photochemistry", Advances in Photochemistry, Vol. 5, Interscience Publishers, (1968).

8. Haagen-Smit, A. and Fox, M., "Automobile Exhaust and Ozone Formation", SAE Paper No. 55421, (January 1955).

9. Anderson, J., Arnoldi, W. and Arons, A. "A Study of the Nitric Oxide in the Exhaust Gases of Internal Combustion Engines", Senior Report, Stevens Institute of Technology, (1937).

10. Wimmer, D. and McReynolds, L., "Nitrogen Oxides and Engine Combustion", SAE Transactions, Vol. 70 (1962).

11. Campau, R. and Neerman, J., "Continuous Mass Spectrometric Determination of Nitric Oxide in Automotive Exhaust", SAE Paper No. 660116, (January, 1966).

12. Kaufman, F. and Decker, L., "Effect of Oxygen on Thermal Decomposition of Nitric Oxide at High Temperatures", 7th Symposium (International) on Combustion, Butterworths Publications, Ltd., London (1959).

13. Wray, K. and Teare, J., "Shock-Tube Study of the Kinetics of Nitric Oxide at High Temperature", Journal of Chemical Physics, Vol. 36, No. 10 (May, 1962).

14. Newhall, H., "Theoretical and Experimental Investigation of Chemical Kinetics During Rapid Expansion of High Temperature Combustion Products", Ph.D. Thesis, University of California, Berkeley, (1966).

15. Herzberg, G., "Infrared and Raman Spectra of Polyatomic Molecules", D. Van Nostrand Co., Inc., Princeton, New Jersey, (1946).

16. Dimitriades, B., "Methods for Determining Nitrogen Oxides in Automotive Exhausts", United States Dept. of the Interior Bureau of Mines Report of Investigations 7133, (May, 1968).

17. Eyzat, P. and Guibet, J., "A New Look at Nitrogen Oxides Formation in Internal Combustion Engines", SAE Paper No. 680124 (January, 1968).

18. LaVoie, G., Heywood, J. and Keck, J., "Experimental and Theoretical Study of Nitric Oxide Formation in Internal Combustion Engines", Combustion Science and Technology, Vol. 1, No. 4, (February, 1970).

19. LaVoie, G., "Spectroscopic Measurements of Nitric Oxide in Spark Ignition Engines", Massachusetts Institute of Technology, Fluid Mechanics Laboratory Publication No. 70-4, (March, 1970).

20. Newhall, H., "Kinetics of Engine-Generated Nitrogen Oxides and Carbon Monoxide", 12th Symposium on Combustion, (1969).

21. Kopa, R., "Control of Automotive Exhaust Emission by Modifications of the Carburetion System", SAE Paper No. 660114, (1966).

22. Benson, J., "Reduction of Nitrogen Oxides in Automobile Exhaust", SAE Paper No. 690019, (1969).

23. Nicholls, J., El-Messiri, I. and Newhall, H., "Inlet Manifold Water Injection for Control of Nitrogen Oxides - Theory and Experiment", SAE Paper No. 690018, (1969).

24. Reid, R., Mingle, J. and Paul, W., "Oxides of Nitrogen from Air Added in Exhaust Ports", SAE Paper No. 660115 (1966).

25. Shelef, M., Otto, K. and Gandhi, H., "The Heterogeneous Decomposition of Nitric Oxide on Supported Catalysts", Ford Motor Company Scientific Laboratory Preprint.

26. Baker, R. and Doerr, R. "Catalytic Reduction of Nitrogen Oxides in Automobile Exhaust", Journal of the Air Pollution Control Association, Vol. 14, No. 10, (October, 1964).

27. Schwochert, H., "Performance of a Catalytic Converter on Non-Leaded Fuel", SAE Paper No. 69053, (May, 1969).

28. Fenimore, C. and Jones, G., "Nitric Oxide Decomposition at 2200-2400°K", Journal of Physical Chemistry, Vol. 61, (May, 1957).

29. Starkman, E., Stewart, H. and Zvonow, V., "An Investigation into the Formation and Modification of Emission Precursors", SAE Paper No. 690020, (January, 1969).

30. Patterson, D., "Cylinder Pressure Variation, A Fundamental Combustion Problem", SAE Paper No. 660129, (1966).

31. Personal Communications, Professor Robert F. Sawyer, University of California, Berkeley, California.

32. Huls, T. and Nickol, H., "Influence of Engine Variables on Exhaust Oxides of Nitrogen Concentrations from a Multi-cylinder

Engine", SAE Paper No. 670482, (May, 1967).

33. Cole, D. and Mirsky, W., "Mixture Motion - Its Effect on Pressure Rise in a Combustion Bomb; A New Look at Cyclic Variation", SAE Paper No. 680766, (October, 1968).

34. Peters, B. and Borman, G., "Cyclic Variations and Average Burning Rates in a S.I. Engine", SAE Paper No. 700064, (January, 1970).

35. Bannister, F. and Mucklow, G., "Wave Action Following Sudden Release of Compressed Gas From a Cylinder", The Institution of Mechanical Engineers. Proceedings, Volume 159, (1948).

36. Herzberg, G., "Spectra of Diatomic Molecules", 2nd Edition, 8th Printing, D. Van Nostrand Co. Inc., Princeton, New Jersey, (1963).

37. Penner, S., "Quantitative Molecular Spectroscopy and Gas Emissivities", Addison-Wesley Publishing Co., Inc., Reading, Mass., (1959)

38. Pierson, R., Fletcher, A., St Clair Gantz, E., "Catalog of Infrared Spectra for Qualitative Analysis of Gases", Analytical Chemistry, Vol. 28, No. 8, (August, 1956).

39. Sullivan, J. and Holland, A., "A Congeries of Absorption Cross-Sections for Wavelengths less than 3000A", NASA Contractor Report, CR-371, (January, 1966).

40. Marmo, F., "Absorption Coefficients of Nitrogen Oxide in the Vacuum Ultraviolet", Journal of the Optical Society of America,.

Vol. 43, No. 12, (Dec. 1953).

41. Gaydon, A., "Dissociation Energies of Spectra of Diatomic Molecules", John Wiley and Sons, Inc. New York, (1947).

42. Smakula, A., Swinehart, C., Whitaker, G., O'Dell, E. and Johnson, R., "Harshaw Optical Crystals", Publication of the Harshaw Chemical Co.

43. Union Carbide Crystal Products Bulletin F-917-D

44. Baum, W. and Dunkelman, L., "Ultraviolet Radiation of the High Pressure Xenon Arc", Journal of the Optical Society of America, Vol. 40, No. 11, (November, 1958).

45. Jones, L. and Taylor, L., "Far Ultraviolet Absorption Spectra of Unsaturated Aromatic Hydrocarbons", Analytical Chemistry, Vol. 27 No. 2, (February, 1955).

46. Jaffé, H. and Orchin, M., "Theory and Application of Ultraviolet Spectroscopy" John Wiley and Sons, New York, (1962).

47. Mellon, M., "Analytical Absorption Spectroscopy", The Encyclopedia of Spectroscopy, Clarke, G. Ed.,Reinhold Publishing Co., New York, (1960)

48. Fink, E. and Welge, K., "Lebensdauern und Löschquerschnitte Angeregter Zustände", Zeitschrift für Naturforschung, Vol. 23, (1968).

49. Nicksic, S. and Harkins, J., "Spectrophotometric Determination of Nitric Oxide in Auto Exhaust", Analytical Chemistry, Vol. 34, No. 8, (1962).

50. Brown, W., Gendernalik, S., Kerley, R. and Marsee, F., "Effect of Engine Intake-Air Moisture on Exhaust Emissions", SAE Paper No. 700107, (January, 1970).

51. Edson, M., and Taylor, C., "The Limits of Engine Performance - Comparison of Actual and Theoretical Cycles", Digital Calculations of Engine Cycles, SAE Progress in Technology Series, Vol. 7 (1964)

52. Starkman, E. and Newhall, H., "Characteristic of the Expansion of Reactive Gas Mixtures as Occurring in Internal Combustion Engine Cycles", SAE Paper No. 650509, (May, 1965)

53. Vickland, C., Strange, F., Bell, R. and Starkman, E., "A Consideration of the High Temperature Thermodynamics of Internal Combustion Engines", Digital Calculations of Engine Cycles, SAE Progress in Technology Series, Vol. 7 (1964)

54. Gaydon, A. and Hurle, I. "The Shock Tube in High-Temperature Chemical Physics", Reinhold Publishing Co., New York, (1963)

55. Hudson, R., Carter, V. and Stein, J., "An Investigation of the Effect of Temperature on the Schumann-Runge Absorption Continuum of Oxygen, 1580-1950A", Journal of Geophysical Research, Vol. 70, No. 9, (May, 1966)

56. Evans, J. and Schexndyder, C., "An Investigation of the Effect of High Temperature on the Schumann-Runge Ultraviolet Absorption Continuum of Oxygen", NASA Technical REport R-92, (1961)

57. Montroll, E. and Shuler, K., "Studies in Non-Equilibrium Rate Processes. I. The Relaxation of a System of Harmonic Oscillators", Journal of Chemical Physics, Vol. 26, No. 3, (March, 1957)

58. Cottrell, T. and McCoubrey, J., "Molecular Energy Transfer in Gases", Butterworths and Co. London, (1961)

59. Wray, K., "Shock-Tube Study of the Vibrational Relaxation of Nitric Oxide", Journal of Chemical Physics, Vol. 36, No. 10, (May, 1962)

60. Kodak Publication P-9, "Kodak Plates and Films for Science and Industry", (1967)

61. Saltzman, B., "Colorimetric Microdetermination of Nitrogen Dioxide in the Atmosphere", Analytical Chemistry, Vol. 26, No. 12, (December, 1954)

62. Singh, T., Sawyer, R., Starkman, E. and Caretto, L., "Rapid Continuous Determination of Nitric Oxide Concentration in Exhaust Gases", Journal of the Air Pollution Control Association, Vol. 18, No. 2, (February, 1968)

63. Beatty, R., Berger, L. and Schrenk, H., "Determination of the

Oxides of Nitrogen by the Phenoldisulfonic Acid Method", Bureau of Mines Report of Investigations R. I. 3687, (February, 1943)

64. Shapiro, A., "The Dynamics and Thermodynamics of Compressible Fluid Flow", Volume 1, The Ronald Press Co., New York, (1953)

65. Rothbart, H., "Cams-Design, Dynamics and Accuracy", John Wiley and Sons, New York, (1956)

66. "Janaf Thermochemical Tables", National Bureau of Standards PB 168370, (August, 1965)

67. "Selected Values of Chemical Thermodynamic Properties" Circular of the National Bureau of Standard 500, (February, 1952)

68. Zeleznik, F. and Gordon, S., "A General IBM 704 or 7090 Computer Program for Computation of Chemical Equilibrium Compositions, Rocket Performance, and Chapman-Jouguet Detonations", NASA TND-1454, (October, 1962)

69. "Selected Values of Properties of Hydrocarbons", Circular of the National Bureau of Standards, C461, (November, 1947)

70. Clarke, J., "Initiation and Some Controlling Parameters of Combustion in the Automobile Engine", SAE Transactions, Vol. 70, (1962)